REPORT DOCUMENTATION PAGE

Form Approved
OMB No. 0704-0188

1. REPORT DATE (DD-MM-YYYY)	2. REPORT TYPE	3. DATES COVERED (From - To)
23/06/2007	Final	4/1/03 to 9/30/06

4. TITLE AND SUBTITLE

Rapid Assessment of the Roll of Microstructural Variability in the Fatigue Behavior of Structural Alloys using Ultrasonic Fatigue

5a. CONTRACT NUMBER

5b. GRANT NUMBER
F49620-03-1-0069

5c. PROGRAM ELEMENT NUMBER

6. AUTHOR(S)

J. Wayne Jones

5d. PROJECT NUMBER

5e. TASK NUMBER

5f. WORK UNIT NUMBER

7. PERFORMING ORGANIZATION NAME(S) AND ADDRESS(ES)

Regents of the University of Michigan
Div. of Research Development and Admin.
Wolverine Tower, Room 1058
3003 S. State St.
Ann Arbor, MI 48109-1274

8. PERFORMING ORGANIZATION REPORT NUMBER
F007992

9. SPONSORING / MONITORING AGENCY NAME(S) AND ADDRESS(ES)

Bret Connor /NA
Program Manager: Metallic Materials Prog.
375 North Randolph Street
Arlington, Virginia 22203

10. SPONSOR/MONITOR'S ACRONYM(S)
AFOSR

11. SPONSOR/MONITOR'S REPORT NUMBER(S)

12. DISTRIBUTION / AVAILABILITY STATEMENT

Approved for public release,
distribution unlimited

AFRL-SR-AR-TR-07-0201

13. SUPPLEMENTARY NOTES

14. ABSTRACT

Ultrasonic fatigue (20kHz) has been used to investigate the role of microstructural variability on fatigue life variability for very long fatigue lives, betwe 10^7 and 10^9 cycles, in structural aerospace materials. This AFOSR program has been augmented by support from DARPA (Dr. Leo Christodoulou) and summary of the results from the combined support is described in this report. Four distinctly different structural alloys have been studied: (1) a partic reinforced aluminum alloy, 2009Al/15SiCp, where clustering of SiC particles and the presence of processing-related inclusions is expected to contr fatigue life, (2) an alpha/beta titanium disk alloy, Ti-6Al-2Sn-4Zr-6Mo, that has been processed to have a fine, homogeneous, two-phase microstructu that is essentially free of inclusions or other defects; (3) a polycrystalline nickel-base disk alloy, Rene 88DT which has a small but finite number of lar grains that influence fatigue crack initiation; and a single crystal nickel-base superalloy for blade applications, PWA 1484. In this program, and advanc ultrasonic fatigue system capable of fatigue testing aerospace materials at 20 kHz and at temperatures form ambient to 1000°C has been developed. For t polycrystalline materials, the magnitude of fatigue life variability was observed to be strongly dependent on the microstructure-dependent crack initiatic processes, which, in turn, were different for each material. For 2009Al/15SiCp, crack initiation occurred in almost all cases at 20-30 μm diamet inclusions. Less than half an order of magnitude variation in fatigue life at 10^9 cycles was observed and is explained by the absence of a significant cra initiation lifetime. However, for the alpha/beta processed titanium alloy, transgranular crack initiation occurred either at large alpha grains or at clusters smaller alpha grains and variability in fatigue life of three orders of magnitude was observed. For the Rene 88DT alloy, clusters of two or more lar grains, on the order of five times the average grain size controlled crack initiation. In the single crystal alloys crack initiation was controlled by carbide and the mode of propagation (crystallographic, or non-crystallographic) depended on temperature and frequency. This work has demonstrated th ultrasonic fatigue methodologies offer a useful approach to identifying the microstructure feature that controls fatigue crack initiation.

15. SUBJECT TERMS

16. SECURITY CLASSIFICATION OF:	17. LIMITATION OF ABSTRACT	18. NUMBER OF PAGES	19a. NAME OF RESPONSIBLE PERSON

RAPID ASSESSMENT OF THE ROLE OF MICROSTRUCTURAL VARIABILITY

IN THE FATIGUE BEHAVIOR OF STRUCTURAL ALLOYS USING

ULTRASONIC FATIGUE

AFOSR GRANT NO: F49620-03-1-0069

J. Wayne Jones
Department of Materials Science and Engineering
College of Engineering
University of Michigan
Ann Arbor, MI 48109-2136

Abstract

Ultrasonic fatigue (20kHz) has been used to investigate the role of microstructural variability on fatigue life variability for very long fatigue lives, between 10^7 and 10^9 cycles, in structural aerospace materials. This AFOSR program has been augmented by support from DARPA (Dr. Leo Christodoulou) and a summary of the results from the combined support is described in this report. Four distinctly different structural alloys have been studied: (1) a particle reinforced aluminum alloy, 2009Al/15SiCp, where clustering of SiC particles and the presence of processing-related inclusions is expected to control fatigue life, (2) an alpha/beta titanium disk alloy, Ti-6Al-2Sn-4Zr-6Mo, that has been processed to have a fine, homogeneous, two-phase microstructure that is essentially free of inclusions or other defects; (3) a polycrystalline nickel-base disk alloy, Rene 88DT which has a small but finite number of large grains that influence fatigue crack initiation; and a single crystal nickel-base superalloy for blade applications, PWA 1484. In this program, and advanced ultrasonic fatigue system capable of fatigue testing aerospace materials at 20 kHz and at temperatures form ambient to 1000°C has been developed. For the polycrystalline materials, the magnitude of fatigue life variability was observed to be strongly dependent on the microstructure-dependent crack initiation processes, which, in turn, were different for each material. For 2009Al/15SiCp, crack initiation occurred in almost all cases at 20-30 μm diameter inclusions. Less than half an order of magnitude variation in fatigue life at 10^9 cycles was observed and is explained by the absence of a significant crack initiation lifetime. However, for the alpha/beta processed titanium alloy, transgranular crack initiation occurred either at large alpha grains or at clusters of smaller alpha grains and variability in fatigue life of three orders of magnitude was observed. For the Rene 88DT alloy, clusters of two or more large grains, on the order of five times the average grain size controlled crack initiation. In the single crystal alloys crack initiation was controlled by carbides, and the mode of

Acknowledgement/Disclaimer

This work was sponsored (in part) by the Air Force Office of Scientific Research, USAF, under grant number F49620-03-1-0069. The views and conclusions contained herein are those of the authors and should not be interpreted as necessarily representing the official policies or endorsement, either expressed or implied, of the Air Force Office of Scientific Research or the U.S. Government.

propagation (crystallographic, or non-crystallographic) depended on temperature and frequency. This work has demonstrated that ultrasonic fatigue methodologies offer a useful approach to identifying the microstructure feature that controls fatigue crack initiation.

Objectives

The objectives this research are: (1) to advance current predictive capability for fatigue life in relevant structural materials with complex and variable microstructures; (2) to provide fundamental links between microstructure variability and fatigue life that informs alloy design for fatigue resistance; and (3) to investigate ultrasonic fatigue methodologies as an effective tool for rapid assessment of fatigue behavior in structural alloys important to Air Force needs, specifically to aid in developing statistically meaningful long life, low stress fatigue failures as a critical part of the analysis of fatigue crack initiation and early crack growth mechanisms in structural materials.

Major Findings and Results

1. Appended to this report are the publications describing the details of experimental techniques for accelerated fatigue studies using ultrasonic fatigue that have been developed and the specific findings regarding the role of microstructure variability and fatigue behavior in a wide range of structural alloys for aerospace applications. The key results and findings are summarized below.

2. Ultrasonic fatigue instrumentation and techniques were developed to allow accurate and reproducible accelerated fatigue studies at a cyclic frequency of 20 kHz and at temperatures from ambient to 1000°C.

3. Very long-life fatigue studies in a SiCp reinforced aluminum alloy, where lifetimes as long as 10^9 were investigated, showed that a processing inclusion, and not SiC particle clustering controlled fatigue crack initiation. This study provided convincing evidence of the capability of accelerated fatigue testing to quickly identify key microstructural features controlling fatigue, even when those features existed in an extremely small population.

4. More subtle effects of microstructure (e.g. clustering and preferred orientation) of alpha grains in the alpha-beta Ti-6242 alloy were shown to be responsible for scatter in fatigue life in this disk alloy. This results allows more accurate modeling of the microstructural "neighborhood" that is critical to fatigue behavior in this duplex alloy. It was also shown that the axial fatigue behavior observed under conventional testing methods was essentially identical (extrapolated lifetimes, crack initiation processes) with that observed in ultrasonic fatigue.

5. In the polycrystalline nickel alloy Rene 88DT, the mechanisms of cyclic damage accumulation have been investigated at ambient temperature and at 593°C.

Persistent slip band formation at room temperature occurs in the largest grains and leads to failure. At elevated temperature, oxide formation suppresses PSB emergence at specimen surfaces and forces crack initiation to occur at large grains or grain clusters in the specimen interior. Techniques have been developed to identify the dependence of large grain orientation and the relative orientations of two-grain clusters on fatigue crack initiation.

6. Techniques have been developed to allow studies at ultrasonic frequencies, high mean stresses and temperatures as high as 1000°C for nickel superalloy single crystals. This capability has allowed an important extension of comparisons of crack initiation behavior and subsequent early crack growth as a function of frequency to the range associated with turbine blade failures.

Personnel Supported at University of Michigan

J. Wayne Jones, Professor
Chris Torbet, Research Engineer
Auralie Salem (MS Degree 2005)
James Huang, (MS Degree 2006)
Chris Sczcepanski, (Ph.D. expected 2007)
Jiashi Miao (Ph.D. expected in 2008)
Amit Shyam (Postdoctoral Fellow, partial support)
Jian Yi (Postdoctoral Fellow, partial support)

Journal and Conference Publications

1. "Ultrasonic Fatigue of a Single Crystal Superalloy at 1000°C", J.Yi, C.J. Torbet, Q. Feng, T.M. Pollock and J.W. Jones, Materials Science and Engineering A, 443 (2007) 142-149.

2. "Fatigue Behavior of SiCp-reinforced Aluminum Composites in the Very High Cycle Regime Using Ultrasonic Fatigue", J. Huang, J.E. Spowart and J.W. Jones, Fatigue and Fracture of Engineering Materials and Structures, v29, n7, July 2006, p 507-517.

3. "On Small Fatigue Crack Growth in Structural Materials", A. Shyam, J.W. Jones and J.E. Allison, Proceedings, Ninth International Fatigue Congress, May 2006.

4. "Fatigue Crack initiation in an Alpha + Beta Alloy", C.J. Szczepanski, S.K. Jha, J.M. Larsen and J.W. Jones, to appear in Proceedings, Ninth International Fatigue Congress, May 2006.

imposed on the gage section can be monitored and controlled by adjusting the amplitude of the input signal. With this approach, a specimen is tested in mechanical resonance at frequencies of approximately 20 kHz. The advantages of this in terms of the ability to accelerate tests are obvious. For example, at 20 kHz, applying 10^8 cycles requires approximately 3 hours and applying 10^9 cycles can be completed typically within 1 day. Therefore, a significant amount of data can be established in a very short period of time in the intermediate fatigue life regime. Thus, the fatigue behavior at cycles more representative of the expected service life can be determined experimentally, rather than estimated from extrapolations.

The technique was first explored in the 1950s and the early work through 1980 was reviewed by Willertz in 1980 [19]. More recently, Mayer has offered a comprehensive review of improvements in the past ten years, especially regarding the use of ultrasonic fatigue for fatigue crack growth threshold studies [20]. In the United States, early work was begun by Tien and co-workers in the late 1970s and early 1980s [21,22] but in recent years, research effort has been concentrated primarily in Japan and Europe, where the technique is enjoying considerable use there as a tool for very long fatigue life prediction [23,24]. The growing interest in ultrasonic fatigue is driven in part by the increased need to predict lifetimes in aging structures and is made possible by dramatic improvements in the accuracy of control instrumentation for ultrasonic fatigue.

Numerous studies have been conducted showing that the fatigue behavior of many important structural materials systems, including aluminum, titanium and nickel based alloys can be determined effectively by ultrasonic fatigue methods [19,20,23]. Importantly, frequency effects may not be significant for many structural materials unless environmental attack is occurring simultaneously. The objective of the work described in this paper is to examine the potential use of ultrasonic fatigue in the study of the relationship between microstructural variability and fatigue life in structural turbine alloys, especially at long fatigue lives. We describe an ultrasonic fatigue test system capable of operation at temperatures as high as 600°C under variable mean stress loading. Initial results of high temperature ultrasonic fatigue studies are presented for the disk alloy Rene' 88 DT [25].

Experimental Procedure

The ultrasonic fatigue test system that has been developed for fatigue studies on superalloys and other high temperature materials is shown in Figure 1. A high accuracy ultrasonic amplifier drives the piezoelectric transducer. Feedback from an inductive vibration gage is used to control vibration amplitude and frequency to within 1%. Cycles can be applied in pulses as short as 25 ms (500 cycles) to prevent specimen heating during cycling at room temperature. Specimens with diameters of 5-6 mm and overall dimensions similar to specimens used in conventional fatigue testing are typically used. Other specimen shapes, such as hourglass specimens are also used. The transducer is isolated from the mean load by a specially constructed cage and the transducer, load train and specimen are designed such that the specimen is in resonance at or near 20 kHz, with displacement anti-nodes occurring at the specimen ends. The mean load is applied at a flange which is located at an exact displacement node and therefore, does not affect the ultrasonic load train. Specimen heating is accomplished by induction heating and Figure 2 shows the induction coil arrangement around a standard cylindrical ultrasonic fatigue specimen of Rene' 88 DT. The temperature at the center of the specimen is measured and controlled with a non-contact infra-red pyrometer. The induction coil design is optimized to provide uniform heating along the entire length of the gage section. Induction heating in this manner produces a temperature variation of $\pm$ 3°C in the gage section of the cylindrical specimen.

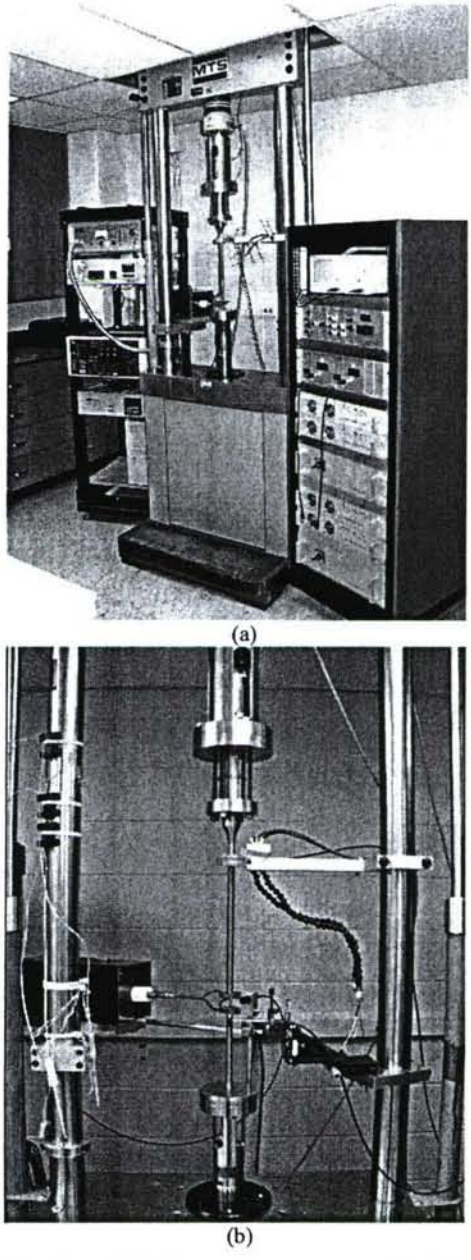

Figure 1: The ultrasonic fatigue testing system capable of testing with superimposed mean stresses at elevated temperature (a) the entire system with the controls and (b) the ultrasonic fatigue load train.

Fatigue tests were conducted at a load-ratio of 0.05 and temperatures of 20°C and 593°C. The desired mean stress was

applied using a servohydraulic fatigue testing system and the alternating stress was accomplished with ultrasonic loading. Fatigue cycles were applied in pulses of 500 ms followed by a pause of 900 ms at 20°C. This was done to prevent the specimen from heating as a result of high frequency cycling. At 593°C, however, ultrasonic loading was continuous since the heat generated was compensated by the temperature control system. There was no statistically significant influence of pulsed loading at elevated temperature since both pulsed and continuously loaded specimens yielded similar lifetimes under a given condition.

Closed loop control of specimen displacement is achieved during fatigue. This is accomplished by measuring the displacement amplitude of the load train at the specimen using an inductance transducer. This feedback signal is then used to control specimen strain. The feedback signal is calibrated to specimen strains using the output of strain gages attached to the gage section. A high temperature strain gage was used to measure the response of the system as it is heated from 20 to 593°C under displacement control. It was found the strain in the specimen center increased by approximately 6% as a result of heating to 593°C. This factor of 1.06 (which was verified by modeling temperature effects on resonance) was used to calibrate for imposed strains at 593°C by making strain measurements at room temperature.

At higher test stresses, the strain gaging technique requires extrapolation of the feedback signal/specimen strain data, rather than interpolation. Consequently, the instrument is now equipped with a high resolution, non contacting fiber optic displacement gage, also shown in Figure 2. In this figure, this probe is measuring in a lateral mode although longitudinal mode measurements are also possible. This optical probe system provides a means to continuously measure displacement at anti-nodal points in the specimen without disrupting the mechanical conditions required for resonance. An example of the linear relationship between the displacement at the specimen end and gage section strain, as measured by strain gages, is shown in Figure 3. Importantly, the optical gage can be used without interruption at all displacement amplitudes, and is not affected by electrical noise resulting from induction heating.

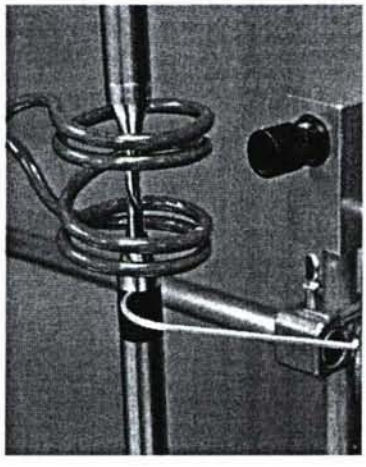

Figure 2: A Rene' 88 DT specimen with the induction heating setup. Also shown here is the non contacting fiber optic displacement gage.

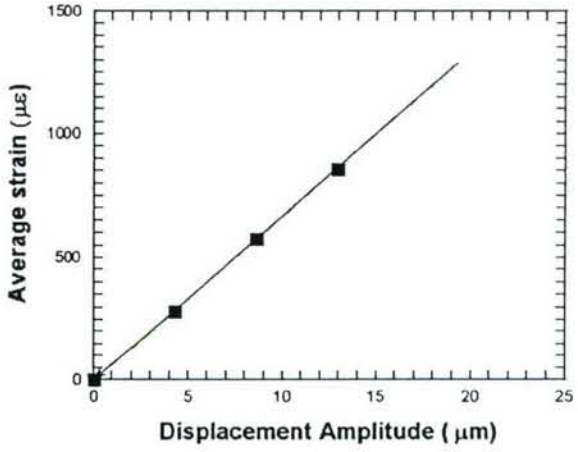

Figure 3: An experimentally generated linear calibration of average strain at the center of the gage section with the displacement amplitude at the end surfaces of the ultrasonic fatigue specimen. με represents microstrains.

Specimen dimensions were fixed using an analytical solution for resonance, as described in the next section. The gage section of the fatigue specimen was 16 mm long and had a diameter of 5 mm and overall dimensions are shown in Figure 4(a). The material for this investigation came from the circumferential orientation of a pancake shape forging. The forging had received a supersolvus heat treatment prior to aging. In order to conserve material for the fatigue tests, the ends of the specimen were made of Inconel 718 and were inertia welded to the Rene' 88 DT gage section. Electropolishing was used to remove approximately 0.1 mm from the diameter of the gage section. This was done to eliminate surface compressive residual stresses arising from the low stress grinding process [26]. Electropolishing was conducted using an electrolyte of 55% ethanol with 35% butyl cellusolve and 10% perchloric acid at 40 V and -30°C.

The microstructure of Rene' 88 DT was examined by optical microscopy and the grain-size distribution was determined using standard linear intercept methods. The fatigue fracture surfaces were studied using scanning electron microscopy (SEM). The distance of the crack initiation site from the surface was measured in all cases where a sub-surface crack initiation event occurred.

Micronotches were machined on some fatigue specimens with the use of femtosecond pulsed lasers. The specimens were mounted on a stage on an optics worktable. A Ti:sapphire femtosecond laser system was used to produce 1000 laser pulses per second at a wavelength of 780 nm, with each pulse 120 fs in duration. The laser pulses were directed through a shutter which opened for 100 ms (100 pulses) on to a 50 mm focal length plano-convex lens and focused onto the specimen surface. The shutter opening time was used to control the depth of the notch. Notches of depth < 30 μm and width 10 μm could be made using this procedure. Details of the laser notching procedure and its effects in aluminum alloys and nickel-base superalloys could be found elsewhere [27,28]. An important feature of the femtosecond laser micromachining approach is the elimination of any melting or

heat affected zones typically encountered with conventional laser drilling techniques [28].

Modeling of Ultrasonic Fatigue

A simple model for a fatigue specimen vibrating at a resonant frequency of f_{res} consists of two blocks of mass 'm' joined by a spring with a spring constant 'k'. In a dumbbell shaped specimen, the grip section approximates the mass and the weightless gage section represents the 'spring'. The resonant frequency is then

$$f_{res} = \frac{1}{2\pi}\sqrt{\frac{k}{m}} \qquad (1)$$

which gives the expected result of low mass objects having a higher resonant frequency. The angular frequency is given by the relationship $\omega = 2\pi f_{res}$. Equation (1), although approximate can give useful insights to specimen design.

A much better representation of the displacement and strain distribution of the fatigue specimen vibrating in resonance can be achieved by solving the displacement equation for the propagation of planar tension-compression waves in a resonant part [20]. A dynamic force balance (neglecting damping effects) in the longitudinal direction which allows for changing cross-sectional area yields the following equation

$$u'' + (A'/A)\,u' + \omega^2(\rho/E)u = 0 \qquad (2)$$

where, u = u (x,t) is the displacement in the longitudinal (x) direction, A is the cross-sectional area and A' is its gradient, ρ is the density and E is the elastic modulus in the longitudinal direction. It is to be noted that time has been factored out in this equation and the partial derivative of the displacement would give the instantaneous strain in the x-direction. In the absence of area gradients, the analytical solution of equation (2) would indicate a sinusoidal variation [20]. If elastic modulus gradients exist in the specimen (for example, as a result of heating the specimen) a general force balance yields the following displacement equation

$$u'' + [(A'/A) + (E'/E)]\,u' + \omega^2(\rho/E)u = 0 \qquad (3)$$

where E' represents a modulus gradient. The strain and displacement distributions in fatigue specimens were obtained by solving Equation (2) for the room temperature case and by solving Equation (3) for elevated temperatures. The solutions were obtained numerically by executing a fourth order Runge Kutta Nystrom (RKN) method within a Java™ computer program. The boundary conditions were implemented in the following fashion: starting at the center of the gage section which is a displacement node (with maximum known strain); the appropriate displacement equation was iteratively evaluated until the specimen ends which are displacement anti-nodes (with zero strain) are reached. The known temperature variation of the modulus of the superalloy and an experimentally measured temperature profile across the specimen was embedded within the code. Since the strain solutions are symmetric (and the displacement solutions are anti-symmetric), only one half of the displacement/strain distribution in the specimen was determined in the above manner.

By solving equation (3), the displacement and strain distribution in the resonating fatigue specimen can be determined as a function of temperature and stress. An example is shown in Figure 4. Figure 4(a) is a schematic figure showing the superalloy specimen dimensions. Figure 4(b) shows model predictions of displacement and strain distribution for this half-specimen with an alternating resonant stress of 361 MPa (for R = 0.05, this represents a maximum stress of 760 MPa) at the gage center. Results are presented for 20 and 593°C, which are the temperatures of interest in this investigation. Modulus differences at the two temperatures account for the different strains at the center of the specimen. The calculations in Figure 4(b) assume resonant frequencies of 19.6 kHz and 19.2 kHz at 20 and 593°C, respectively which are close to the observed resonance frequencies. The lower resonance frequency at the higher temperature arises from the increased compliance of the system. Since the displacement and strain distributions are now known as a function of temperature, we can use this information to relate the displacement amplitude at the ends of the specimen to the strain (and therefore stress) amplitude at the center of the specimen.

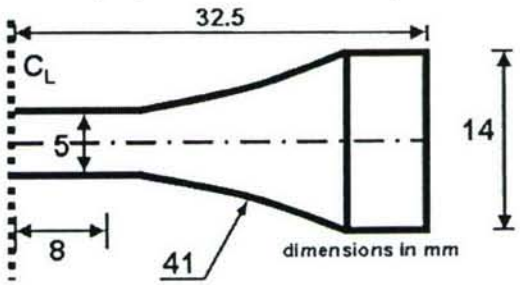

(a)

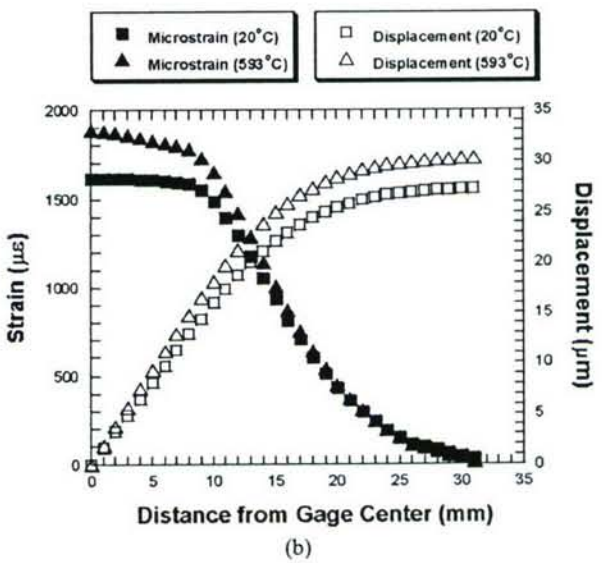

(b)

Figure 4: (a) A schematic of half of the ultrasonic fatigue specimen dimensions with a resonant frequency of 19.6 kHz at 20°C. All dimensions are in mm. (b) Model prediction for strain and displacement distribution across this ultrasonic fatigue specimen. The alternating stress at the center is 361 MPa for both temperatures.

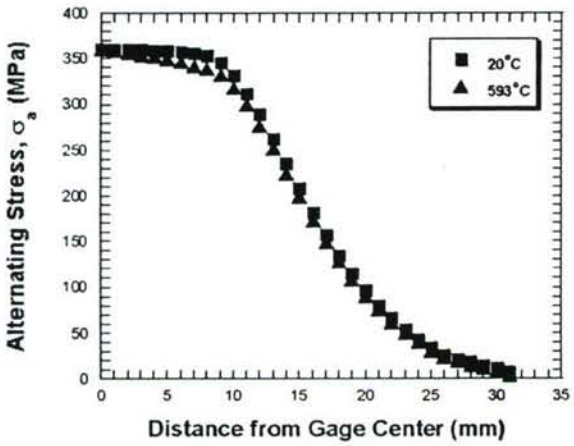

Figure 5: Comparative distribution of stresses in the specimen at the two temperatures.

Figure 5 shows the resulting stress distribution for the strain distribution shown in Figure 4(b). It can be seen that while the stresses vary by less than 2% within the gage section at room temperature, this variation is less than 5% at 593°C. This difference is due to the changing modulus to density ratio between 20 and 593°C as would be predicted by either equation (2) or (3). Although these stress gradients are reasonable, further improvements could be achieved by refining specimen design.

Results

Microstructural Characterization

An optical micrograph showing the microstructure of Rene' 88 DT is shown in Figure 6. This micrograph is representative of the grain structure variation associated with the circumferential orientation in the forging. Annealing twins are prevalent in the microstructure. The supersolvus heat treatment leads to a relatively coarse and equiaxed distribution of grains. In order to determine the grain size distribution, 500 grains were measured using the intercept method and the results of this procedure are summarized in Figure 7. The grain-size distribution is log-normal with a long tail and an average size close to 18.3 μm. The results indicate that there is a finite probability of finding grains with as much as five times the average grain size.

Stress-life response at ultrasonic frequencies

The S-N behavior of Rene' 88 DT at an ultrasonic frequency and a load-ratio of 0.05 at 20 and 593°C has been plotted in Figure 8. The resonant frequency of specimens was close to 19.6 kHz at room temperature and due to increased compliance of the system at elevated temperature, the frequency decreased by approximately 300 Hz at 593°C. Both low stress ground (as-machined) and electropolished specimens were used to generate the results shown in Figure 8. Fatigue lifetimes decreased at 593°C compared to 20°C. Although failures were observed only at 850 MPa at ambient temperatures, at elevated temperature, the variability in fatigue life increased as stress level was decreased.

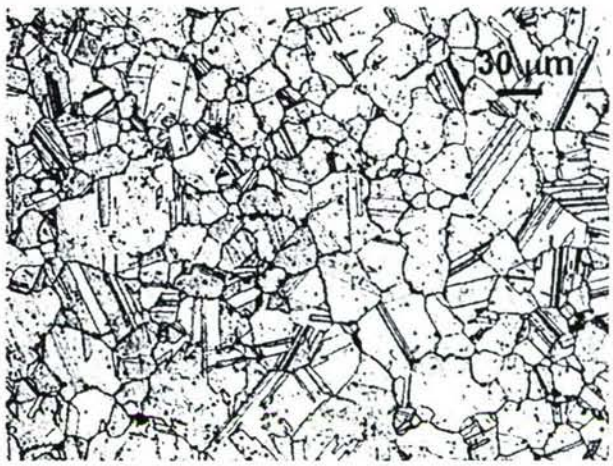

Figure 6: Optical micrograph of Rene' 88 DT.

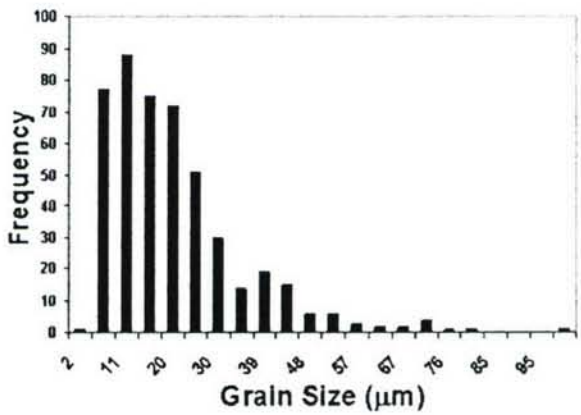

Figure 7: Lognormal distribution of grain size in Rene' 88 DT.

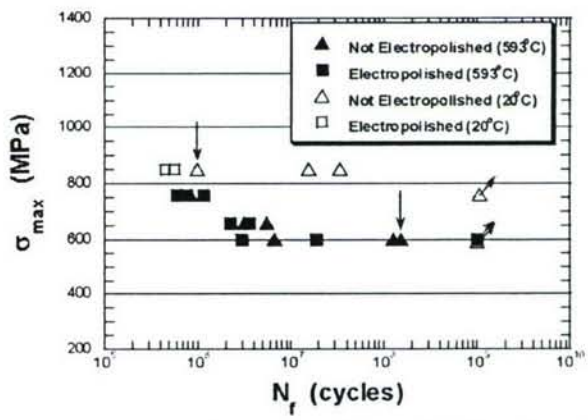

Figure 8: The stress life response of Rene' 88 DT at ultrasonic frequencies and a load-ratio of 0.05. The data-points with downward pointing arrows are specimens with laser machined micronotches.

At 593°C, the variability in lifetimes was within an order of magnitude at 760 and 660 MPa but increased to almost three orders of magnitude at 600 MPa. On two samples, laser machined micronotches were used to initiate fatigue cracks and these data points are indicated with downward pointing arrows in Figure 8.

Fractography

Fractographic examinations were conducted on all specimens that failed under ultrasonic loading conditions. All cracks initiated at sub-surface locations at 593°C. An example of sub-surface initiation is shown in the SEM image of Figure 9. Two different types of crack initiation were observed: crystallographic initiation at large grains (Figure 10(a)) and crack initiation at inclusions (Figure 10(b)). Crystallographic crack initiation was more commonly observed and a large grain (such as the one shown in Figure 10(a)) could be identified with most of these sites. In the few cases where the crack initiated from an inclusion, a larger than average grain could once again be identified in the neighborhood of the inclusion. Regardless of the nature of the crack initiation, the cracks propagated in a transgranular manner producing a rough fracture surface with the roughness decreasing as the crack size increased. This transition from relatively rough to a smoother surface can be seen in Figure 9. At crack lengths just below the transition to the fast fracture region, some striations could also be seen on the fracture surface. Evidence of striation formation is indicated by arrows in the SEM micrograph in Figure 11.

Figure 12(a) shows the fractographic features associated with a crack that initiated from a laser micronotch in as-machined specimen with a maximum stress of 850 MPa at room temperature. Details of the notch are shown in Figure 12(b) and, as anticipated, there are no indications of a damaged area around the notch. The shape of this notch on the fracture surface is a half-cone and its maximum width is approximately 10 μm with a depth of about 25 μm. Fractographic observations suggest that the cracks that initiate from these notches quickly assume a semi-circular shape like cracks that naturally initiate from surface flaws. Similar behavior has been observed in other studies of crack initiation and growth from laser micronotches [27].

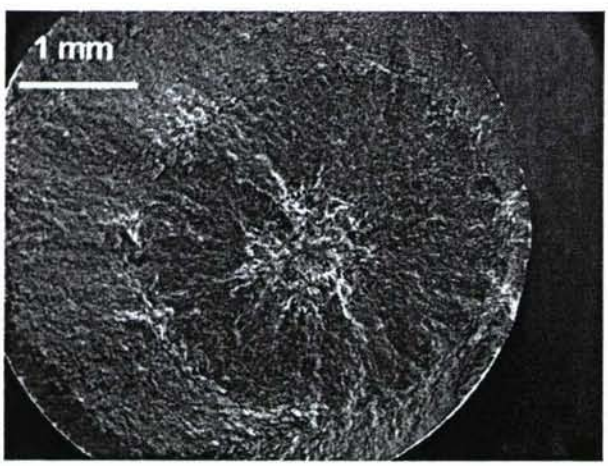

Figure 9: A subsurface crack initiation site for 850 MPa maximum stress at 20°C.

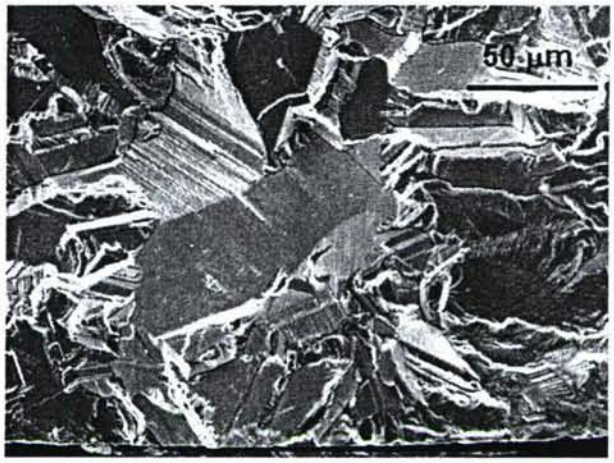

(a)

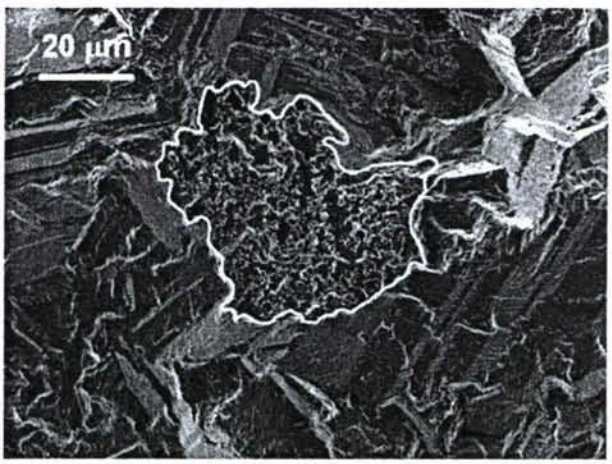

(b)

Figure 10(a) A crystallographic crack initiation site, 593°C with maximum stress of 760 MPa (b) a crack initiating from an inclusion, 20°C with maximum stress of 850 MPa.

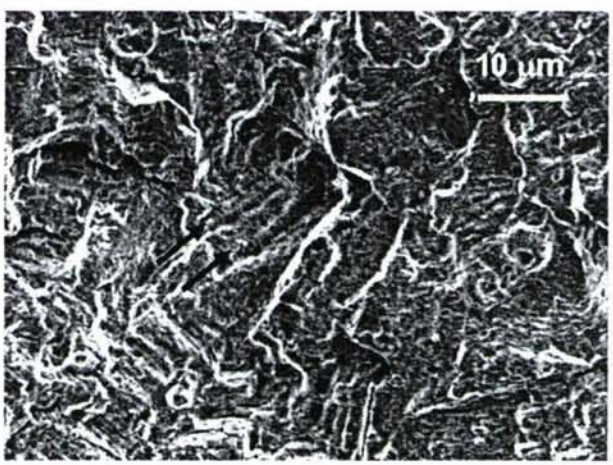

Figure 11: Micrograph indicating the presence of fatigue striations just prior to the fast fracture regime.

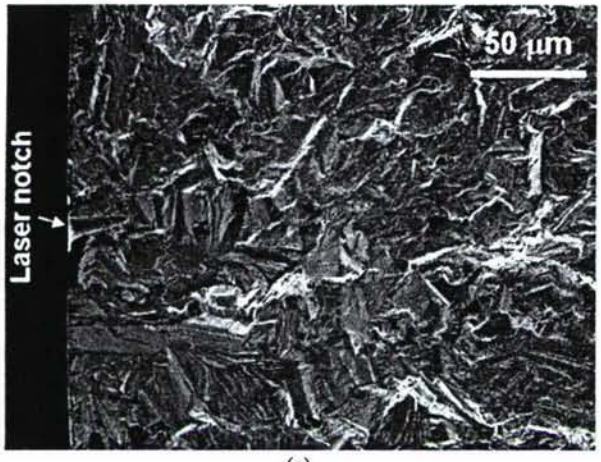

(a)

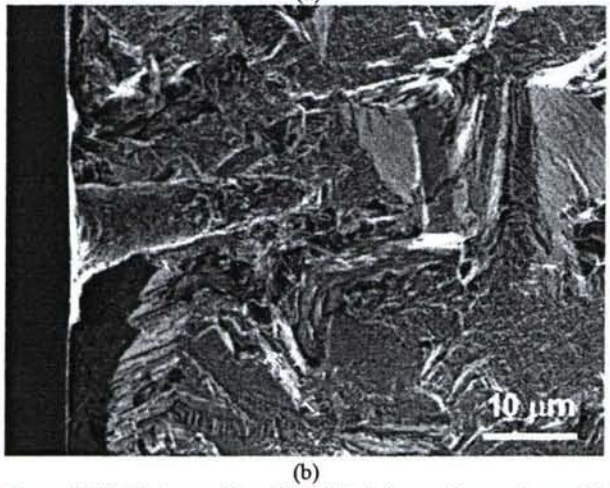

(b)

Figure 12(a) Features of crack initiated from a laser micronotch and (b) higher magnification image of the notch.

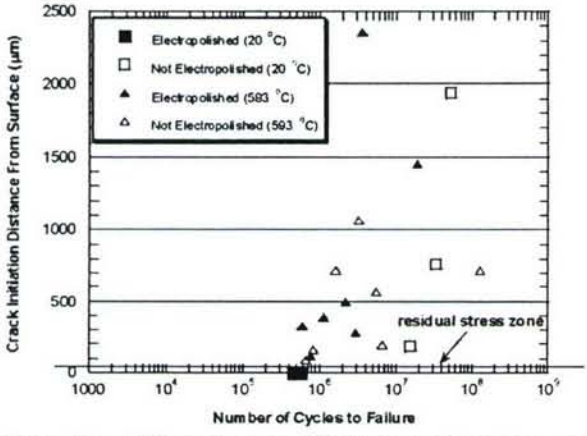

Figure 13: Effect of electropolishing on sub-surface crack initiation. The horizontal line at an initiation distance of 50 μm indicates the boundary of the zone containing compressive residual stresses from machining.

Discussion

We have demonstrated the applicability of ultrasonic fatigue to test turbine disk superalloys at positive mean-stresses and elevated temperatures (<600°C). With adjustments in the load train and specimen design, we can test at temperatures higher than 600°C. Fatigue is a property of concern for many turbine engine components [29]. Of particular relevance for disk materials is quantification of any possible reduction in fatigue life due to small processing defects or particular features of the microstructure [30]. Ultrasonic testing provides opportunities for probing failures from such small defects that may be activated at very long lifetimes under nominally elastic fatigue conditions. In this section, we examine these opportunities in light of our preliminary results.

Sample Surface Conditions

As shown in Figure 8, surface condition influences the fatigue life at room temperature but not at elevated temperature. This is further illustrated in Figure 13, where the fatigue crack initiation locations are plotted against fatigue life. At room temperature, electropolished samples have a lifetime two orders of magnitude less than as-machined specimens. This behavior is consistent with the existence of surface residual compressive stresses from machining. Recent work [26] has determined that compressive residual stresses as high as 450 MPa can exist within the as-machined layer of this superalloy. The inhibition of crack initiation by residual stress is consistent with surface crack initiation in electropolished specimens and only subsurface initiation for as-machined specimens. On the other hand, as shown in Figure 13, only sub-surface initiation occurs at elevated temperature and there is no discernible effect of surface condition on lifetime. It is possible that surface oxide formation may play a role in retarding crack initiation by limiting surface slip [31]. It is more likely that at elevated temperature, greater homogenization of deformation [32] throughout the gage volume results in smaller surface slip offset and therefore favors an interior crack initiation-site with a large grain and/or inclusion while surface/near-surface modes remain dormant. Clearly, the role of surface condition is important and more work is required for a definitive explanation of these results.

Micromechanisms of Crack Initiation and Growth

The results indicate that large grains in the size-range defined by the far right tail of the grain-size distribution shown in Figure 7 play a dominant role in crack initiation. This indicates that fatigue damage accumulation occurs more readily in the weaker regions of the microstructure, in this case large favorably oriented grains. In some cases inclusions in the neighborhood of large grains are crack initiation sites.

Crack propagation is initially crystallographic along with attendant rougher fracture surfaces but when the plastic zone size becomes larger than the average grain size and multiple slip systems can be activated, this leads to a smoother fracture surface [33]. Transitions in crack growth mechanisms have been related to both the monotonic [34] and reversed [34-36] plastic zone sizes for several disk superalloys. The monotonic plastic zone (r_{pzs}) size is given by [37]

$$r_{pzs} \approx \frac{1}{6\pi}\left(\frac{K_{max}}{\sigma_{ys}}\right)^2 \qquad (4)$$

where, K_{max} represents the maximum stress intensity in the fatigue cycle and σ_{ys} is the monotonic yield stress. Assuming an approximate stress intensity solution for an embedded elliptical crack in a flat plate [38], and using yield stress values from Huron [39] equation (4) can be used to predict the boundary for the transition from a crystallographic growth mode to a nominally mode I growth mode. In Figure 9, the crack size at which the calculated maximum plastic zone size is equivalent to the average grain-size is shown. As can be seen, this correlates well with the observed transition in crack growth mode.

The total life of any component consists of the crack initiation life, the small crack propagation life and the long crack propagation life. Taylor and Knott [40] among others have argued that a transition from small to long crack growth mechanisms occurs when the size of the crack is approximately 10 times the size of the characteristic microstructural dimension such as the grain size. If this is true, microstructural fracture mechanics operates when the crack is less than 200 μm in length in this superalloy. The laser micronotching studies, in this context, provide a unique opportunity for studying the interaction of small cracks with the underlying microstructure. The notches are loaded at an ultrasonic frequency and therefore growth rates smaller than at the conventionally defined fatigue threshold (10^{-10} m/cycle) can also be recorded using this technique. Extension of our current experimental capabilities to probe cracks at small length scales comparable to microstructural dimensions and growing at average rates smaller than one lattice spacing per cycle is currently in progress.

Comparison with stress-life data at conventional frequency

A key issue in ultrasonic fatigue is whether fatigue behavior is dependent on frequency, especially when elevated temperature fatigue is studied. In Figure 14, we compare fatigue lifetime derived from ultrasonic fatigue tests with lifetimes resulting from a frequency of 10 and 20 Hz for specimens machined from the same forging [26]. All of the data generated at lower frequency was on electropolished specimens in load-control using a standard servohydraulic test system. For comparative purposes, we have reproduced the ultrasonic frequency fatigue data from electropolished specimens only at room temperature and all the data at elevated temperature (since there is no effect of surface finish condition at 593°C). It can be seen that the fatigue strength at 593°C is significantly lower in the ultrasonic tests. The elevated temperature S-N curve at ultrasonic frequency has shifted down by 250-300 MPa when compared to the low frequency S-N curve. It is important to note the differences in the two techniques. The ultrasonic technique is nominally elastic, so direct comparison to a stress-controlled test at low frequency under conditions where there are significant cyclic plastic strains is not straightforward [26]. Although limited amount of comparable data was generated at room temperature, Figure 14 suggests that the fatigue lives are similar at an ultrasonic frequency and 10 Hz under ambient conditions with a slight increase in fatigue life at 19.6 kHz. A small increase in fatigue life for the superalloy Inconel 718 at ultrasonic frequency under ambient conditions has been reported earlier by Chen *et al.* [41]. The crack initiation sites, however, are the same at both the frequencies. Ultrasonic fatigue techniques can therefore, be used as a tool to quickly identify the weakest links in the microstructure.

Beyond the likely differences in the overall plastic strain distribution in these two types of specimens, some of the variation in fatigue lives with temperature and frequency may be associated with thermally activated deformation mechanisms. These mechanisms could be different in the vicinity of the crack initiation sites. At room temperature, deformation is strain-rate insensitive and this manifests as little or no effect of loading frequency on fatigue lives or crack growth rates. As temperature is increased from 20 to 593°C (at 10 Hz) or when frequency is decreased from 19.6 kHz to 10 Hz (at 593°C), the fatigue lives increase. It is known that increasing temperature (at the same strain rate) and strain rate (at the same temperature) have opposite effects on thermally activated deformation [42]. It is also known that for several superalloys, fatigue cracks grow at faster rates as temperature is increased and/or frequency is decreased [32]. The above discussion, therefore, indicates that any decrease in fatigue lives at ultrasonic frequencies (at 593°C) may be due to favorable crack initiation conditions resulting from high frequency deformation. The favorable condition at high frequency could be higher values of slip offset (or more heterogeneously distributed slip) which makes it easier to initiate a fatigue crack [43]. Atomic force microscopy studies of slip offsets to investigate this hypothesis are currently in progress.

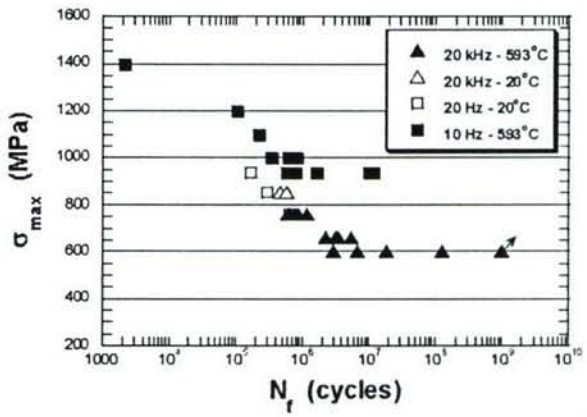

Figure 14: Comparison of the S-N response of Rene' 88 DT between conventional (10 Hz) and ultrasonic (20 kHz) frequencies.

Conclusions

- An ultrasonic fatigue test system has been developed that is capable of superposed mean stresses and elevated temperatures up to 700°C.
- The fatigue behavior of Rene' 88 DT has been examined at ultrasonic frequencies in lifetimes ranging from 10^5 to 10^9 for a load-ratio of 0.05 at 20 and 593°C.
- Fatigue lifetime is dependent on surface condition at ambient temperature but not at elevated temperature, where all crack initiation sites were sub-surface.

- All the crack initiation sites were associated with larger grains or at inclusions near large grains.

- It was demonstrated that micronotches produced by femtosecond pulsed laser machining could be used effectively to study crack initiation and propagation from defects whose sizes are comparable to characteristic microstructural dimensions.

- These results indicate the potential for using fatigue as a tool for examining the role microstructural variability on fatigue life.

Acknowledgements

This work was supported by AFOSR under Grant F4620-03-1-0069, Dr. Craig Hartley, Program Manager. The authors acknowledge the support of Mr. David Maxwell in coordinating the production of fatigue specimens.

References

1. J. Schijve, "Fatigue predictions and scatter", *Fatigue Fract. Engng. Mater. Struct.*, 17 (1994) 381-396.

2. R.E. Little, E.H. Jebe, *Statistical Design of Fatigue Experiments*, Wiley, 1975.

3. S. Suresh, *Fatigue of Materials*, 2nd Ed., Cambridge University Press, 1998.

4. K.S. Ravichandran, R.O. Ritchie, Y. Murakami, Eds., *Small Fatigue Cracks: Mechanics, Mechanisms and Applications*, Elsevier, 1999.

5. K. J. Miller, E.R. de los Rios, eds, *The Behavior of Short Fatigue Cracks*, EGF Pub, 1987, 461-478.

6. J. Schijve, P. De Rijk, "The fatigue crack propagation in 2024-T3 alclad sheet materials from seven different manufacturers", Nat. Aerospace Lab., NRL, Amsterdam, TR M.2162, 1966.

7. D.A. Virlker, B. M. Hillberry, P.K. Goel, "The statistical nature of fatigue crack propagation", *J. Engng Mat. Tech.*, 1011 (1979) 148-153.

8. C. Laird, "*Fatigue*", in Physical Metallurgy, R.W. Cahn and P. Haasen, Eds, Elsevier, 1986, 2294-2397.

9. D.L. Davidson, J. Lankford, "Fatigue crack growth in metals and alloys: mechanisms and micromechanics", *Int. Mater. Rev.*, 37 (1992) 45-76.

10. W Schutz, P. Heuler, "A review of fatigue life prediction models for the crack initiation and propagation phases", in *Advances in Fatigue Science and Technology*, Kluwer Academic Publishers, 1989, 177-219.

11. L. Lawson, E.Y. Chen, M. Meshii,, "Near threshold fatigue: a review", *Int. J. Fatigue*, 21 (1999) S15-S34.

12. J.W. Porvan, Z. H. Zhai, "A review of fatigue crack initiation", in *Time-Dependent Fracture: Proceedings of the 11th Canadian Fracture Conference*, Martinus Nijhoff Publishers, 1985.

13. M. Goto, Statistical investigations of the behaviour of microcracks in carbon steels", *Fatigue Fract. Engng Mater. Struct.*, 14 (1991) 833-845.

14. M. Goto, Y. Yanagawa, H. Nisitani, "Statistical property in the initiation and propagation of microcracks of a heat-treated 0.45% steel", *JSME Int.* 22 (1990) 235-242.

15. H. Nisitani, M. Goto, "A small crack growth law and its application to the evaluation of fatigue life", in *The Behavior of Short Fatigue Cracks*, K. J. Miller and E.R. de los Rios, eds, EGF Pub, 1987, 461-478.

16. M. Goto, "Statistical investigation of the behavior of small cracks and fatigue life in carbon steels with different ferrite grain sizes", *Fatigue Fract. Engng Mater. Struct.* 17 (1994) 635-649.

17. Q.C. Wang, D. Apelian, D.A. Lados, "Fatigue behavior of A356-T6 aluminum cast alloys. Part I: Effect of casting defects", *J. Light Metals*, 1 (2001) 73-84.

18. Q.C. Wang, D. Apelian, D.A. Lados, "Fatigue behavior of A356-T6 aluminum cast alloys. Part II: Effect of microstructural constituents, *J. Light Metals*, 1 (2001) 85-97.

19. L.E. Willertz, "Ultrasonic fatigue", *Int. Met. Rev.*, 25 (1980) 65-78.

20. H. Mayer, "Fatigue crack growth and threshold measurements at very high frequencies", *Int. Mat. Rev.*, 44 (1999) 1-36.

21. J.K. Tien, "High-Power, Ultrasonic Fatigue Testing Machine", *Rev. Sci. Instrum.*, 46 (1975) 840-846.

22. J.M. Wells, O. Buck, L.D. Roth and J.K. Tien, eds., *Ultrasonic Fatigue, Proceedings*, TMS/AIME, 1982.

23. S. Stanzl-Tschegg, H. Mayer, Eds., *Proceedings of the International Conference on Fatigue in the Very High Cycle Regime, Institute of Meteorology and Physics*, Vienna, 2001.

24. S. Stanzl-Tschegg, "Ultrasonic Fatigue", in *Fatigue '96: Sixth International Fatigue Congress*, Elsevier Science Inc., 1996, 1887-1898.

25. D.D. Krueger, R.D. Kissinger, R.G. Menzies, "Development and introduction of a damage tolerant high temperature nickel-base disk alloy, Rene' 88 DT", in *Superalloys 1992*, S.D. Antolovich *et al.*, eds., TMS-AIME, 1992, 277-286.

26. M.J. Caton, S.K. Jha, A.H. Rosenberger, J.M. Larsen, "Divergence of Mechanisms and its effect on variability in Fatigue life of Rene' 88 DT", *Superalloys 2004*.

27. A. Shyam, Y.N. Picard, J.W. Jones, J.E. Allison, S.M. Yalisove, "Small fatigue crack propagation from micronotches in the cast aluminum alloy W319", *Scripta Mater.*, 50 (2004) 1109-1114.

28. Q. Feng, Y.N. Picard, H. Liu, S.M. Yalisove, G. Mourou, T.M. Pollock, "Femtosecond laser micromachining of single-crystal superalloys", *Superalloys 2004*.

29. B.A. Cowles, "High cycle fatigue in aircraft gas turbines - an industry perspective", *Int. J. Fract.*, 80 (1996) 147-163.

30. E.S. Huron, P.G. Roth, "The influence of inclusions on low cycle fatigue life in a P/M nickel-base disk superalloy", in *Superalloys 1996*, R.D. Kissinger *et al.*, eds., TMS-AIME, 1996, 359-367.

31. J. E. King, "Role of oxides in fatigue crack propagation", *Mater. Sci. Technol.*, 6 (1990) 19-31.

32. J. E. King, "Fatigue crack propagation in nickel-base superalloys - effects of microstructure, load ratio, and temperature", *Mater. Sci. Technol.*, 3 (1987) 750-764.

33. A. Shyam, W.W. Milligan, "Effects of deformation behavior on fatigue fracture surface morphology in a nickel-base superalloy", *Acta Mater.*, 52 (2004) 1503-1513.

34. P.A.S. Reed, W.F. Gale, J.E. King, "Intrinsic threshold in polycrystalline Udimet 720", *Mater. Sci. Technol.*, 9 (1993) 281–287.

35. J.E. King, "Effects of grain size and microstructure on threshold value and near-threshold crack growth in powder-formed Ni-base superalloy" *Met. Sci.* 16 (1982) 345–355.

36. J. Luo, P. Bowen, "Small and long fatigue crack growth behaviour of a PM Ni-based superalloy, Udimet 720", *Int. J. Fatigue*, 26 (2004) 113-124.

37. T.L. Anderson, *Fracture Mechanics – Fundamentals and Applications*, 2nd Edition, CRC Press, 1994, 72-75.

38. Y. Murakami, Ed. in chief, *Stress Intensity Factors Handbook*, Vol. 2, Pergamon, 1987, 712-713.

39. E.S. Huron, "Serrated yielding in a nickel-base superalloy", in *Superalloys 1992*, S.D. Antolovich *et al.*, eds., TMS-AIME, 1992, 675-684.

40. D. Taylor, J.F. Knott, "Fatigue crack propagation behaviour of small cracks; the effect of microstructure", *Fatigue Fract. Eng. Mater. Struct.*, 4 (1981) 147–155.

41. Q. Chen, N. Kawagoishi, K. Othubo, E. Kondo, M. Sakai, T. Kizaki "Ultrasonic fatigue strength in Inconel 718", in *Fifth International Symposium on Superalloys 718, 625, 706 and Various Derivatives*, E.A. Loria, ed., TMS-AIME, 2001, 573-582.

42. G. E. Dieter, *Mechanical Metallurgy*, SI Metric Edition, McGraw-Hill, 1988, 275-324.

43. J.C. Williams, E.A. Starke Jr., "Progress in structural materials for aerospace systems", *Acta Mater.*, 51 (2003) 5775-5799.

Materials Damage Prognosis
Edited by J.M. Larsen, L. Christodoulou, J.R. Calcattera, M.L. Dent, M.M. Derriso, W.J. Hardman, J.W. Jones, and S.M. Russ
TMS (The Minerals, Metals & Materials Society), 2005

CHARACTERIZATION OF THE ROLE OF MICROSTRUCTURE ON THE FATIGUE LIFE OF Ti-6Al-2Sn-4Zr-6Mo USING ULTRASONIC FATIGUE

C. J. Szczepanski[1]; A. Shyam[1]; S. K. Jha[2]; J. M. Larsen[3]; C. J. Torbet[1]; S. J. Johnson[1]; J. W. Jones[1]

[1]University of Michigan, Materials Science and Engineering, Ann Arbor, MI-48109 USA
[2]Universal Technology Corporation, Dayton, Ohio 45432 USA
[3]Air Force Research Laboratory, Materials and Manufacturing Directorate, AFRL/MLLMN, Wright-Patterson AFB, OH-45433 USA

Keywords: Titanium alloys, Ultrasonic Fatigue, Crack Propagation, Small Fatigue Cracks; Gigacycle Fatigue, Fatigue Variability

Abstract

The effect of microstructural variability on the fatigue life of the α + β titanium alloy, Ti-6246, has been examined in the very long life fatigue regime using ultrasonic fatigue. Tests were conducted at ambient temperatures at a frequency of 20 kHz and a load ratio of 0.05. Fatigue lifetimes were characterized in the regime from 10^5 to 10^9 cycles. Microstructural features associated with crack initiation and their locations relative to the specimen surface are examined and compared to the behavior observed in fatigue tests at a conventional frequency of 20 Hz. The growth behavior of small fatigue cracks initiated from femtosecond pulsed laser machining was examined. The worst-case fatigue life in Ti-6246 is modeled from the small crack propagation behavior of the alloy.

Introduction

The U.S. Air Force typically spends approximately two-thirds of its annual jet propulsion budget on the maintenance and sustainment of gas turbine engines. Much of this cost is due to the lifetime retirement cycle in which components are retired based on their original design lifetime. This approach to lifing is often conservatively calculated to allow for uncertainties in usage and behavior. As part of the Engine Structural Integrity Program (ENSIP) [1] the Air Force performs inspections for damage and cracking at the half-life of fracture-critical turbine engine components. This methodology employs nondestructive evaluation (NDE) techniques such as eddy current measurements and ultrasonic techniques for certifying the condition of components before returning them to service. Beyond the ENSIP approach, technology is being developed to facilitate the management of turbine engines based on the philosophy of materials damage prognosis [2,3], which utilizes a combination of advanced, physically based, life methods and techniques for real-time determination of material damage states. The eventual goal of the prognosis project is to develop a predictive methodology where decisions to fly, based on the condition of the gas turbine components, can be made by deployed asset commanders.

The present study fits into the overall goal of the prognosis approach because of the need to couple understanding of fatigue scatter with a fundamental knowledge of the effects of microstructure on fatigue behavior. Understanding the statistical nature of fatigue and its fundamental relationship to microstructure will allow for the development of accurate predictions of fatigue lives. The objectives of this study are to understand the fatigue behavior of Ti-6Al-2Sn-4Zr-6Mo (in wt%) at ultrasonic and conventional frequencies in order to develop a methodology for predicting fatigue behavior at low stresses and long lifetimes and to determine the role of microstructural variability on fatigue lifetimes.

The excellent mechanical properties of α + β titanium alloys have led to their widespread use in gas turbine engines. Because of this, there have been many research efforts devoted to characterizing the fatigue properties as a function of the microstructure for this class of alloys. Work by Jago *et al.*[4] has found that the primary α grain size and total volume fraction α phase (grains and lathes) were the most important microstructural parameters in determining fatigue crack initiation and growth behavior. In other work [5], the fatigue resistance was found to be dependent on the lamellar α volume fraction.

Recent research has found a bimodal distribution of fatigue lifetimes in Ti-6246[6]. This was found to be a result of two distinct crack initiation mechanisms [7]. Ongoing research efforts aim to understand these mechanisms of crack initiation. Much research has been devoted to understanding the mechanical properties of Ti-6246, but these studies have not tied the microstructure of the material to the mechanical properties at a fundamental level. The goal of this research is to couple microstructural features with the fatigue lifetimes so that models may predict fatigue lives as a function of microstructure. In order to fully understand the fatigue behavior of a material, it is necessary to test at a range of stresses. Generally, it is impractical to run fatigue tests past 10^7 cycles at conventional frequencies. Thus, we have employed ultrasonic fatigue instrumentation operating at frequencies of approximately 20 kHz. Ultrasonic fatigue testing has been used to characterize the fatigue behavior of materials for decades [8,9], but recent advances in testing equipment have increased the reliability of this technique as a valid means for characterizing materials in the low stress-long lifetime regime.

Material and Experimental Procedure

Material

The material used in this study was cut from a forged and heat treated pancake. It has a duplex microstructure with equiaxed α (hcp) grains in a transformed β (bcc) matrix. The microstructure of this material was observed with optical and scanning electron microscopy (SEM) (Philips XL30/FEG.) An optical micrograph of the microstructure is shown in Figure 1. The primary α grains appear light, while the transformed β phase is dark with light interspersed α lathes.

Specimen Design

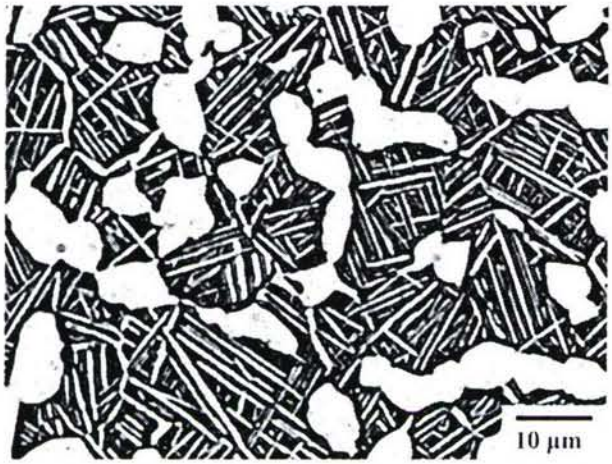

Figure 2. An optical micrograph of the material tested in this study indicating a microstructure of globular primary α grains in a transformed β matrix.

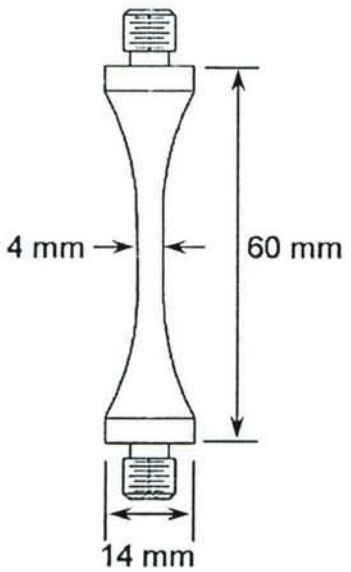

Figure 1. A schematic of the fatigue specimens used in ultrasonic frequency fatigue testing.

Ultrasonic fatigue specimens were designed using the Runge-Kutta method to insure that they would be in resonance near 20 kHz. Details of this method can be found elsewhere [10]. Figure 2 is a schematic of the specimen with the major dimensions labeled. The gage section of the specimen is of the size typically used in servo-hydraulic fatigue experiments. The specimens are large enough to insure that a statistically significant volume of material is sampled in each test. Specimens were machined using low stress grinding and were subsequently electropolished to remove compressive residual stresses. The polishing was completed using the following solution: 59% methanol, 35% ethylene glycol monobutyl ether, 6% (60%) perchloric acid. This solution was kept at -40°C while the voltage was maintained at 40V for effective polishing. With these conditions, approximately 150 μm was removed from the specimen surface reducing the diameter by 300μm.

Fatigue Testing

The fatigue testing completed at the University of Michigan (UM) employed an ultrasonic frequency of 20 kHz. The tests completed at the Air Force Research Laboratory (AFRL) were performed at a frequency of 20 Hz in load-control on conventional servo-hydraulic equipment [11]. All tests were conducted at room temperature with a load ratio 0.05. A schematic of the ultrasonic testing setup is shown in Figure 3. Ultrasonic fatigue tests are run in displacement control, which uses a Hall-effect sensor to measure the high frequency displacement of the load train. Using this feedback, the command signal adjusts the amplitude of the input pulse to achieve the necessary displacements. The system is designed such that the specimen ends are displacement maxima while the center of the gage section is a displacement node. The center of the specimen is therefore, a strain anti-node. Strain gages affixed to the gage section of the specimen allow the measurement of resultant strain in the specimen. The stress amplitude is calculated using the strain measurements and the modulus of the material. By adjusting the amplitude of the input pulse, we control the strain in the specimen and thus the stress. The top λ-rod shown in Figure 3 is a wavelength long at 20 kHz. It is used both to isolate the specimen from the transducers and allow for ease in setup of the experiment. The lower half λ-rod is used for the application of mean stress at a displacement node so that there will be no damping of the acoustic pulse.

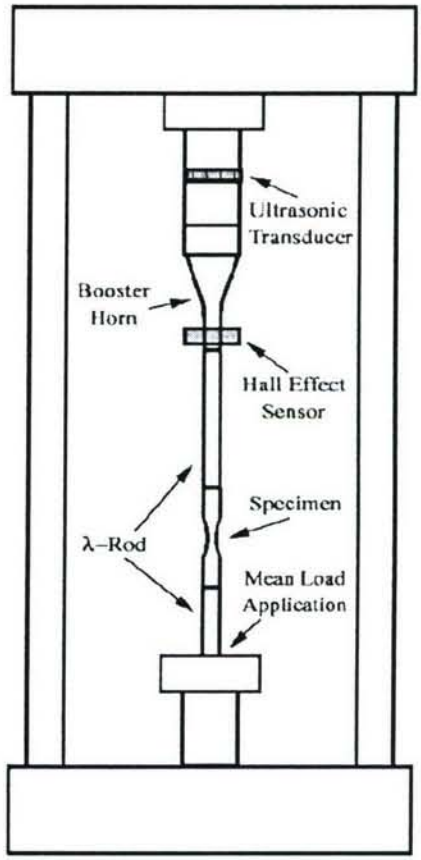

Figure 3. A schematic of the experimental setup is shown with the ultrasonic frequency components depicted as they are loaded in an MTS load frame for mean stress testing.

Crack Growth

In addition to the fatigue testing described above, some specimens were reserved for studying crack growth rates. The growth rates were measured from cracks that initiated from laser machined surface notches. Defects are often introduced as radii or notches to examine crack growth rates in materials. However, the process of introducing defects into these specimens often has deleterious effects on the microstructure surrounding the notch. This can be avoided using femtosecond pulsed lasers because the pulse time is shorter than the time required for heat to diffuse into the material.

Additionally, the intensity of the pulse ablates material directly from a solid to plasma. Consequently, we have been able to produce specimens in which there is minimal damage and which are free of debris on the surface surrounding the notch. Figure 4

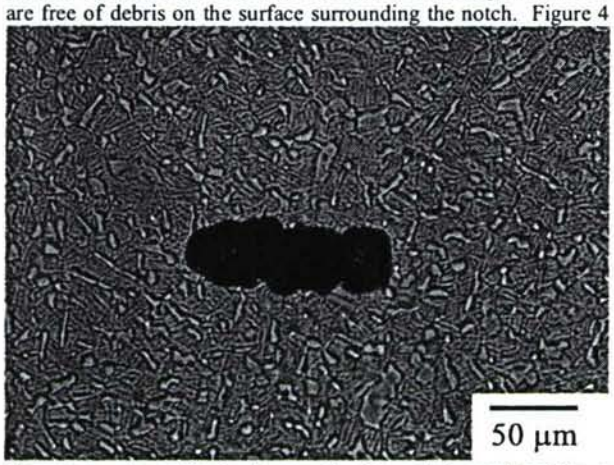

Figure 4. An optical micrograph of a notch produced by a femtosecond pulsed laser in Ti-6246.

shows a notch that has been machined on the flat of a specimen. Due to the absence of a damage zone around the notch, we have the ability to study the crack growth rates of materials in the small-crack regime at near-threshold crack growth rates.

This technique has been used to study other materials, as well [12]. The specimen design shown in Figure 2 was modified for use in this part of the study. Flats of approximately 2 mm width were machined in the gage section of the specimens with a 50 cm radius grinding wheel. They were machined on radially opposing sides of the specimen to maintain symmetry and to insure that the specimens would resonate without bending at 20 kHz. The flats were important in focusing the laser on the specimen surface during the machining process. During testing, images of the crack were taken using a Questar telescope and a PC running the IMAQ Vision Builder® software from National Instruments. This setup allowed for observation of crack growth in real time. The flats on the specimen provided a constant plane of focus for the optical measurement of crack lengths during testing. Measurements of the crack length were then taken approximately every 1000 cycles following initiation. The crack growth rates measured from these images are shown in Figure 9. These data are plotted using the Newman-Raju [13] solution for stress intensity assuming a semicircular surface crack.

Results and Discussion

Microstructural Characterization

As the demand for accuracy of fatigue lifetime predictions continues to increase, new methods for automating the task of microstructural characterization are being developed [14,15]. For this reason, the IMAQ Vision Builder® (by National Instruments) software was used for this task, with the goal that a script could be written to automate the process and remove user subjectivity from the quantitative measurement of the microstructure. Measurements of the average grain size were collected along with a distribution of the grain sizes. The primary α grain size was measured to be 3.7 μm with a volume fraction of 27%. The grain size was measured using the line intercept method, and the volume fraction was found with the point count method. The histogram of the grain size distribution is shown in Figure 5a. The largest grains are approximately 20 μm in diameter. Fatigue cracks were observed to initiate from these large alpha grains.

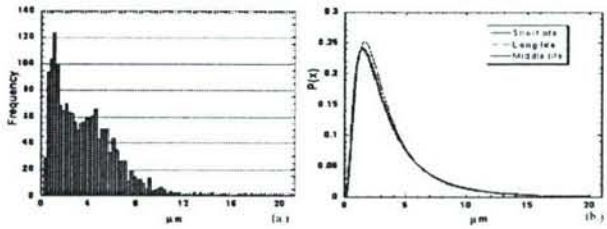

Figure 5. Grain size distribution in Ti-6246 **(a)** histogram, **(b)** lognormal probability density function.

Although, the probability of finding grains this size is low, the larger grains and grain clusters tend to be the crack initiating features so it is, therefore, important to characterize their distribution. Lognormal statistics were used to plot the probability density function for the distribution of grain sizes as shown in Figure 5b. It can be seen that the distribution of α grains was reasonably approximated by a lognormal distribution.

In Figure 5b, the three curves labeled short, middle, and long lives represent the data acquired from three different specimens, ranging in lifetimes over approximately two orders of magnitude. The specimens were all tested at 700 MPa, but the short-life specimen failed after approximately 2 x 10^5 cycles, while the longest-life specimen lasted for almost 2 x 10^7 cycles. These specimens were examined to verify that the scatter in lifetimes was not a result of statistically significant variations in microstructure. It was found that the average grain size and the grain size distribution were essentially the same for the short, middle, and long-life specimens.

Fatigue Testing

Figure 6 shows the combined stress-life (S-N) curve for conventional and ultrasonic fatigue tests. Data at 820 MPa and above were acquired using conventional testing (20 Hz). Data at 700 MPa and below were obtained using ultrasonic testing (20 kHz). The S-N behavior from both techniques was found to be consistent in terms of crack initiation sites and scatter in fatigue lifetimes. The percentage of failures that had subsurface initiation sites were seen to increase as the stress level decreased. This was found in both conventional and ultrasonic frequency testing. It was also found that the amount of scatter in lifetimes was consistent in conventional and ultrasonic frequency. The bimodal

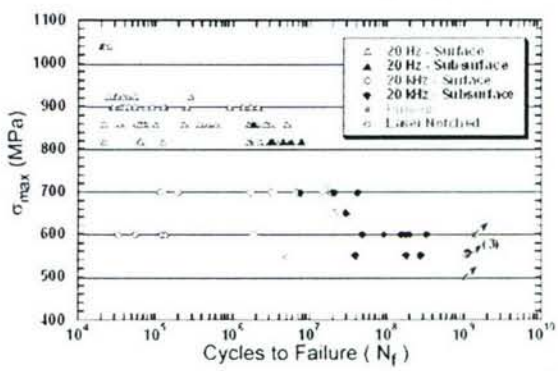

Figure 6. Fatigue lifetime as a function of maximum stress for conventional and ultrasonic fatigue testing

distribution, which has been described in the literature [6] for conventional frequencies is also observed here in tests at

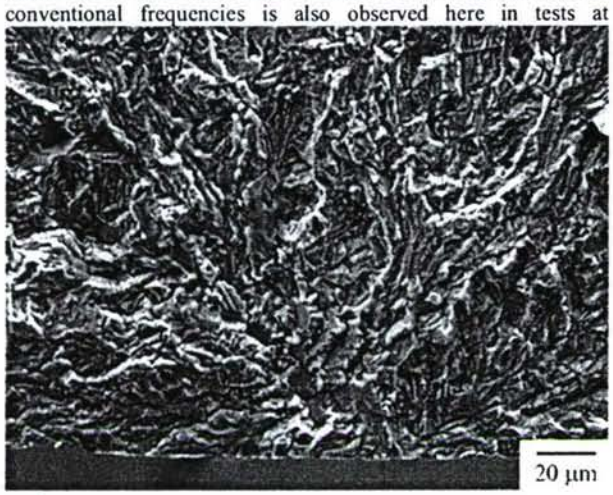

a.

b.

Figure 7. SEM fractographs of the crack initiation site at a cluster of α grains.

ultrasonic frequency. The four short-life data points at 600 MPa were from specimens that have been laser notched where notches were considerably larger than the largest α grain diameter.

Fractography

It was found that crack initiation sites were predominantly at α grains. Fatigue failures observed in these tests initiated at one of two distinct features. Cracks initiated from either large α grains or from clusters of average-sized α grains which are, presumably, oriented favorably for slip. In both cases, the effective size of the initiation site was on the order of 15-20 μm in diameter. Clusters of α grains as an initiation site were found in both subsurface and surface crack initiation. The case of the large α grains being responsible for initiation was only observed in some subsurface failures. Figure 7a displays a fracture surface of a specimen in which initiation occurred at a cluster of α grains. Figure 7b is a higher magnification image of this fracture surface. Figure 8 illustrates a failure in which the crack initiated at a large α grain of approximately 15-20 μm. No correlation between the initiation sites and lifetimes could be drawn from fractographic analysis.

Crack Propagation

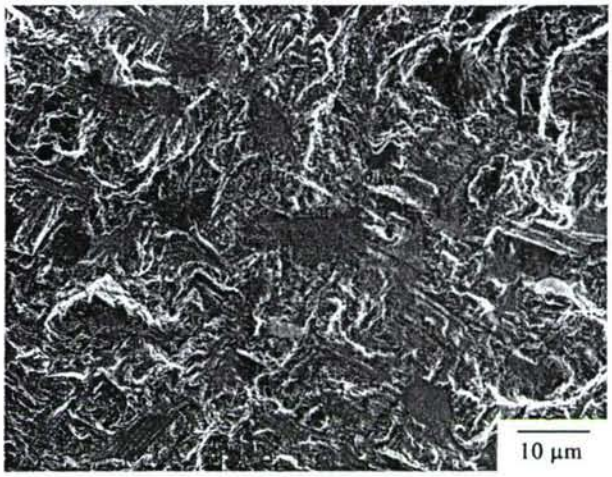

Figure 8. Scanning electron fractograph illustrating a crack initiating from a large α grain.

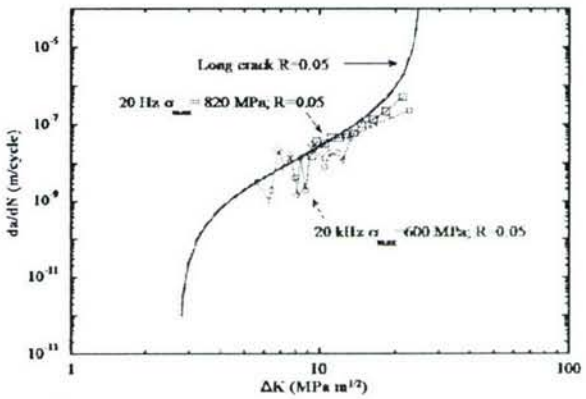

Figure 9. Crack growth rates in ultrasonic and conventional frequency testing.

The fatigue crack propagation rates shown in Figure 9 for ultrasonic frequencies were measured for cracks initiating from notches such as the one shown in Figure 4. The length of these notches is approximately 110 μm (~30 times the average grain size) so these data may not show small-crack effects. Initiation of cracks typically occurred between 10^4 and 10^5 cycles. The crack growth rates shown at 20 kHz are in good agreement with crack propagation rates at conventional frequency. It appears that there may be a slight effect of frequency on the propagation rates, but further study is needed to confirm this. A dependence on frequency might be expected as crack growth is known to be sensitive to strain rates and its influence on the development of plasticity at the crack tip.

Failure Prediction

Figure 10 shows the S-N data that have been obtained at ultrasonic frequencies in Ti-6246. Also shown in the plot is a band which predicts fatigue lifetime for different initial crack sizes. This band is bounded by two lines, which are calculated

using the crack propagation rates observed at ultrasonic frequencies. The predictions were made by integrating these crack growth rates over the number of cycles to failure. These predictions are based on an extrapolation of the Paris-region crack

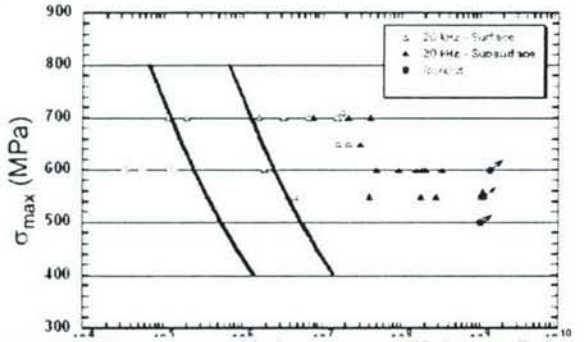

Figure 10. The SN curve with the worst-case lifetime predictions overlaid on the plot.

growth rates, and have not otherwise been corrected for possible small fatigue crack effects. The short-lifetime line is calculated assuming that a crack will initiate in the first cycle from a grain with a diameter of 25 μm. This value was selected since it agrees with the largest experimentally observed crack initiation sites. The longer-lifetime line represents the lifetime one would expect from specimens where a fatigue crack initiates from a 5 μm grain in the first cycle of loading. This corresponds to the size of the smallest initiation site that was seen in this study. The fatigue lifetimes observed here indicate that, as expected, most cracks do not initiate in the first cycle of loading, although the worst-case cracks clearly initiate very early.

The open circles to the left of the predictions represent the lifetimes of the specimens that had been laser notched for crack growth studies. The notches machined in this study are larger (~110 μm) than the sizes of defects typically found in crack initiation. As the sizes of the notches are reduced to converge with the typical defect size (~15-25 μm), we would expect to see the data move to longer lifetimes and be in line with the predictions from the crack growth model.

Conclusions

The fatigue behavior observed at ultrasonic frequencies is consistent with that seen at conventional frequencies for Ti-6246 in terms of fatigue lifetimes and fatigue crack growth rates. Two categories of failure initiation features are observed in this alloy: clusters of α grains and large isolated single grains. The crack initiation occurred at a feature that was approximately 15-25 μm in diameter for all cases. The measured crack growth rates were used to make predictions of the worst-case lifetimes in Ti-6246. These predictions are consistent with experimentally observed worst-case lifetimes. From this study it appears that ultrasonic fatigue methods can be used to obtain critical information on the role of microstructure in the very long life regime.

Acknowledgements

This work was supported by the Air Force Office of Scientific Research (F49620-03-1-0069) with Dr. Craig Hartley, Program Manager.

References

[1] U.S. Air Force, Engine Structural Integrity Program, Military Standard 1783B, Aeronautical Systems Center, Wright-Patterson Air Force Base, OH, 31 May 2002, <http://www.dscr.dla.mil/fscap2/Policy/MilHDBK1783B.pdf>

[2] L. Christodoulou and J. M. Larsen, "Using Materials Prognosis to Maximize the Utilization Potential of Complex Mechanical Systems," *JOM*, March 2004, 15-19.

[3] L. Christodoulou and J. M. Larsen, "Materials Damage Prognosis: A Revolution in Asset Management," in this proceedings, TMS, 2005.

[4] G. Jago, J. Bechet, C. Bathias. "Microstructures/property relationships in Ti-6.2.4.6 alloy: A microstructural approach to the fatigue damage," *Titanium '95: Science and Technology*. **Vol. II**, (1996) 1203-1210.

[5] G. Jago, J. Bechet. "Influence of microstructure of (α+β) Ti-6.2.4.6 alloy on high cycle fatigue and tensile test behavior," *Fatigue Fract. Engr. Mater. Struct.* **22**, (1999) 647-655.

[6] S. K. Jha, J. M. Larsen, A. H. Rosenberger, G. A. Hartman. "Dual fatigue failure modes in Ti-6Al-2Sn-4Zr-6Mo and consequences on probabilistic life prediction," *Scripta Materialia.* **(48)**, (2003) 1637-1642.

[7] S. K. Jha, J. M. Larsen, A. H. Rosenberger, G. A. Hartman. "Variability in fatigue life of Ti-6Al-2Sn-4Zr-6Mo," *Materials Science and Engineering A. Accepted May 2003.*

[8] H. Mayer. "Fatigue crack growth and threshold measurements at very high frequencies," *International Materials Reviews*. **44**, Number 1, (1999) 1-34.

[9] L. Willertz. "Ultrasonic fatigue," *International Metals Reviews*. No. 2, (1980) 65-78.

[10] A. Shyam, C. J. Torbet, S.K. Jha, J.M. Larsen, M.J. Caton, C.J. Szczepanski, T.M. Pollock, J.W. Jones. "Development of Ultrasonic Fatigue for Rapid, High Temperature Fatigue Studies in Turbine Engine Materials," *Superalloys 2004*. (2004) 259-268.

[11] S. K. Jha, J. M. Larsen, C.G. Annis, A. H. Rosenberger, "Prediction of the Worst-Case Fatigue Failures of an α + β Titanium Alloy," in this proceedings.

[12] A. Shyam, Y. N. Picard, J. W. Jones, J. E. Allison, S. M. Yalisove. "Small fatigue crack propagation from micronotches in the cast aluminum alloy W319," *Scripta Materialia.* **50** (2004) 1109-1114.

[13] J.C. Newman Jr., I.S. Raju. "An empirical stress-intensity factor equation for the surface crack," *Engr Fract. Mech.* **15** (1981) 185-192.

[14] J. Chraponski, W. Szkliniarz. "Quantitative metallography of two-phase titanium alloys," *Materials Characterization.* **46** (2001) 149-154.

[15] J. Tiley, T. Searles, E. Lee, S. Kar, R. Banerjee, J. C. Russ and H. L. Fraser. "Quantification of microstructural features in α/β titanium alloys," *Materials Science and Engineering A* **372** (2004) 191-198.

Proceedings
9th International Fatigue Conference
May 2006

FATIGUE CRACK INITIATION IN AN α + β TITANIUM ALLOY

C.J. Szczepanski*[1], S.K. Jha[2], J.M. Larsen[3], J.W. Jones[1]

[1] Department of Materials Science and Engineering, University of Michigan, Ann Arbor, MI 48109, USA
[2]Universal Technology Corporation, Dayton, OH 45433, USA
[3]Air Force Research Laboratory, AFRL/MLLMN, Wright-Patterson Air Force Base, Dayton, OH 45433, USA

ABSTRACT

Ultrasonic fatigue has been employed to examine the fatigue behavior of Ti-6Al-2Sn-4Zr-6Mo in the range of 10^6 to 10^9 cycles. Fatigue tests have been conducted at stresses, σ/σ_Y, ranging from ~0.45-0.62 for two different heats of material. The variability in fatigue lifetimes was 2.5-3 orders of magnitude at all stress levels. Facets, which correspond in size to large primary α grains, were found at the sites of crack initiation. Observation of the crack initiation sites did not reveal morphological features that could be correlated with variability in lifetime. Surface and subsurface crack initiation sites were found to exhibit similar lifetimes. In general, the amount of faceted failure in the region of crack initiation was greater than that observed as the crack propagated. The topography of the fracture surface was quantified and shows that most of the facets are oriented nearly normal to the stress axis.

KEYWORDS

Ultrasonic fatigue, crack initiation, titanium alloys, faceted failure

INTRODUCTION

Engineering components used in various applications including automotive and gas turbine engines typically accumulate 10^6 to 10^9 cycles in their intended lifetime [1-3]. To make accurate lifetime predictions in the regime of very high cycle fatigue (VHCF), it is necessary to understand the fatigue behavior in this range of stresses and lifetimes. The technique of ultrasonic fatigue affords the opportunity to acquire fatigue lifetime data in the VHCF regime in reasonable times. This technique was developed in the 1950's, but recent advances in the control instrumentation allows for specimens to be tested under conditions similar to those used at conventional frequencies [4,5]. These techniques have been employed recently in studies on a number of commercially important alloy systems [6-9].

In a number of structural alloys [8,10], processing-related defects lead to the premature failure of components and thus obscure the fatigue lifetime variability that is related to microstructural heterogeneity such as grain size distribution, crystallographic texture, and clustering of constituent phases. However, current titanium alloy processing technology can produce relatively clean materials with a very low defect number density[11]. In these alloys, the opportunity exists to observe the role of microstructural heterogeneity in damage accumulation that may be associated with variability in fatigue crack initiation and growth.

Fatigue crack initiation is generally assumed to account for the majority of fatigue lifetime in applications where imposed stresses are low relative to the yield stress[12]. Thus, to predict the lifetimes of components in the gigacycle regime, it is important to develop a full understanding of the process of fatigue crack initiation. Hall [11] has reviewed the fatigue crack initiation behavior of $\alpha + \beta$ titanium alloys, where he defines crack-like discontinuities as the feature of a size where it can be assumed that a fatigue crack has initiated and can be described by models for short crack growth. Generally, slip in α_p grains was found to be integral to the formation of a crack-like discontinuity (CLD). In some cases, the slip bands in α_p caused decohesion of the α_p grain from the β matrix. This was intensified in cases where a number of α_p grains were in close proximity. RaviChandran and Jha [13] recently found for a β-Ti alloy, Ti-10V-2Fe-3Al, that the clustering of α_p grains was the critical parameter in crack initiation and thus total fatigue life. Evans [14] considers fatigue crack initiation in $\alpha + \beta$ titanium alloys an issue of stress redistribution in the matrix due to the interaction of $\alpha + \beta$ grains based on their orientation relative to the stress axis. These results suggest that crack initiation in two-phase alloys may not be dependent solely on the largest defect or unfavorably oriented grain. Our recent study of Ti-6246 [6] indicates that crack initiation occurs across individual primary α grains or in neighborhoods of primary α grains. These grains are found relatively frequently in the microstructure and consequently their size alone does not distinguish them as crack initiating features. In fatigue studies at higher stresses for Ti-6246, [15-19], it was also found that facets on the fracture surface resulted from failure of the α_p phase. It has also been observed [18], that crack initiation occurred at α-β interfaces due to dislocation pile-up at these interfaces.

While bulk or average microstructural properties can be used to predict average fatigue behavior [20], it is likely that the large variability in fatigue behavior observed in alloys where fatigue life is controlled by crack initiation, may depend strongly on the variability of so-called microstructural neighborhoods. The nature of microstructural heterogeneity that ultimately determines fatigue behavior may depend on a number of microstructural features, ranging from crystallographic orientation and the size of individual grains to the characteristics of clusters of grains [13,21], and numerous microstructural characterization techniques have been used to relate microstructure to fatigue lifetime variability [22-24]. However, for the case of very long fatigue lifetimes ($>10^8$ cycles) only limited studies of microstructural variability and fatigue have been studied. It is the objective of the current work to examine the influence of microstructural variability and very high cycle fatigue behavior for the $\alpha + \beta$ alloy Ti-6246.

EXPERIMENTAL PROCEDURE

Fatigue studies were completed on two heats of $\alpha + \beta$ processed Ti-6Al-2Sn-4Zr-6Mo (wt.%) at ultrasonic (20 kHz) and conventional frequencies (20 Hz). Cylindrical specimens with a gage length and diameter of 12.5mm and 4mm, respectively, were used. As shown in Figure 1, the bi-modal microstructure of the two heats is nominally the same; both materials have an equiaxed primary α phase in a transformed β matrix. One set of fatigue specimens came from a forged and heat treated pancake while another set was taken from a retired disk. The grain size of the α_p phase was measured using the line-intercept method and the volume fraction was measured using the point count method. These measurements are summarized in Table 1 for both materials. Grain size follows a log-normal distribution. While the average α_p grain size for each material is less than 5 μm, some grains are on the order of 20 μm in diameter.

Conventional load-controlled fatigue tests were performed on servo-hydraulic fatigue machines at the Air Force Research Laboratory (AFRL) while ultrasonic fatigue studies were conducted at the University of Michigan. Details of the ultrasonic fatigue technique can be found elsewhere [6-9]. All tests were run at a stress ratio R=0.05 in ambient laboratory air.

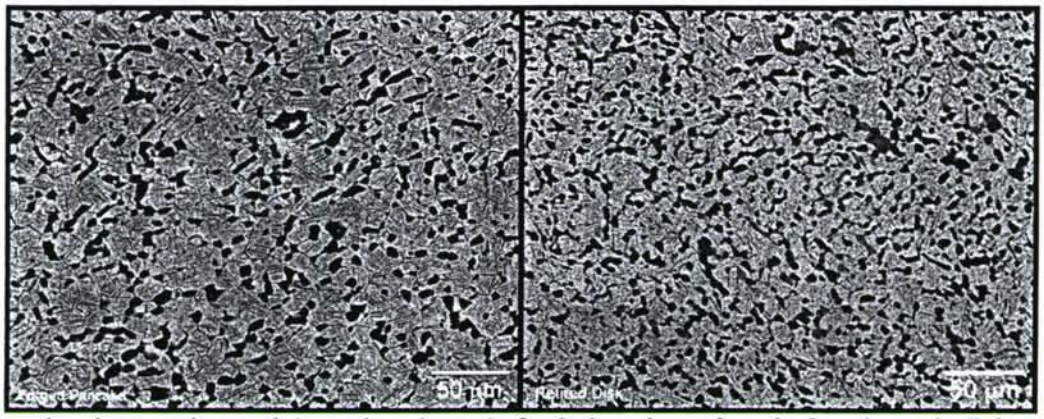

Figure 1. Scanning electron micrograph (secondary electron) of etched specimens from the forged pancake (left) and the retired disk material (right) are shown. The α_p phase appears dark while the transformed β phase is lighter.

TABLE 1
Microstructural characterization

Material	Average α_p grain size	V_f α_p
Forged Pancake	3.7 μm ± 2.6 μm	27% ± 2.9%
Retired Disk	4.6 μm ± 2.4 μm	38.6% ± 4.6%

Fractography

Scanning electron microscopy (SEM) was used to observe the fracture surfaces of failed specimens. Individual images were used to create montages with the necessary resolution and field of view to analyze the fracture surfaces of selected specimens. Facets were generally observed on the fracture surfaces with greater numbers in the initiation and early crack growth region. To quantify the degree of faceting, area fraction measurements were made for concentric annuli centered at the crack initiation site. The location of the crack initiation site was determined by following the macroscopic markings on the fracture surface. The topography of the fracture surface and, particularly, the orientation of the facets relative to the tensile axis, were determined by analysis of stereo pairs of fractographs, using the MeX software package.

Orientation Imaging Microscopy (OIM)

Metallographic specimens were prepared for orientation imaging microscopy (OIM) by mechanical polishing and subsequent electropolishing. The OIM was performed in a Cambridge S360FE scanning electron microscope. Orientation data was gathered using a TSL™ OIM system. A working distance and sample tilt of 25 mm and 70°, respectively, were used. The accelerating voltage was 20 kV and the probe current was 10 nA. A step size of 0.1 μm was employed. The sample was moved in automated stage control to cover a large area in a single scan.

RESULTS AND DISCUSSION

Fatigue Lifetime Data

The results of conventional and ultrasonic fatigue tests for both materials are shown in Figure 2(a). Data shown for σ_{max}=820 MPa and above was collected at conventional frequencies. Specimens tested at 20 kHz

were tested at stresses of 700 MPa and below. Open symbols represent surface failures, while solid symbols indicate subsurface crack initiation. Circles are used to indicate runouts, where testing was stopped after 10^9 cycles. Runouts were only observed at ultrasonic frequencies. Lifetimes fell into the same general trend for specimens tested at ultrasonic and conventional frequencies. Subsurface crack initiation was more frequent at lower stresses (longer lifetimes) for both test methods.

The results of tests at ultrasonic frequencies are detailed in Figure 2(b). There is greater scatter in the lifetimes of the forged pancake specimens compared to the retired disk specimens, the minimum lifetime of specimens from the retired disk is slightly greater than for the forged pancake, and there is overlap in the lifetime to failure for cracks that were initiated from surface and subsurface sites. The decreased scatter in fatigue lifetime of the disk material may result from a more homogeneous distribution of crack initiating features[25].

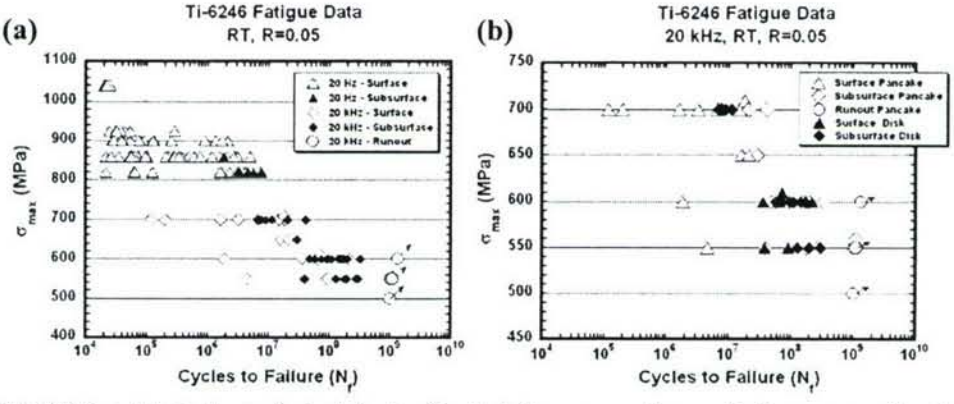

Figure 2. (a) The lifetime data is shown for both heats of material to compare the results from conventional and ultrasonic frequencies. **(b)** Ultrasonic frequency fatigue data for both forged pancake and retired disk specimens.

Fractography

Crack Initiation Site Analysis

Most fracture surfaces of specimens exhibited varying degrees of faceted failure at or near the site of crack initiation. Figure 3(a) and (b) are examples of the facets observed near the crack initiation site for surface and subsurface crack initiation sites, respectively. The projected size of these facets was on the order of the size of the larger α_p grains and are likely to be the result of a cleavage process in the α_p grains. Initial analyses determined that neither difference in the size of the facets, defined as projected maximum diameter, nor their location relative to the specimen surface of facets near the presumed initiation sites correlated with fatigue lifetimes.

The crack initiation sites appeared to be the result of cleavage of clusters of α_p grains. To quantify the amount of faceting observed on the fracture surfaces, measurements of area fraction were made as a function of crack size. These values for area fraction can be compared based on the calculated stress intensity values for cracks of various sizes. Figure 4 is an example of the image of a typical fracture surface that has been prepared for this analysis. The facets have been highlighted with black, while the concentric white circles are centered at the presumed crack initiation site. Using the Newman Raju stress intensity solutions [26] for surface crack initiation and Murakami [27] for subsurface penny-shaped cracks, crack sizes for integer values of K_{max} ranging from 2 to 7 MPa $m^{1/2}$ were calculated. The circles were drawn on the fractograph to correspond to these values. This analysis was completed for a number of specimens that failed from both surface and subsurface crack initiation sites. All specimens either failed at stresses of 600 or 700 MPa and the lifetimes to failure ranged from 10^6 to 10^8 cycles. Table 2 lists the lifetimes and stresses for the specimens from which area fraction of the facets were measured for reference. The

specimens selected for this analysis were chosen to ensure that a representative range of fatigue lifetimes and stresses was sampled.

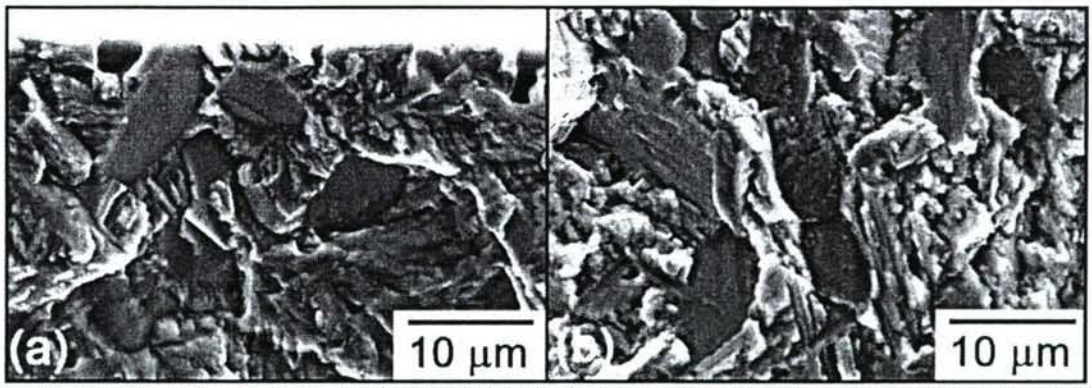

Figure 3. Facets are observed near the crack initiation site for a **(a)** surface initiation and **(b)** subsurface initiation.

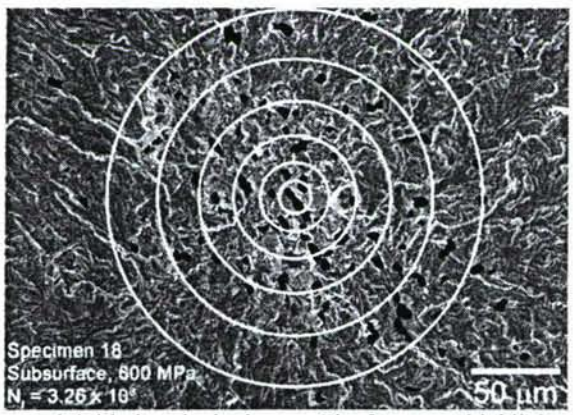

Figure 4. A subsurface crack initiation site is shown. The facets are highlighted with black, while the concentric white circles correspond to integer stress intensity values ranging from 2 to 7 MPa $m^{1/2}$.

The facets correspond to primary α grains and thus it was desirable to characterize the distribution of alpha grains with the same method used to characterize facets. Figure 5(a) displays the results from the facet analysis on the fracture surface while Figure 5(b) shows the results from the analysis of the metallographic surface. As shown in Figure 5(a), the area fraction of facets decreases as the crack propagates for subsurface failures from the pancake specimen. The dashed horizontal line marks the area fraction of α_p measured from a metallographic specimen (Figure 1) and the lines labeled max and min correspond to the maximum and minimum values for area fraction of α_p as shown in Figure 5(b). The same trends were observed for surface crack initiation and for specimens from the retired disk, i.e. the area covered by faceted failure will decrease as the crack propagates.

Figure 5(a) illustrates that the amount of faceted fracture is independent of lifetime to failure. The area fraction of α_p in the bulk microstructure, as shown in Table 1, is approximately 30%. However, when smaller sample sizes are used, local deviations from the mean can be substantial as illustrated in Figure 5(b). These values were acquired by randomly sampling the forged pancake micrograph shown in Figure 1 and measuring the area fraction of the α_p phase. The area fraction of facets on the fracture surface would exhibit values consistently closer to the maximum if clustering of α_p were the most important factor in crack initiation. As the data in Figure 5(a) illustrates, the area fraction of facets will vary significantly from one sample to the next. This suggests that other features, such as crystallographic orientation, of α_p grains have more of an effect in determining the site of crack initiation than the amount of clustering.

TABLE 2
Fatigue results

Specimen Number	14	9	10	18

Cycles to Failure	4.12×10^7	4.7×10^7	8.99×10^7	3.26×10^8
Stress (MPa)	700	600	600	600

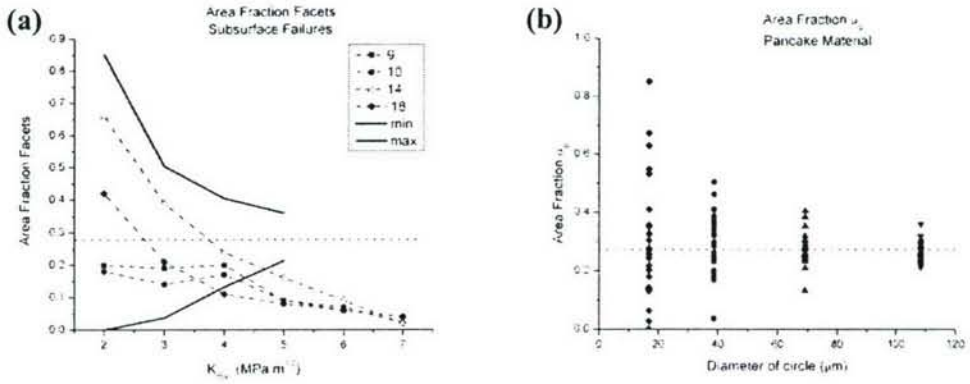

Figure 5. (a) Area fraction measurements for the facets observed in specimens with a subsurface crack initiation site. **(b)** The area fraction of α_p observed in the metallographic specimen from the pancake.

Facet Orientation

The results from the analysis of the fracture surface using stereo pairs to create 3 dimensional reconstructions of the fracture surface indicate that for eight of the ten facets measured in this analysis, the facet normal was oriented less than 15° with respect to the tensile axis. Measurements of the facets were made in two orthogonal directions. Using the values from these profiles and geometric relationships, it is possible to calculate the angle between the facets and the stress axis. The data for the orientation of the facet normals with respect to the tensile axis are shown in Table 3. The facets analyzed in this investigation are highlighted in the fractograph shown in Figure 6. The facets are labeled from top left to bottom right across the fracture surface. The circles superimposed on the fracture surface are the boundaries for integer stress intensity values ranging from 2 though 7 MPa $m^{1/2}$. With the exception of facets 7 and 8, which are indicated with arrows, the facets are not oriented at the angle of critically resolved shear stress. This indicates that the mechanism of crack initiation is not due to shearing that would be predicted by the Schmid factor. Facets 7 and 8 appear to be far enough from the crack initiation site that they did not influence the crack to initiate at that point in the microstructure.

TABLE 3
Facet angles with respect to stress axis

Facet	1	2	3	4	5	6	7	8	9	10
Angle	7.53	14.37	13.23	14.32	8.04	9.42	46.01	39.12	0	10.17

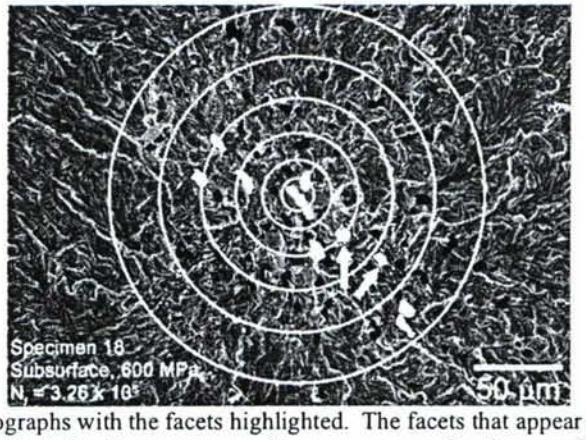

Figure 6. A montage of SEM fractographs with the facets highlighted. The facets that appear light were measured with the three dimensional reconstruction, while the darker facets were used to measure area fraction as a function of crack size. The arrows mark the facets that are oriented nearly 45° to the stress axis.

Crystallographic Orientation

As noted previously, the size and orientation of the crack initiating α_p grain (or grains) by themselves do not seem to control the variability in lifetime. This indicates the important role of the crack initiation neighborhood in addition to the faceted α grain(s) in causing failure initiation and fatigue variability. It is thought that the deformation heterogeneity as caused by local microstructural deviations from the mean characteristics (especially, local crystallographic orientations) may drive the crack initiation and the fatigue variability behavior of this material. The crack initiation region was sectioned using focused ion beam (FIB) machining to reveal the underlying microstructure and enable OIM measurements [28]. Initial results indicated that the crack initiating α_p grain had close to basal orientation with respect to the loading axis, and the surrounding region was oriented for prism <a> type deformation. Orientation imaging microscopy was completed to analyze the differences in texture between the forged pancake and the retired disk that would explain the different scales of fatigue variability in the two cases. The pole figures corresponding to (0001), (10-10), and (11-20) directions are compared in Figure 7 (a) and (b) for the pancake and the disk material respectively. Clearly, these materials have different textures. Additionally, the (0001) pole figures indicate an increased number of basal poles close to the loading axis in the disk material. The difference in the spatial distribution of basal α between the two microstructures is illustrated in Figure 8(a) and (b) where, the close to basal grains have been highlighted. At this point, it is not clear how this difference in the texture correlates with the fatigue variability behavior of the two materials. However, it can be speculated that the increased occurrence of close to basal α_p in the disk sample may increase the possibility of a more even distribution of critical regions for crack initiation therefore, decreasing the scale of variability. Nevertheless, studying the role of texture in affecting the distribution of critical neighborhoods in a sample will be important for a complete understanding of the differences in the fatigue variability behavior of the two microstructures.

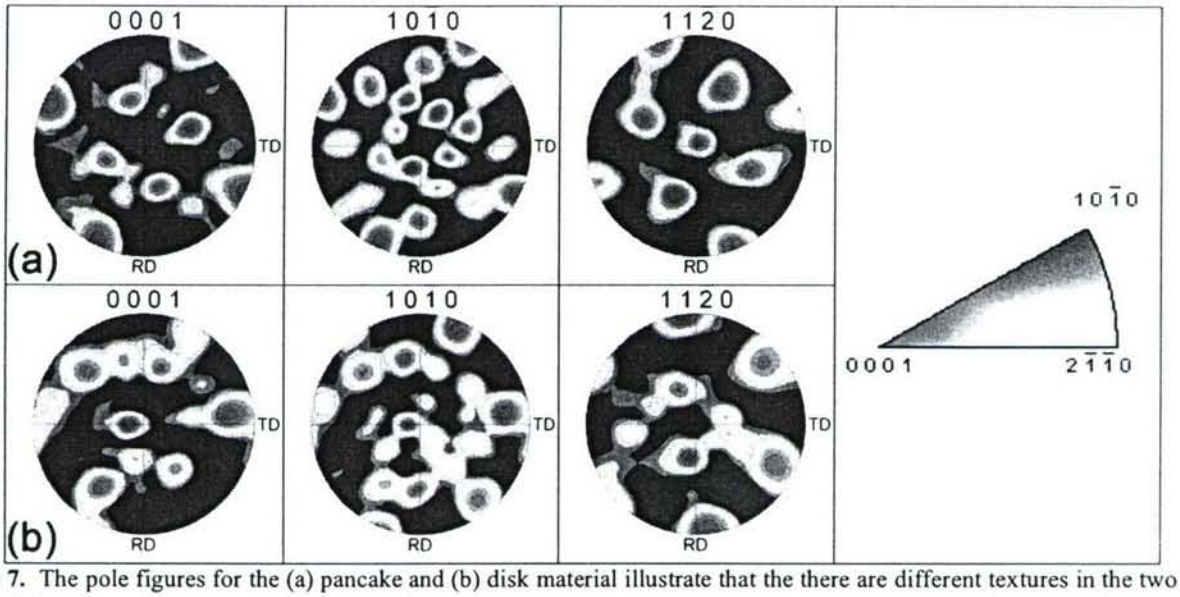

Figure 7. The pole figures for the (a) pancake and (b) disk material illustrate that the there are different textures in the two heats of material.

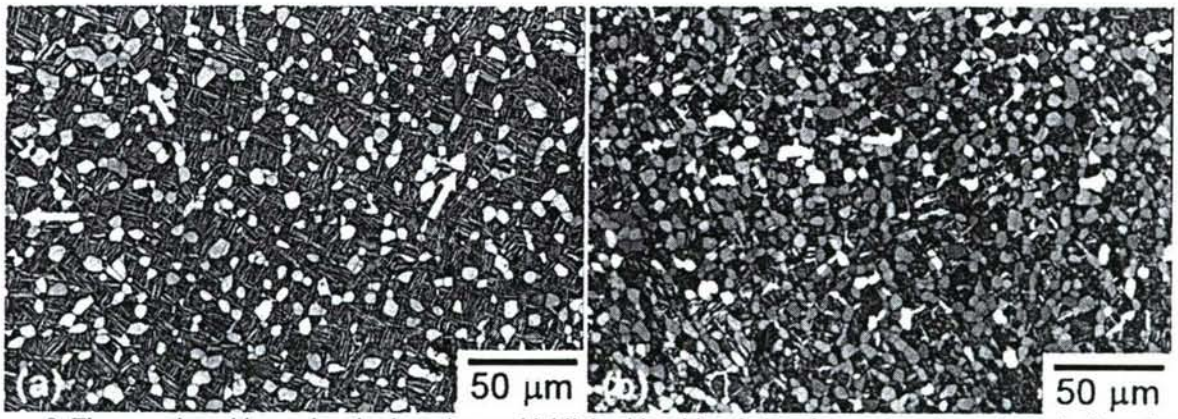

Figure 8. The α_p grains with near basal orientation are highlighted in white. Only a few such grains exist (as indicated with arrows) in (a), while for (b) there are many more grains with this crystallographic orientation (BSE image).

CONCLUSIONS

The results indicate that fatigue lifetimes of specimens are not affected by testing frequency. Specimens tested at conventional and ultrasonic frequencies follow similar trends. There is an increasing likelihood of subsurface crack initiation sites as the testing stress is decreased for both conventional and ultrasonic frequencies. On average, specimens with subsurface crack initiation sites exhibit longer lifetimes regardless of testing frequency. Fatigue cracks that initiate from subsurface sites are expected to propagate slower than surface initiated cracks since they are growing in near vacuum conditions. The morphology of the crack initiation sites is the same in that the initiating features are α_p facets at conventional and ultrasonic frequencies. The amount of scatter in the fatigue lifetime data is the same regardless of frequency. These statements, taken together, support the view that fatigue lifetimes and, by extension, the crack initiation lifetimes, are not altered by the change in testing frequency.

The crack initiating features are α_p grains, which often produce a faceted morphology upon failure. The amount of faceted failure varied from specimen to specimen and the area covered by the facets near the site of crack initiation does not correlate with fatigue lifetimes. The maximum area fraction measurements for the α_p were well above the measured area fractions of facets on a fracture surface. This indicates that the spacing of α_p grains alone is not the critical factor in determination of the crack initiation site. This finding suggests that the site of crack initiation is determined by other factors such as crystallographic orientation of grains within a given neighborhood of material.

Facets are not isolated to the site of crack initiation, as they are also observed in regions of fatigue crack propagation. The area fraction of faceted failure decreases below the volume fraction of the α_p phase as the crack propagates. This would indicate that either the propagating crack avoids the α_p phase or that the mode of failure within α_p grains changes with crack size so that the resulting morphology on the fracture surface is not a facet.

Using three dimensional surface reconstructions, the angle of facet normals with respect to the stress axis is less than 15° for the facets that are located at the crack initiation site. The same can be said for a majority of the facets across the region of crack propagation. This indicates that these facets are not created because they are the planes of the maximum critically resolved shear stress. More likely, the facets are formed based on the characteristics and deformation behavior of a given neighborhood of material such as crystallographic orientation or localized plasticity.

The textures of the pancake and disk material are noticeably different in terms of the distribution of α_p grains with respect to the loading axis. The material taken from the retired disk displays much less scatter in fatigue lifetimes than material from the forged pancake. Primary alpha grains with basal poles nearly

parallel to the loading axis were more homogeneously distributed in the disk material than the pancake material.

ACKNOWLEDGEMENTS

This work was supported by the Air Force Office of Scientific Research (F49620-03-1-0069), Dr. J. Tiley, Program Manager.

REFERENCES

[1] H Mughrabi; "On the life-controlling microstructural fatigue mechanisms in ductile metals and alloys in the gigacycle regime," *Fatigue Fractures of Engineering Materials Structures*, **22**, (1999) 633-641.

[2] MJ Caton, JW Jones, H Mayer, S Stanzl-Tschegg, JE Allison; "Demonstration of an endurance limit in cast 319 aluminum," *Metallurgical and Materials Transactions A*, **34A,** no. 1, (2003) pp. 33-41A.

[3] BA Cowles; "High cycle fatigue in aircraft gas turbines – an industry perspective," *International Journal of Fracture*, **80**, (1996) 147-163.

[4] H Mayer. "Fatigue crack growth and threshold measurements at very high frequencies," *International Materials Reviews*. **44**, Number 1, (1999) 1-34.

[5] L Willertz. "Ultrasonic fatigue," *International Metals Reviews*. No. 2, (1980) 65-78.

[6] CJ Szczepanski; A Shyam; SK Jha; JM Larsen; CJ Torbet; SJ Johnson; JW Jones; "Characterization of the role of microstructure on the fatigue life of Ti-6Al-2Sn-4Zr-6Mo using ultrasonic fatigue," In *Materials Damage Prognosis*, Eds. JM Larsen, L Christodoulou, JR Calcattera, ML Dent, MM Derriso, WJ Hardman, JW Jones, and SM Russ, TMS, 2005.

[7] A Shyam, CJ Torbet, SK Jha, JM Larsen, MJ Caton, CJ Szczepanski, TM Pollock, JW Jones; "Development of ultrasonic fatigue for rapid, high temperature fatigue studies in turbine engines," *Superalloys 2004*, Eds. KA Green, TM Pollock, H Harada, TE Howson, RC Reed, JJ Schirra, S Walston; TMS, 2004.

[8] X Zhu, A Shyam, JW Jones, H Mayer, JV Lasecki, JE Allison; "Elevated Temperature Fatigue Behavior of a 319 Cast Aluminum Alloy in the Gigacycle Regime," Proceedings of the 3rd International Conference on Very High Cycle Fatigue (VHCF-3), Sept. 16-19, 2004, Ritsumeikan University, Kusatsu, Japan, pp 553-560.

[9] AR Moore, CJ Torbet, A Shyam, JW Jones, DM Walukas, RF Decker; "Fatigue behavior of thixomolded magnesium AZ91D using ultrasonic techniques," *Magnesium Technology 2004* as held at the 2004 TMS Annual Meeting; Charlotte, NC; USA; 14-18 Mar. 2004. pp. 263-268. 2004

[10] J Huang, JE Spowart, JW Jones; "Fatigue behavior of SiC_p-Reinforced aluminum composites in the very high cycle regime using ultrasonic fatigue," *Fatigue and Fracture of Engineering Materials and Structures,* in press (2006).

[11] JA Hall; "Fatigue crack initiation in alpha-beta titanium alloys," *Int. J. Fatigue*, **31** Suppl. 1, (1997) S23.

[12] S Suresh, Fatigue of Materials Second edition, Cambridge University Press, Cambridge UK, 2001.

[13] KS Ravi Chandran, SK Jha; "Duality of the S-N fatigue curve caused by competing failure modes in a titanium alloy and the role of Poisson defect statistics," *Acta Materialia*, **53** (2005) 1867.

[14] WJ Evans; "Optimising mechanical properties in alpha + beta titanium alloys," *Materials Science and Engineering*, **A243**, (1998), 89-96.

[15] SK Jha, JM Larsen, AH Rosenberger, GA Hartman; "Dual fatigue failure modes in Ti-6Al-2Sn-4Zr-6Mo and consequences on probabilistic life prediction," *Scripta Materiala,* **48**, pp. 1637-1642, 2003.

[16] AS Beranger, X Feaugas, M Clavel; "Low cycle fatigue behavior of an α + β titanium alloy:Ti6246," *Materials Science and Engineering*, **A172**, pp.31-41, 1993.

[17] Y Mahajan, H Margolin. "Low Cycle Fatigue Behavior of Ti-6Al-2Sn-4Zr-6Mo: Part I. The Role of Microstructure in Low Cycle Crack Nucleation and Early Crack Growth," *Metallurgical Transactions A*, **13A**, 1982, 257.

[18] Y Mahajan, H Margolin, "Low Cycle Fatigue Behavior of Ti-6Al-2Sn-4Zr-6Mo: Part II. Cyclic Deformation Behavior and Low Cycle Fatigue," *Metallurgical Transactions A*, **13A**, 1982, 269.

[19] G Jago, J Bechet; "Influence of microstructure of (α+β) Ti-6.2.4.6 alloy on high cycle fatigue and tensile test behaviour," *Fatigue Fractures of Engineering Materials Structures*, **22**, pp.647-655, 1999.

[20]G Lütjering; "Influence of processing on microstructure and properties of (α + β) titanium alloys," *Materials Science and Engineering* **A243**, (1998), 32-45.

[21] K LeBiavant, S Pommier, C Prioul; "Local texture and fatigue crack initiation in a Ti-6Al-4lV titanium alloy," *Fatigue Fractures of Engineering Materials Structures*, **25** (2002) 527-545.

[22] A Tewari, AM Gokhale, JE Spowart, DB Miracle; "Quantitative characterization of spatial clustering in three-dimensional microstructures using two-point correlation functions," *Acta Materialia*, **52**, 307-319, 2004.

[23] H Kumar, CL Briant, WA Curtin; "Mechanical Modeling of Complex Microstructures," Submitted to *Acta Materialia*, 12 May 2004.

[24] J Tiley, T Searles, E Lee, S Kar, R Banerjee, JC Russ, HL Fraser, "Quantification of microstructural features in α + β titanium alloys," *Materials Science and Engineering A* **372** (2004) 191–198.

[25] SK Jha, JM Larsen, AH Rosenberger, "Microstructure and Temperature Effects on the Fatigue Variability Behavior of an a+b Titanium Alloy and Implications for Life Prediction," *Fatigue 2006*.

[26] JC Newman, Jr., IS Raju. "An emprirical stress-intensity factor equation for the surface crack," *Engineering Fracture Mechanics*, **15** (1981) 185-192.

[27] Y Murakami. "Stress intensity factors handbook," Oxford; New York : Pergamon, (1987) p.668.

[28] SK Jha, JM Larsen, AH Rosenberger, C Annis; "Prediction of the worst-case fatigue failures in an α + β titanium alloy," In *Materials Damage Prognosis*, Eds. JM Larsen, L Christodoulou, JR Calcattera, ML Dent, MM Derriso, WJ Hardman, JW Jones, and SM Russ, TMS, 2005.

4th International Conference on Very High Cycle Fatigue
Edited by: J.E. Allison, J.W. Jones, J.M. Larsen and R. Ritchie
TMS (The Minerals, Metals & Materials Society), 2007

THE ROLE OF MICROSTRUCTURE ON THE FATIGUE LIFETIME VARIABILITY IN AN α + β TITANIUM ALLOY, Ti-6Al-2Sn-4Zr-6Mo

C. J. Szczepanski[1]; S. K. Jha[2]; J. M. Larsen[3]; J. W. Jones[1]

[1]University of Michigan, Materials Science and Engineering, Ann Arbor, MI-48109 USA
[2]Universal Technology Corporation, Dayton, Ohio 45432 USA
[3]Air Force Research Laboratory, Materials and Manufacturing Directorate, AFRL/MLLMN, Wright-Patterson AFB, OH-45433 USA

Keywords: Ti-6Al-2Sn-4Zn-6Mo, fatigue crack initiation, microtexture, ultrasonic fatigue, α_p grain clustering

Abstract

Ultrasonic fatigue has been employed as a technique to characterize the fatigue behavior of Ti-6%Al-2%Sn-4%Zr-6%Mo in the very high cycle regime. The microstructure is a two-phase structure with primary α grains (α_p grains) in a transformed β matrix. α_p grains produce a faceted morphology upon failure near the site of fatigue crack initiation. The microstructure at the site of fatigue crack initiation has been examined using orientation imaging microscopy (OIM) and a texture suited for basal and prismatic slip exists there. α_p grains and α laths with similar crystallographic orientations relative to one another have been found just below the crack initiation site in some samples. Based on these findings, it is proposed that the local microtexture is a critical factor in determining the site of fatigue crack initiation. The crystallographic orientations within the α phase material (α_p grains and laths) found near the crack initiation site are aligned with each other such that if one is oriented for slip, it will be easy to transmit slip into adjacent grains. These findings indicate that at low stresses and long lifetimes, the fatigue critical defects are microtextured volumes of material.

Introduction

The exceptional cost of maintenance and repair of turbine engine components has increased interest [1] in developing more accurate physically-based models of fatigue lifetimes in the very long lifetime range of 10^6-10^9 cycles. Ultrasonic fatigue is a technique that provides researchers with a tool for acquiring statistically significant data in the very high cycle fatigue (VHCF) regime in a reasonable period of time. VHCF behavior is becoming of greater technological interest for other engineering alloys, as well. Thus, ultrasonic fatigue techniques have found usefulness in characterizing the fatigue behavior of a number of different alloy systems; including aluminum [2], magnesium [3], nickel-based [4], and titanium [5,6] alloy systems.

Fatigue crack initiation is known to consume the majority of fatigue lifetimes in the VHCF regime and as a result, there is an interest in determining the mechanisms of fatigue crack initiation and how the nearby microstructural neighborhood affects this process. In fatigue studies of alpha + beta titanium alloys, [6-9] cyclic deformation localization is first observed in the alpha phase. Mahajan and Margolin [9] observed that slip traces nucleate within primary alpha grains and at alpha lath/transformed beta interfaces. They concluded that the fatigue properties of α + β titanium alloys could be improved by limiting the accumulated slip in the alpha phase of these materials. This could be achieved either by eliminating the presence of

large α_p grains or by maximizing the distance between individual α_p grains. Hall's review [10] of fatigue in $\alpha+\beta$ titanium alloys also concludes that the fatigue strength of this class of alloys depends predominantly on the spacing between α_p grains since this distance affects the ease of slip transmission to neighboring grains. Hall describes an initiated fatigue crack as a crack-like discontinuity (CLD), after which point the feature behaves as a small fatigue crack. This idea can be extended to assume that the crack initiation may originate from a range of individual features or a collection or cluster of individual features with related properties (e.g. size or orientation) that can favor fatigue crack initiation [11, 12].

In titanium alloys with limited slip systems, grain orientation and/or texture can have a large effect on the active deformation mechanisms [13]. Sinha et. al. [14] studied the dwell-fatigue behavior of Ti-6242 and found that regions of material oriented for basal and prismatic slip were associated with the fatigue crack initiation sites. Le Biavant et. al. [15] observed the presence of microtextured regions in Ti-6Al-4V and found that these regions were the distinguishing characteristic of the fatigue crack initiation sites. These studies indicate that while individual α_p grains may not act as fatigue crack initiation sites, microstructural neighborhoods composed of such grains with similar crystallographic orientations can favor crack initiation. It is also possible that, as the stress range decreases and lifetimes increase into the VHCF range, the nature and frequency of occurrence of these favorable clusters can play a more important role in controlling fatigue life. Thus, in the present study, an investigation of the nature of the crack initiation regions in the VHCF regime is undertaken in an effort to better understand the relationship between microstructure variability and fatigue life.

Material and Experimental Procedures

Material

The material used in this study is Ti-6Al-2Sn-4Zr-6Mo, an alpha + beta forged near-alpha alloy. Figure 1 illustrates the microstructure of this material which has an equiaxed primary alpha phase (dark phase) distributed in a matrix of transformed beta (lighter phase). The α_p grain size was measured using the linear intercept method and can be described as log-normally distributed about a mean grain size of 3.7 ± 2.6 μm. The volume fraction of the primary alpha phase is ~30%, as determined by the point count method. Cylindrical fatigue specimens have a uniform gage section of 16 mm in length and 4 mm in diameter. All specimens were electropolished prior to testing to eliminate residual stresses from machining.

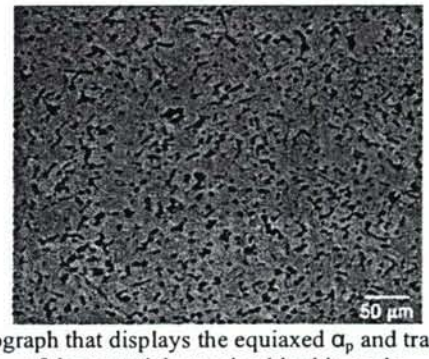

Figure 1. Secondary electron micrograph that displays the equiaxed α_p and transformed beta matrix microstructure of the material examined in this study.

Experimental Procedures

Ultrasonic fatigue tests were conducted with a positive mean stress ratio of 0.05 at room temperature in laboratory air as previously described [5]. Specimens were tested at ultrasonic frequencies near 20 kHz in displacement control using feedback from a Hall Effect sensor. Foil strain gages were applied to the specimen to calibrate the displacement amplitude with the input signal. An interferometric strain displacement gage was developed which allowed direct

measurement of the strains using fiducial marks on the specimen surface. Data acquired with this technique was used to further calibrate the system.

The fracture surfaces of failed specimens were examined in an XL30 FEG SEM. Orientation imaging microscopy (OIM) was used to gather crystallographic data from the grains near the crack initiation site. OIM patterns were collected in the same SEM with detectors and software made by TSL. Since deformation free surfaces are required for the acquisition of OIM patterns, the final polishing steps were found to be critical to pattern acquisition. Accordingly, specimens were prepared by hand polishing down to 0.05 μm alumina with subsequent polishing completed in a Buehler Vibromet II vibratory polisher on 0.05 μm colloidal silica for 3 hours. Without vibratory polishing, no Kikuchi bands were detectable in the OIM detector.

Results and Discussion

Ultrasonic Fatigue Testing

Fatigue tests have been completed at 20 kHz and at 20Hz on the same heat of material and the results are shown in Figure 2. **The S-N curve for Ti-6246 at room temperature and R=0.05 demonstrates that variability in the fatigue lifetime data exists for lives in the VHCF regime.**

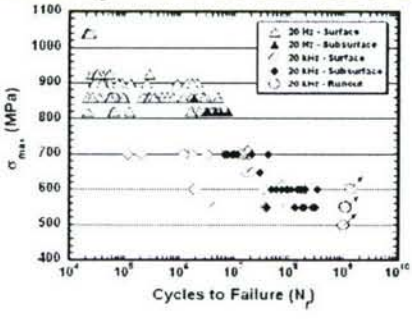

, where cycles to failure is plotted again maximum stress (R = 0.05). No effect of frequency on the fatigue lifetimes for this alloy and microstructure was observed. However, there is an increasing tendency towards subsurface crack initiation at lower stress levels. This trend is observed at conventional frequencies and continues into the lower stress, long-lifetime regime characterized at ultrasonic frequencies.

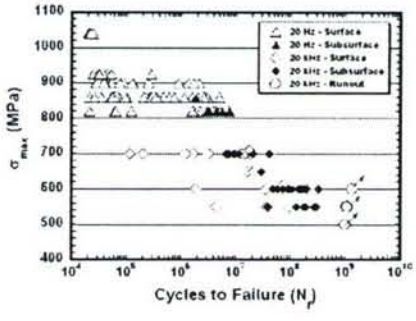

Figure 2. The S-N curve for Ti-6246 at room temperature and R=0.05 demonstrates that variability in the fatigue lifetime data exists for lives in the VHCF regime.

Fractographic Analysis

As shown in Figure 3, the crack initiation sites were always found to contain a cluster of a few α_p facets, which are formed by the fracture of α_p grains. The α_p facet sizes follow a normal distribution and, as **Error! Reference source not found.** shows, the average facet diameter is 6.0 ± 1.8 μm. This is slightly larger than the measured α_p grain size of 3.7 ± 2.6 μm. Figure 4 illustrates that the average α_p facet is the same size as commonly occurring α_p grains. Thus, the α_p facets are not considered to be unique because of their size.

The crack initiation sites exhibit clusters of α_p facets which are highlighted in the fractograph shown in Figure 5. Arrangements of α_p grains/laths that promote transmission of slip into neighboring grains/laths, such as clusters or contiguous α_p grains are known to be crack initiating features [**Error! Bookmark not defined., Error! Bookmark not defined., Error! Bookmark not defined.**]. Thus, a quantitative measurement of α_p facet clusters was completed [16] to assess the distribution of α_p grain clusters within the general microstructure. By measuring the area fraction of the α_p grains on a local scale and comparing these measurements to area fraction measurements of facets on the fracture surface it was found that α_p clusters of this size are commonly found in the general microstructure. Examples of some of these α_p clusters are circled in Figure 5. This analysis supports the theory that something other than α_p cluster size or severity must be responsible for fatigue crack initiation.

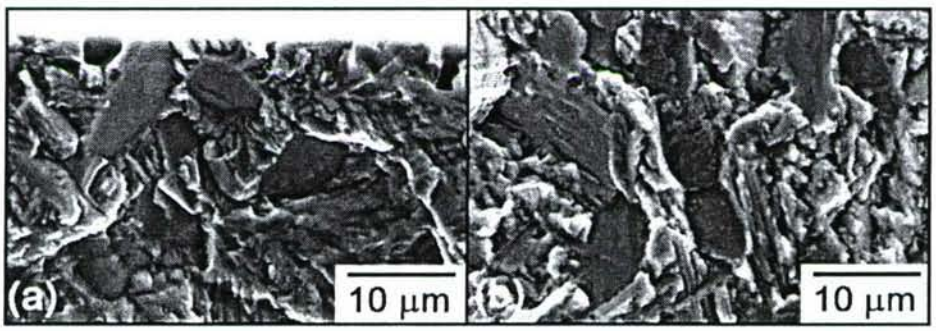

Figure 3. Clusters of α_p facets as shown here are found at the site of fatigue crack initiation.

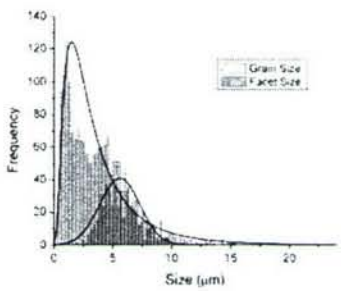

Figure 4. This histogram displays the distribution of α_p facet size and α_p grain size.

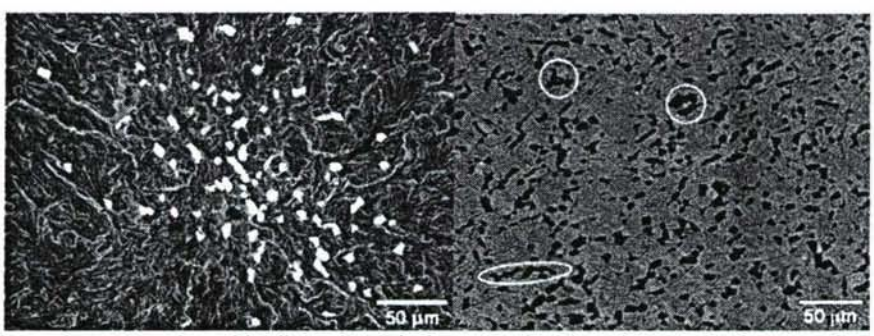

Figure 5. The α_p facets have been highlighted in this fractograph. The micrograph of a general metallographic surface indicates that there are a number of α_p clusters that are as large or larger than the clusters of α_p facets on the fracture surface.

Stereo pairs were created to examine the spatial orientation, relative to the tensile axis, of the facets near the fatigue crack initiation site. Some of these facets were inclined for maximum resolved shear stress while others were nearly perpendicular to the loading axis. Of the 47 facets

measured with this technique, the average angle of inclination with respect to the plane formed normal to the loading axis is 30°. The larger facets were mostly found to be inclined greater than 35° with respect to the horizontal plane. It appears that facets on the order of 10 μm are found to be oriented for slip at the site of fatigue crack initiation.

Crystallographic Orientation of α_p Facets

It is clear that the α_p facets form along a crystallographic direction favorable for slip. Mechanisms of stress redistribution at the local level have been developed [17,18] to explain the presence of facets on fatigue fracture surfaces in titanium alloys because of the limited slip systems available. It was desired to determine the crystallographic orientations relative to the tensile axis so that these slip planes could be identified. The FIB was used to selectively micro-machine through some of the facets observed at the site of fatigue crack initiation. Through the combined approach of stereology and OIM it was possible to resolve the spatial and crystallographic orientation of the α_p facet and the α_p grain containing the facet. A total of 7 facets were analyzed using this combined approach. In each case, the facet plane was parallel to the basal plane of the material. This is illustrated in Figure 6 and the data is shown in Table 1. The spatial orientation describes the angle of inclination of the facet relative to horizontal, i.e. a facet with a low spatial orientation is nearly perpendicular to the tensile axis. The crystallographic orientation describes the orientation of the basal pole of the material with respect to the tensile axis. From these initial results, the facet plane is a fractured basal plane of the α_p grain and therefore, basal type slip is an active deformation mode for this material and stress level. In light of the previous studies [**Error! Bookmark not defined.**,**Error! Bookmark not defined.**] on fatigue facet formation in titanium alloys, it should be stated that the hypothesized Stroh-type mechanism is not the mechanism of crack initiation. It certainly appears that some facets form perpendicular to the tensile axis, but this would be expected to occur in some number of α_p grains. Most of the larger facets near the site of crack initiation are oriented for basal slip.

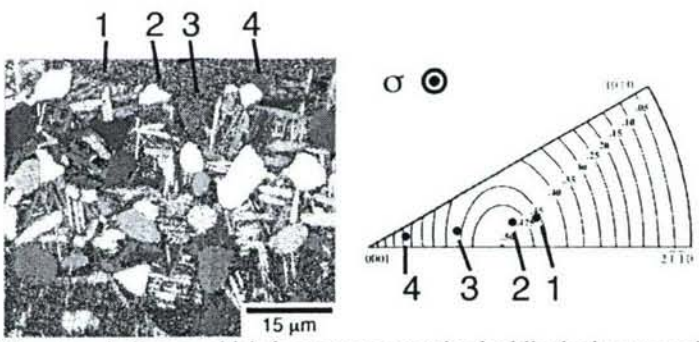

Figure 6. The OIM pattern indiactes which facets were examined while the inverse pole figure plots the crystallographic orientations of those facets.

Table 1. Crystallographic and Spatial Orientations of the α_p Facets

Facet	1*	2	3	4
Spatial Orientation	44°	42°	25°	15°
Crystallographic Orientation	55°	48°	30°	13°

* This feature is not a α_p facet. It is a transformed beta grain that fractured along a basal plane of the α laths.

Texture of Crack Initiation Site

The α_p grains in which facets form are not unique relative to the general microstructure. Thus, there must be some mechanism for slip transmission between adjacent α_p grains such that a given neighborhood of material is more susceptible to crack initiation than adjacent areas [**Error! Bookmark not defined.**]. To ascertain the likelihood of this theory, serial sectioning was used to reveal the volume of material just beneath the crack initiation site for analysis of

texture in the OIM. A typical OIM pattern and the corresponding discrete inverse pole figure are shown in Figure 7. The loading direction in the OIM pattern is vertical in the plane of the page. The inverse pole figures shown in the figure are typical of those collected from the near-crack initiation region. The Schmid factor iso-curves are shown on the discrete pole figures for both basal and prismatic slip and the arrows indicate the location of the maximum Schmid factor. The clusters of dots near the maximum Schmid factor indicate that the α material near crack initiation is oriented to activate both basal and prismatic slip. In a number of cases the slip planes for basal and prismatic slip were well aligned relative to adjacent grains, suggesting that both basal and prismatic slip are active slip systems. These results are consistent with the work of Bridier et. al. [19] in which a procedure of serial sectioning coupled with EBSD analysis was used to determine that the grains near the crack initiation site were oriented to maximize the resolved shear stress (highest Schmid factor) on the basal and prismatic planes. Judging from the observed texture and the fact that the CRSS for prismatic and basal slip are approximately equal [20], it is reasonable to suggest that both types of slip were operative.

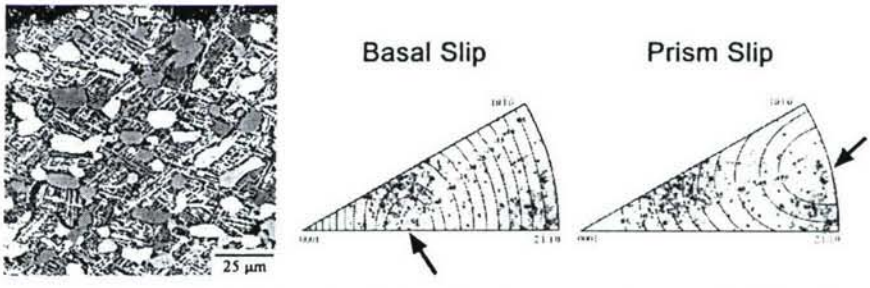

Figure 7. OIM pattern for the material found just below the fracture surface for one of the failed specimens. In this pattern, different colors correspond to different crystallographic orientations.

Summary and Conclusions

The fatigue behavior has been characterized at conventional and ultrasonic frequencies for Ti-6246. Fatigue cracks have been found to initiate at both surface and subsurface locations. In both cases, a cluster of α_p facets are observed near the site of fatigue crack initiation. The individual α_p facets form in α_p grains of relatively average size that are commonly distributed throughout the matrix. The crystallographic orientation of the facets was measured for a number of samples that failed from subsurface crack initiation and it was found that the facets are formed from the fracture of α_p grains along the basal plane. Stereology was completed and it was determined that the facets are often oriented to maximize the resolved shear stress. The local texture of the crack initiation site was examined using OIM and the alpha material is suited for basal and prismatic slip. Since the α_p facets are not continuous, the local microtexture is believed to be necessary for promoting slip in nearby α grains. Thus, the crack initiating volume is composed of α_p grains that fracture along the basal plane surrounded by regions of material suited for easy basal and prismatic slip.

Acknowledgements

The authors would like to thank Chris Torbet (University of Michigan) for his technical assistance with experimental equipment. This work was funded by the Air Force Office of Scientific Research (F49620-03-1-0069, Dr. J.Tiley, Program Manager).

References

[1] *Materials Damage Prognosis*, Materials Science and Technology 2004; New Orleans, LA, September 26-30, 2004.

[2] X Zhu, A Shyam, JW Jones, H Mayer, JV Lasecki, JE Allison; "Elevated Temperature Fatigue Behavior of a 319 Cast Aluminum Alloy in the Gigacycle Regime," Proceedings of the 3rd International Conference on Very High Cycle Fatigue (VHCF-3), Sept. 16-19, 2004, Ritsumeikan University, Kusatsu, Japan, , pp 553-560
[3] AR Moore, CJ Torbet, A Shyam, JW Jones, DM Walukas, RF Decker; "Fatigue behavior of thixomolded magnesium AZ91D using ultrasonic techniques," *Magnesium Technology 2004* as held at the 2004 TMS Annual Meeting; Charlotte, NC; USA; 14-18 Mar. 2004. pp. 263-268.
[4] A Shyam, CJ Torbet, SK Jha, JM Larsen, MJ Caton, CJ Szczepanski, TM Pollock, JW Jones; "Development of ultrasonic fatigue for rapid, high temperature fatigue studies in turbine engines," *Superalloys 2004*, Eds. KA Green, TM Pollock, H Harada, TE Howson, RC Reed, JJ Schirra, S Walston; TMS, 2004.
[5] CJ Szczepanski, S.K. Jha, J.M. Larsen, J.W. Jones. "Fatigue crack initiation in an $\alpha + \beta$ titanium alloy," in *Fatigue 2006*. Symposium on Titanium Fatigue. *Electronic Proceedings.*
[6] G Jago, J Bechet; "Influence of microstructure of $(\alpha+\beta)$ Ti-6.2.4.6 alloy on high cycle fatigue and tensile test behaviour," *Fatigue Fractures of Engineering Materials Structures*, **22**, pp.647-655, 1999.
[7] SK Jha, JM Larsen, AH Rosenberger, GA Hartman; "Dual fatigue failure modes in Ti-6Al-2Sn-4Zr-6Mo and consequences on probabilistic life prediction," *Scripta Materiala,* **48**, pp. 1637-1642, 2003.
[8] AS Beranger, X Feaugas, M Clavel; "Low cycle fatigue behavior of an $\alpha + \beta$ titanium alloy:Ti6246," *Materials Science and Engineering*, **A172**, pp.31-41, 1993.
[9] Y Mahajan, H Margolin. "Low Cycle Fatigue Behavior of Ti-6Al-2Sn-4Zr-6Mo: Part I. The Role of Microstructure in Low Cycle Crack Nucleation and Early Crack Growth," *Metallurgical Transactions A*, **13A**, 1982, 257.
[10] JA Hall; "Fatigue crack initiation in alpha-beta titanium alloys," *Int. J. Fatigue*, **31** Suppl. 1, (1997) S23.
[11] SK Jha, JM Larsen, AH Rosenberger; "Random heterogeneity scales and probabilistic description of the long-lifetime regime," *VHCF-4* (2007).
[12] J Miao, TM Pollock, JW Jones; "Very high cycle fatigue behavior of nickel-based superalloy René 88DT at 593 °C," *VHCF-4* (2007).
[13] S Zaefferer; "A study of active deformation systems in titanium alloys: dependence on alloy composition and correlation with deformation texture," *Materials Science and Engineering* **A344** 2003, 20-30.
[14] V Sinha, JE Spowart, MJ Mills, JC Williams; "Observations on the faceted initiation site in the dwell-fatigue tested Ti-6242 alloy: crystallographic orientation and size effects," *Metallurgical and Materials Transactions A*, **37A**, 2006, 1507-1518.
[15] K LeBiavant, S Pommier, C Prioul; "Local texture and fatigue crack initiation in a Ti-6Al-4lV titanium alloy," *Fatigue Fractures of Engineering Materials Structures*, **25** (2002) 527-545.
[16] CJ Szczepanski, SK Jha, JM Larsen, JW Jones. "Fatigue crack initiation in an $\alpha + \beta$ titanium alloy," in *Fatigue 2006*. Symposium on Titanium Fatigue. *Electronic Proceedings*
[17] WJ Evans, MR Bache; "Dwell-Sensitive fatigue under biaxial loads in the near-alpha titanium alloy IMI685," *International Journal of Fatigue, 1994; 16; 443-52.*
[18] DF Neal and PA Blenkinsop; "Internal Fatigue Origins in α-β titanium alloys," *Acta Metallurgica*, **24**, 1976, 59-63.
[19] F Bridier, P Villechaise, J Mendez; "Analysis of the different slip systems activated by tension in a α/β titanium alloy in relation with local crystallographic orientation," *Acta Materiala*, **53**, 2005, 555-567.
[20] JC Williams, RG Baggerly, NE Paton; "Deformation behavior of HCP Ti-Al alloy single crystals," *Metallurgical and Materials Transactions*, **33A**, 2002, 837-850.

ELSEVIER

Materials Science and Engineering A 443 (2007) 142–149

MATERIALS SCIENCE & ENGINEERING A

www.elsevier.com/locate/msea

Ultrasonic fatigue of a single crystal Ni-base superalloy at 1000 °C

J.Z. Yi *, C.J. Torbet, Q. Feng, T.M. Pollock, J.W. Jones

Department of Material Science and Engineering, University of Michigan, H.H. Dow Build, Ann Arbor, MI 48109, USA

Received 24 May 2006; received in revised form 8 August 2006; accepted 9 August 2006

Abstract

An ultrasonic fatigue testing system capable of operating at temperatures up to 1000 °C has been developed and utilized to study the fatigue behavior of a single crystal superalloy (PWA 1484) at a temperature of 1000 °C and loading frequency of approximately 20 kHz. The stress-life data generated from the ultrasonic testing system were comparable to those from conventional servo-hydraulic fatigue tests for similar single crystal alloys. Interior Ta-rich carbides were the major microstructural feature responsible for crack initiation in the alloy. Crack growth under ultrasonic loading frequency at 1000 °C for PWA 1484 occurred in a crystallographic manner on {1 1 1} octahedral slip planes, in contrast to the normal Mode-I growth mode typically observed for single crystal superalloys at high temperature (>850 °C) with conventional servo-hydraulic loading frequencies (<100 Hz).

Keywords: Fatigue; High temperature; Superalloy

1. Introduction

Vibrations in gas turbine engines are a potential cause for fatigue failure of turbine airfoils during engine operation [1,2]. Such vibrations may arise from a wide range of stimuli, such as the turbulent flow around the airfoil itself, and can range in frequency from a few Hz to many thousands of Hz. If the excitation frequencies are close to one of the natural resonant frequencies of the blade, or if the amplitude of the stimulus is high enough, then high cycle fatigue failure of the blades may occur. High pressure turbine blades for high performance aircraft engines are typically composed of single crystal nickel-base superalloys, as they provide a combination of superior creep, stress rupture, oxidation resistance and thermal-mechanical fatigue capabilities over polycrystalline alloys. Hence, the fatigue behavior of single-crystal superalloys loaded by vibratory stresses is a major concern regarding the safety and reliability of gas turbine engines. However, the availability of a materials database for fatigue under conditions relevant to turbine blade operation is severely limited to date due to lack of reliable and efficient testing methodologies at frequencies in the kHz range and at temperatures up to 1000 °C.

In general, fatigue tests in the very long lifetime regime ($>10^8$ cycles) are prohibitively time consuming with conventional servo-hydraulic testing equipment, where a maximum loading frequency on the order of 100 Hz is typical. For this reason, few studies of high cycle fatigue behavior of nickel-base single crystals at very long lifetimes using conventional instrumentation have been performed [2]. While high temperature fatigue studies of these materials at very high frequencies in the range of 10–20 kHz have not been reported, a number of studies at temperatures up to 600 °C have been recently completed on a wide range of structural alloys, including aluminum [3,4], steel [5], titanium [6,7] and polycrystalline superalloys [8]. Thus, ultrasonic fatigue techniques offer a potentially attractive approach for investigation of the high cycle fatigue behavior of superalloy single crystals at very high vibratory loading frequencies [9]. In this paper, we describe a novel approach using ultrasonic fatigue testing instrumentation to examine the fatigue behavior of a nickel-base superalloy single crystal cycled at 20 kHz at a temperature of 1000 °C.

2. Material and development of experimental procedure

The material used in this investigation is a single crystal superalloy, designated PWA1484. The nominal composition (wt%) of the alloy is 5.6 Al, 8.7 Ta, 5.0 Cr, 2.0 Mo, 10.0 Co, 3.0

* Corresponding author. Tel.: +1 734 615 5162; fax: +1 734 615 5168.
E-mail address: jzyi@engin.umich.edu (J.Z. Yi).

0921-5093/$ – see front matter © 2006 Elsevier B.V. All rights reserved.
doi:10.1016/j.msea.2006.08.028

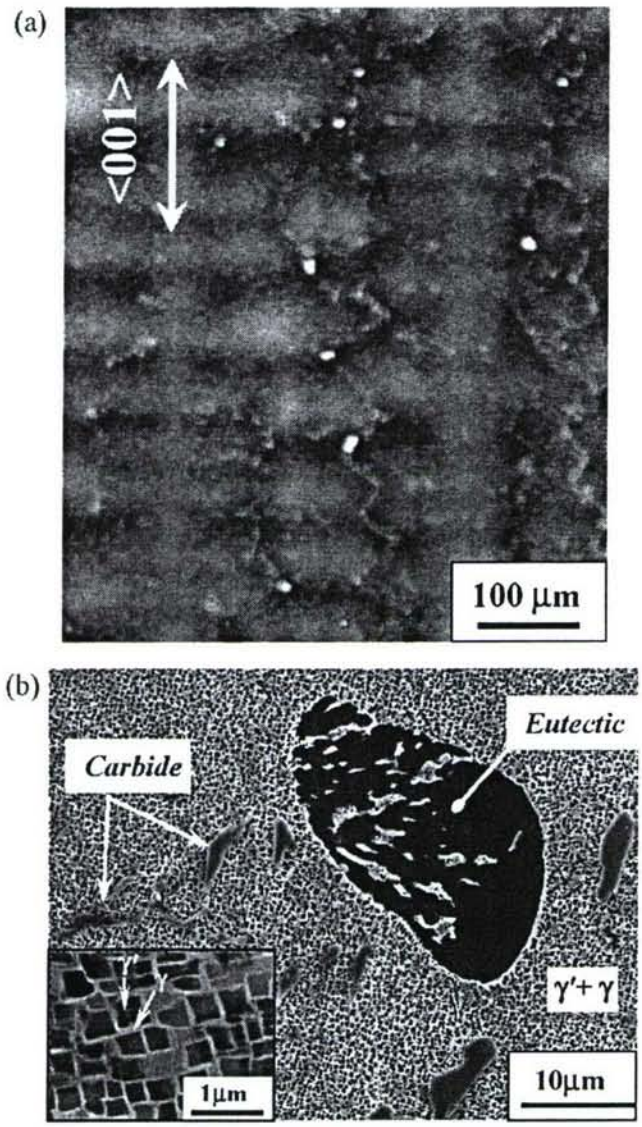

Fig. 1. (a) Directionally-solidified dendritic structure of PWA1484 single crystal superalloy sectioned parallel to the solidification direction; (b) microstructure consisting of carbides and eutectic distributed around interdendritic region, the inset SEM image indicating the cubic γ' particles and γ channels.

Re, 6.0 W, 0.04 B, 0.10 Hf, <0.05 C, and balance Ni [10,11]. Single crystal rods were directionally solidified to produce a ⟨0 0 1⟩ crystal orientation. After solidification, the casting was subjected to hot isostatic pressing (HIP) to eliminate porosity, followed by a standard solution heat treatment and age at GE Aviation. The resulting microstructure, shown in Fig. 1, consists of a dendritic structure with cubic γ' particles with a diameter of approximately 0.5 μm (see the inset in Fig. 1(b)), coarse eutectic ($\gamma+\gamma'$) and carbides distributed in interdendritic regions. The primary dendrite arm spacing is approximately 600 μm. No porosity or other extrinsic defects were observed.

Since specimens are cycled in resonance during ultrasonic fatigue testing, the elastic modulus and density are of primary importance. The density of the alloy is 8.95 g/cm^3, and the Young's modulus was determined according to the well-known relationship [12]:

$$\frac{1}{E} = S_{11} - 2\left(S_{11} - S_{12} - \frac{1}{2}S_{44}\right)(l_1^2 l_2^2 + l_2^2 l_3^2 + l_3^2 l_1^2) \quad (1)$$

E is Young's modulus along a selected crystallographic directions; S_{11}, S_{12}, and S_{44} are compliance coefficients which are experimentally determined; l_1, l_2, and l_3 = direction cosine corresponding to loading axis.

Compliance coefficients as a function of temperature (T, °C) were utilized from room temperature to 1093 °C. By data fitting, the Young's modulus along ⟨0 0 1⟩, as a function of temperature (T, °C) can be approximated by:

$$E_{\langle 100\rangle} = 123.53 - 0.033T + 7.40 \times 10^{-6}T^2 - 1.51 \times 10^{-8}T^3\,(\text{GPa}). \quad (2)$$

Fatigue specimens were machined with the tensile axis parallel to within 5° of the ⟨0 0 1⟩ direction, giving a maximum deviation in modulus of less than 2%. Fatigue tests were conducted at 1000 °C under fully reversed loading ($R=-1$), in an ultrasonic fatigue test system with a nominal resonant frequency of 20 kHz. Fig. 2(a) shows the load train of the testing system, which consists of an ultrasonic transducer, a displacement amplification

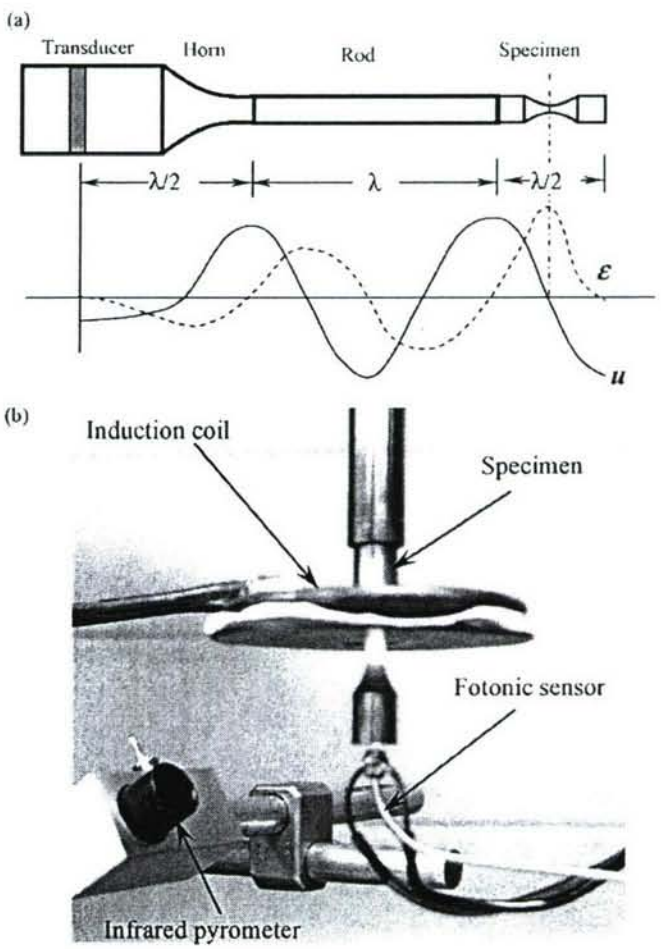

Fig. 2. (a) Schematic of the ultrasonic fatigue testing system, and (b) the ultrasonic apparatus used for fatigue tests at elevated temperature.

horn and the specimen. An induction coil is employed for specimen heating (Fig. 2(b)). The temperature in the specimen gage section is monitored with an infrared pyrometer, and temperature calibration is performed using thermocouples attached to the gage section. Displacement amplitude at the end of the specimen during fatigue is measured using a Fotonic^{TM} displacement transducer with displacement resolution in the range of 1–2 μm (resultant stress accuracy is approximately 5% for the stress range investigated). Vibration amplitude is controlled with a closed-loop system using an inductance transducer for the feedback signal. The lengths of all mechanical vibrating components in the load train are adjusted to vibrate in resonance to obtain specific load amplitudes. In resonance, the total length of the load train is an integral number of the acoustic wavelength, λ, of a tension–compression wave at a frequency of 20 kHz while the specimen length, l, equals $1/2\lambda$ to assure that maximum strain occurs at the specimen gage section mid-length. Assuming a cylindrical specimen with a ratio of length (l) over radius (r), $r/l \gg 1$, with Young's modulus E, and mass density ρ, the resonance length of a rod vibrating at frequency f is given by [13,14]:

$$l = \frac{\lambda}{2} = \frac{1}{2f}\sqrt{\frac{E}{\rho}}, \tag{3}$$

For typical ultrasonic fatigue specimen designs, the governing equation becomes [14]:

$$u'' + u'\frac{\mathrm{d}}{\mathrm{d}x}(\ln A(x) + \ln E(x)) + \left(\frac{2\pi}{\lambda}\right)^2 u = 0 \tag{4}$$

where x is the location along the specimen; $u(x)$ is the displacement; ρ is density of the alloy and $A(x)$ is the cross-sectional area of the specimen. Because temperature, and thus modulus of elasticity, varies along the length of the specimen, $E(x)$ is position dependent.

For the experimental arrangement shown in Fig. 2(b), a constant maximum temperature (e.g. 1000 °C) is maintained in the central gage section and decreases to approximately 600 °C at the specimen ends. The experimentally determined temperature gradient along the specimen length, shown in Fig. 2(c), can be approximated by a normal distribution function with maximum value in the center of the specimen. From Eq. (2) and the measured temperature distribution along the specimen, the position-dependent Young's modulus is estimated and the final specimen dimensions for resonance at the desired test temperature are determined by iteratively solving Eq. (4). In the present study an hour-glass shaped gage section was employed and the specimen dimensions shown in Fig. 3(a). The calculated relative displacement and strain along the specimen axis are shown in Fig. 3(b). Displacement amplitude is adjusted to give the desired stress amplitude under the assumption that deformation is within the elastic range.

As Young's modulus is a function of crystal orientation, it is expected from Eq. (4) that mis-orientation of the tensile axis from the ⟨0 0 1⟩ orientation will cause a change in resonant frequency and vibration amplitude. In this study the specimen tensile axis is always within 5° of the ⟨0 0 1⟩ direction which indicates, based on Eq. (4), that a maximum strain decrease of only 4% relative to the mean imposed strain would be possible.

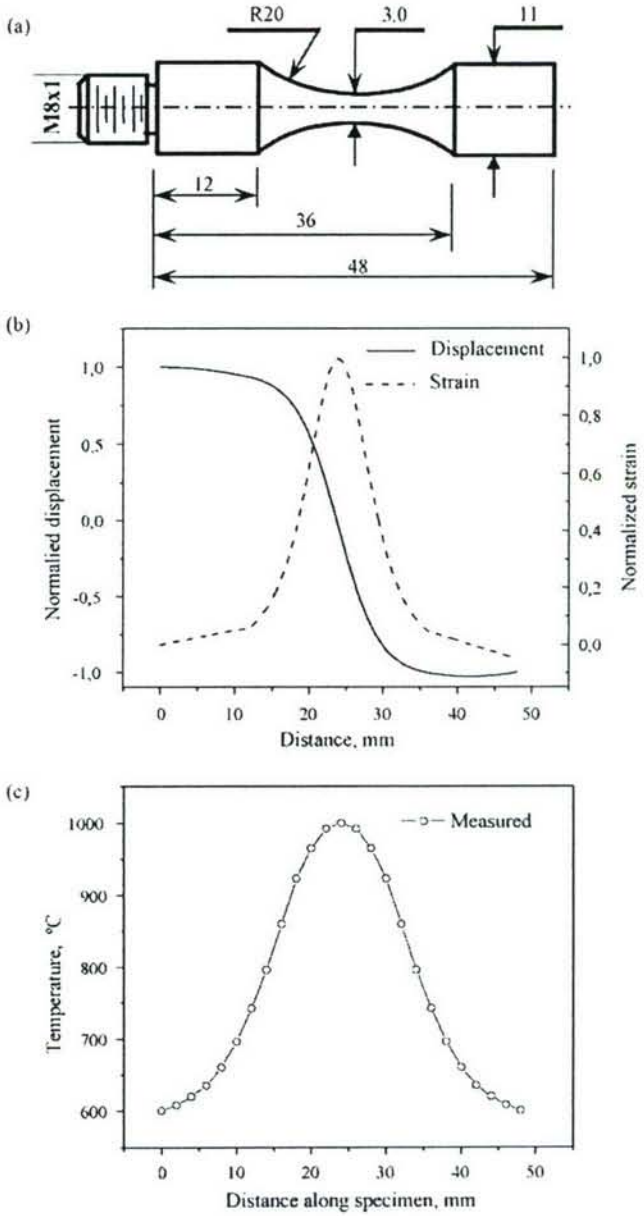

Fig. 3. (a) Ultrasonic fatigue specimen geometry (dimensions in mm); (b) the distributions of relative displacement and strain amplitude along the length of the specimen; and (c) measured temperature along the length of the specimen.

The control system for ultrasonic fatigue allowed all fatigue tests to be operated in an intermittent manner to minimize temperature increases due to heat generation during high frequency cycling. A pulse duration of 250 ms and pause duration of 2000 ms were sufficient for control of the temperature variation to within ±3 °C at 1000 °C. While testing with mean loads is possible within this system, all tests in the presented study were conducted under fully reversed loading conditions.

Testing was automatically terminated when the growth of a fatigue crack or other fatigue damage was sufficient to cause a 5% change in resonant frequency. Specimens that did not fail after 5×10^8 cycles were considered run-outs and then subjected to at least one incremental increase in applied stress range and

tested to failure. Failed specimens, which under fully reverse loading conditions did not experienced full separation within the 5% resonant frequency decrease, were carefully separated to reveal the fatigue crack and all fracture surfaces were examined using a Phillips XL-30 FEG-SEM. Although fatigue-induced plasticity was expected to be minimal, fatigued samples were examined using a Phillips CM-12 TEM to investigate the possible development of dislocation structures attributable to cyclic strain localization. TEM specimens were prepared from 0.5 mm thick disks removed from just below the fracture surface, with the disk sectioned normal to the loading axis. Disks were thinned to less than 100 μm using standard metallographic techniques and a final electropolishing was performed in a solution of 10% perchloric acid, 9% distilled water, 13% butyl cellusolve and 68% methanol at −40 °C and 20 V.

3. Results and discussion

3.1. S–N curve

The stress-life (S–N) data generated by ultrasonic fatigue testing in the lifetime regime of approximately 5×10^5–5×10^8 cycles for the single-crystal superalloy (PWA1484) are shown in Fig. 4. Run outs at $N = 5 \times 10^8$ were observed for three samples at 200, 250 and 300 MPa, respectively. For stress amplitudes between approximately 320 and 420 MPa, fatigue life varied from 10^6 to10^8 cycles. As a limited number of crystals was available for the present study, no replicate tests were carried out in the above lifetime regime. The S–N behavior of the same (PWA 1484) ⟨0 0 1⟩ oriented single crystal superalloy at a higher temperature of 1038 °C, a loading frequency of 59 Hz and $R = -1$ from the work of Wright et al. [2] is shown for comparison in Fig. 4. Specimens in the previous study [2] were platinum-aluminide coated and fatigue testing was performed using a conventional servo-hydraulic test system. As shown in Fig. 4, for the stress ranges examined, fatigue lifetime at a test frequency of 20 kHz is about one and half orders of magnitude longer than observed at 59 Hz. Wright et al. [2] observed no frequency dependence in lifetime in the range of 59–900 Hz at 1038 °C, but did observe such a dependence at a stress ratio of $R = 0.1$ and higher. Such a frequency effect was also reported by MacLachlan and Knowles [15] for CMSX-4 tested at low (0.25 Hz) and high (100 Hz) loading frequencies, at an R-ratio of zero and temperatures of 750 and 950 °C. While a frequency effect at 20 kHz cannot be eliminated in the present study, it is likely that the difference in lifetimes between the conventional tests and the ultrasonic tests is in part due to the different test temperature and the PtAl coating layer on the specimens tested at 59 Hz. Wright et al. [2] reported that crack initiation occurred either on coating layer or internal features for specimen tested at 59 Hz, and both modes could sometimes be seen on a single specimen. The authors also observed that, in both cases, the fracture surface in the vicinity of the origin was quite flat and perpendicular to the specimen axis, and some crystallographic cracking could be seen in the fast fracture area. This is somewhat different from the observations for specimens tested at 20 kHz, where all dominant cracks that led to final failure of the specimens were found to propagate along {1 1 1} crystallographic planes (see Sections 3.2 and 3.3 for more details). Therefore, more studies are needed to clarify the effect of loading frequency, in particular, at ultra-high frequency (>1 kHz), and coating layer on high-cycle fatigue behavior of single crystal Ni-base superalloys.

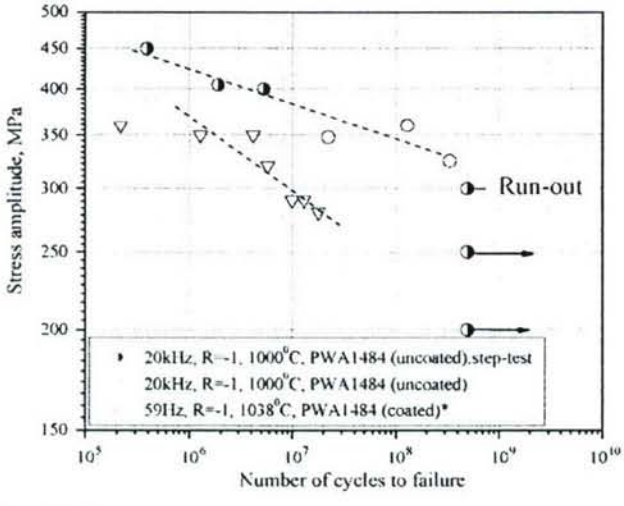

Fig. 4. The S–N curve of PWA 1484 at a stress ratio of $R = -1$, temperature of 1000 °C, and loading frequency of 20 kHz. Conventional S–N data (59 Hz/1038 °C) for aluminide-coated PWA 1484 is shown for comparison [2].

For both sets of data a power-law life model was assumed for the single crystal superalloy based on the Basquin expression,

$$\sigma_a = \sigma_f'(2N_f)^b, \tag{5}$$

where σ_a is the alternating stress, and N_f is the number of cycles to failure. The fatigue strength coefficient, σ_f', is approximately equal to ultimate tensile strength (UTS) of the material, and the constant, b, falls in the range of −0.05 to −0.12 for most metals [16]. As shown in Fig. 4, the S–N data is linear on this log–log plot. By regression, a value of $\sigma_f' = 747$ MPa was obtained. This value is somewhat higher than the yield strength of PWA 1484 along ⟨0 0 1⟩ at 1000 °C (600–650 MPa) [10]. A value of $b = -0.041$ was found to give good fit for the ultrasonic fatigue data. Wright et al. [2] reported a lower value of $b = -0.107$ for the high cycle fatigue data for a PWA 1484 superalloy tested at a temperature of 1038 °C and a wide range of stress ratio ($R < 0.1$) and loading frequency (60–879 Hz).

3.2. Crack initiation

Crack initiation at 20 kHz occurred predominately at subsurface carbides, with only one of six initiations occurring at the specimen surface. Figs. 5(a) and 6(a) shows examples of crack initiation from interiors of the specimens. Further examinations on crack initiation sites at high magnification indicated that Ta-rich carbides are associated with crack initiation, as shown in Figs. 5(b) and 6(b). The addition of minor amounts of carbon in single crystal superalloys serves to: (i) reduce oxygen levels during primary melting [17]; (ii) reduce thermosolutal convective

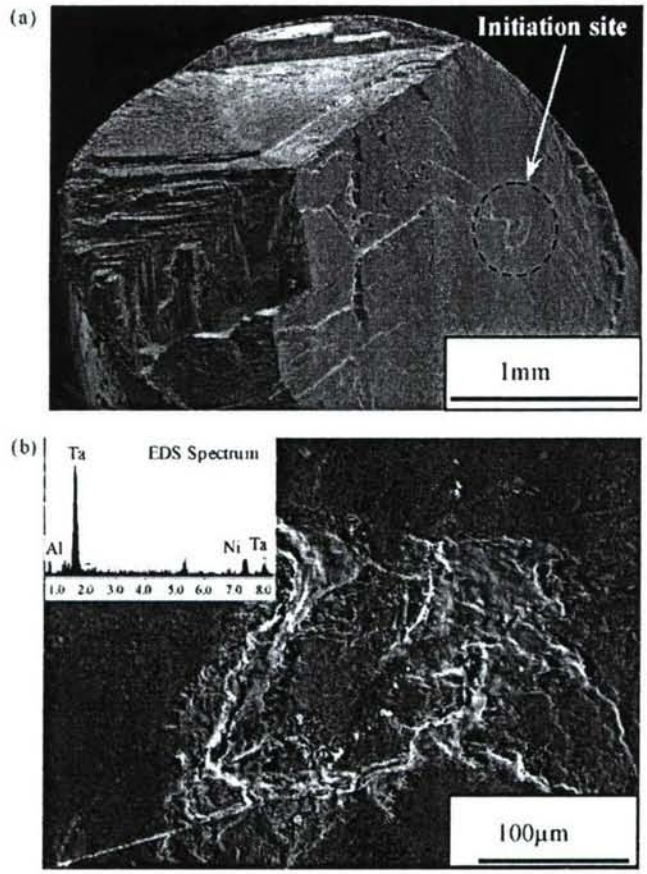

Fig. 5. Fracture surfaces of the specimens failed at (a) $\sigma_a = 400$ MPa, $N_f = 5.8 \times 10^6$ cycles, and (b) $\sigma_a = 350$ MPa, $N_f = 2.2 \times 10^7$ cycles.

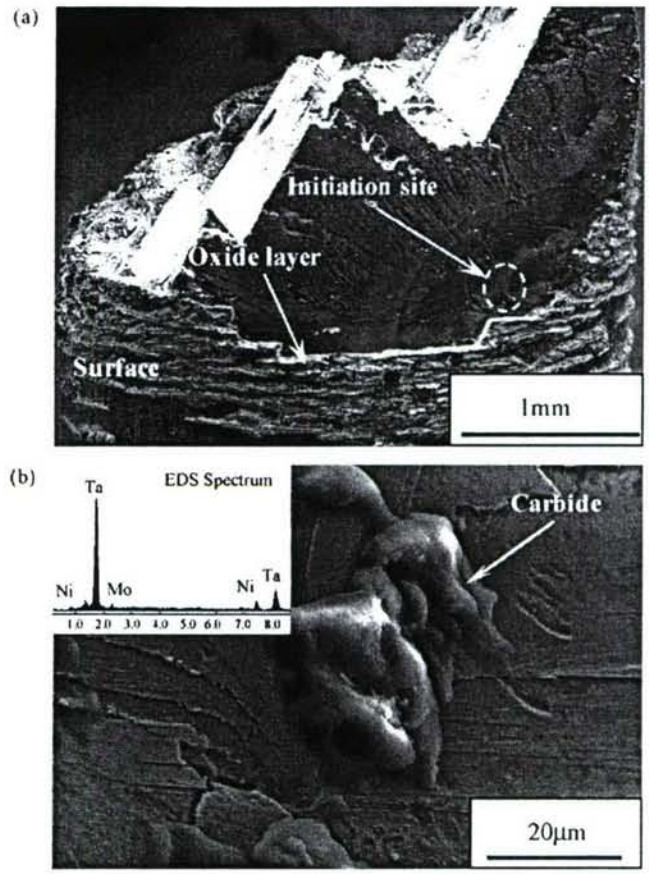

Fig. 6. (a) Blocky carbides associated with crack initiation in PWA 1484 ($\sigma_a = 350$ MPa, $N_f = 2.2 \times 10^7$ cycles), and (b) the EDS spectrum, indicating that the carbides are enriched in Ta.

instabilities during single crystal solidification that are responsible for the formation of defects, such as freckles and misoriented grains [18,19]; (iii) improve the transverse strength of low angle boundaries [20]; and (iv) influence dendritic segregation of elements during solidification [19]. Studies have shown that an addition of less than 0.1 wt% C improves creep rupture life in the temperature range of 850–950 °C for single crystal superalloys because the precipitation of MC carbides (where 'M'

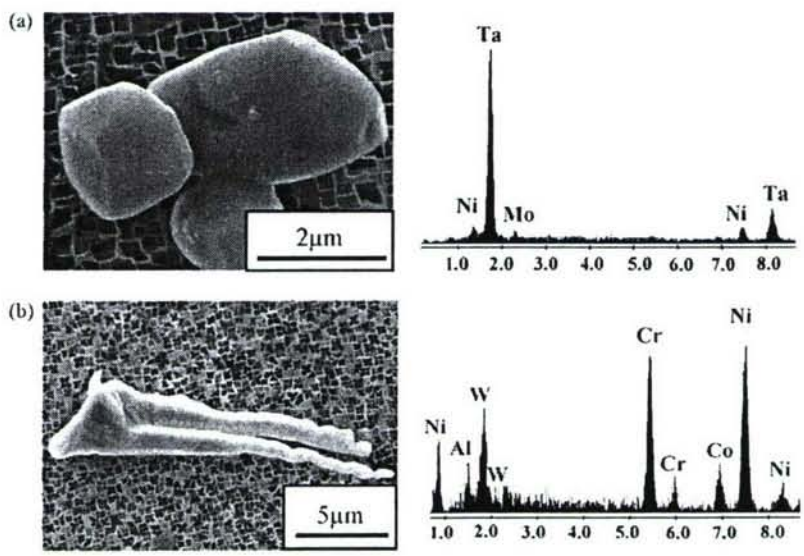

Fig. 7. SEM micrographs and EDS of carbides observed in PWA 1484: (a) blocky and (b) script. The carbides were extracted through electrolytic etching with a current density of ~0.05 A/cm^2 in an HCl and methanol (1:9) solution for approximately 15 min to remove the surrounding nickel material.

denotes metallic elements) during solidification reduces casting porosity [21–23]. However, it has also been observed that carbides raise local stress levels that leads to localized plastic strain during creep [24], low cycle fatigue [25] and thermal-fatigue [26] in superalloys leading to crack initiation [27,28]. In the present study, where porosity is low due to the HIP treatment, carbides are the favored fatigue crack initiation sites. In the alloy examined here, which contains <0.05 wt% C, carbides with blocky and script morphologies were observed in the interdendritic region. Examples of the typical morphologies are shown in Fig. 7 in samples subjected to electrolytic etching for long periods of time to remove the surrounding matrix. EDS analysis indicates that the blocky carbides are mainly enriched in Ta and are thus likely to be MC-type carbides [24,29], whereas the script carbides contain more Cr, and have transformed to $M_{23}C_6$-type carbides during heat treatment [21]. Most of the carbides in this alloy are of blocky shape. This is consistent with the observations that crack initiation occurred at Ta-rich carbides (see Fig. 6(b)).

As noted above, only one sample exhibited crack initiation near the surface and this is shown in Fig. 8. The specimen surface was oxidized during fatigue at 1000 °C, forming a thin layer of 20–30 μm in thickness on the surface, from which the crack apparently originated. These observations indicate that fatigue

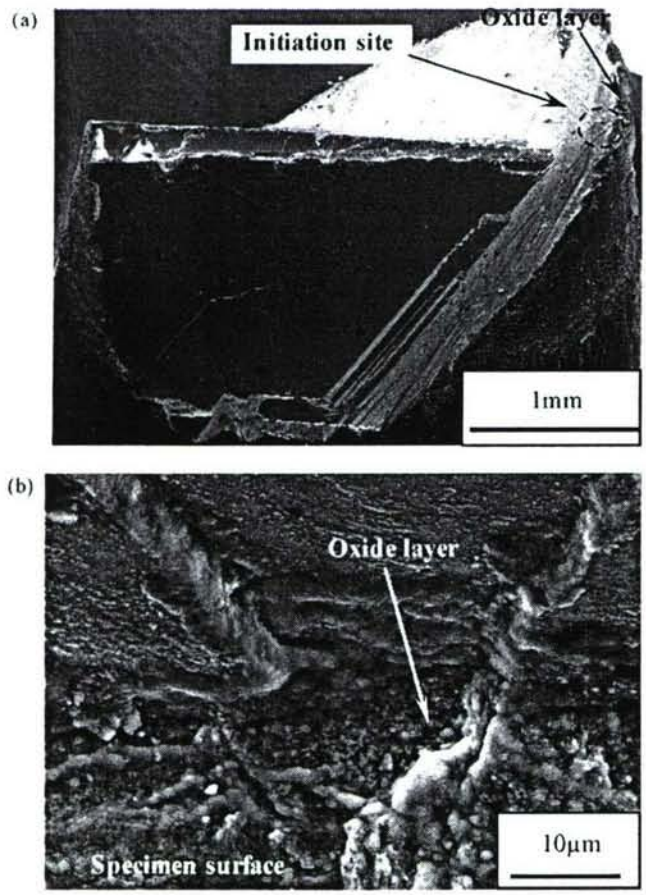

Fig. 8. Fracture surfaces of the specimen failed at $\sigma_a = 360$ MPa, $N_f = 1.3 \times 10^8$ cycles, at 20 kHz. (a) Overview of crack initiation site, and (b) details of the initiation site, indicating the proximity of crack initiation to the surface oxide layer formed during fatigue.

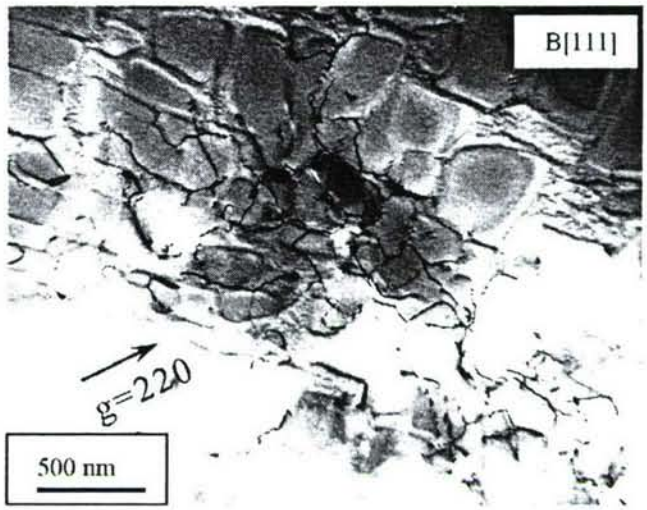

Fig. 9. Typical dislocation substructure observed in a specimen subjected to ultrasonic fatigue at $\sigma_a = 350$ MPa, $R = -1$, 1000 °C and 20 kHz ($N_f = 2.2 \times 10^7$ cycles).

cracks are more likely to initiate from interior carbides under the present testing conditions. Although the exact mechanisms responsible for this behavior require further investigation, it is possible that the surface oxide film that forms on the uncoated samples during testing inhibits cyclic strain localization at the surface [30], thus favoring internal fatigue crack initiation.

A representative TEM images of the substructure developed during fatigue of the alloys is presented in Fig. 9. The foil normal is ⟨0 0 1⟩ and was removed from a region that is approximately 1 mm below the fracture surface in a sample that failed after 2.2×10^7 cycles under $\sigma_a = 350$ MPa. The dislocation density after ultrasonic fatigue is low, compared to that expected to result from creep at 1000 °C. Additionally, no interfacial dislocation networks characteristic of high temperature creep [31] were observed, indicating that no significant general plastic deformation occurred during ultrasonic fatigue. This is also supported by the observation that no change in the γ′ morphology occurred during ultrasonic fatigue (see Figs. 1(b) and 10(b)). However, localized plastic deformation was frequently observed near carbides in the interdendritic regions, and the trace of localized shearing was frequently oriented approximately 50° to the loading axis. An example is shown in Fig. 10. These observations suggest that plastic deformation under ultrasonic cyclic loading preferably occurred around the carbides, and cracks were eventually developed by localized plastic deformation in the form of shear bands along {1 1 1} planes.

3.3. Crack propagation

In the present study fatigue crack propagation from the internal initiation sites at carbides occurred along {1 1 1} octahedral planes under all conditions examined, as shown in Figs. 5(a) and 6(a). There was little reduction in area or elongation of the specimens during the fatigue process and no evidence of creep damage as a primary contributor to failure was observed for the testing conditions examined. A metallographic cross-section parallel to the loading axis shows a trace of the fracture surface, Fig. 11.

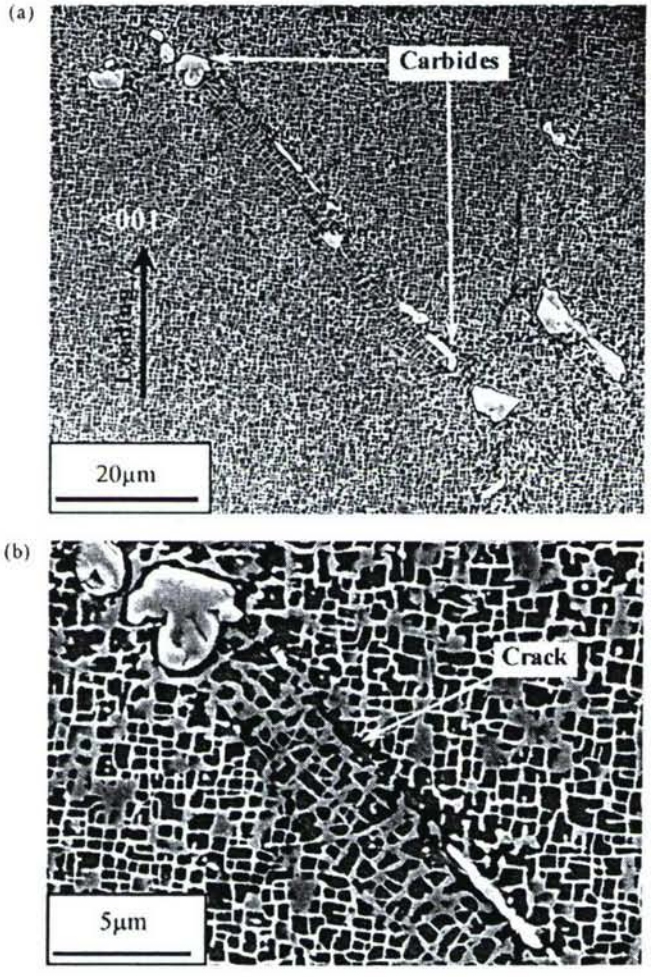

Fig. 10. Secondary cracks observed from cross-section perpendicular to tensile axis in a specimen that failed at $\sigma_a = 360$ MPa, $N_f = 1.3 \times 10^8$ cycles, showing (a) discontinuously distributed carbides in interdendritic region; and (b) cracks generated along the carbides.

The plane of crack propagation is inclined approximately 50° with respect to the ⟨0 0 1⟩ orientation, again suggesting that crack growth occurs on {1 1 1} octahedral planes, rather than perpendicular to the loading axis.

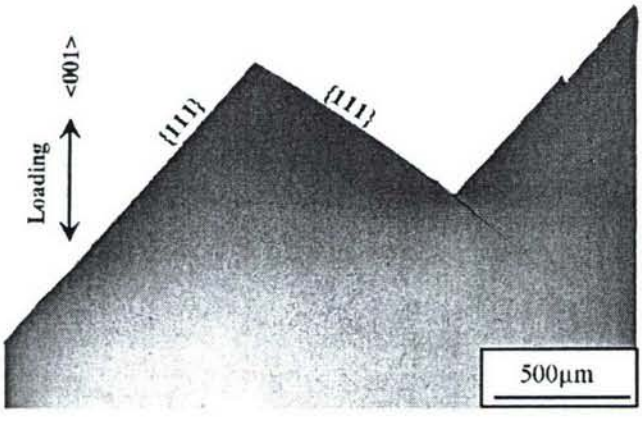

Fig. 11. Cross-section of a failed specimen, indicating that crack propagation occurred along {1 1 1} octahedral planes.

There have been a number of studies, some several decades ago [32–36], and others more recent [1,15,37–40], that have examined fatigue life and fatigue crack propagation behavior in single crystal superalloys as a function of cyclic frequency, temperature and environment. These studies collectively indicate that fatigue crack propagation in nominally [0 0 1] oriented single crystals favors either one of the octahedral {1 1 1} planes or follows a Mode-I path perpendicular to the load axis. Crack propagation on octahedral planes is favored at lower temperatures and higher frequencies (>10 Hz) and is associated with the formation of localized cyclic deformation on {1 1 1} ⟨1 1 0⟩ slip systems. Some evidence suggests that the particular octahedral planes on which crack propagation occurs depends on the combined shear and normal stresses, with the former responsible for damage accumulation from irreversible cyclic deformation and the latter required to cause crack propagation in the damaged regions. Some studies also suggest that at higher temperatures and/or lower frequencies environmental effects, particularly oxidation at the crack tip, are the reason for the transition to non-crystallographic Mode-I type of crack propagation. In this case the fatigue crack propagation rate, da/dN, compared to the rate of crack tip oxidation is thought to be important, with higher temperatures and lower frequencies enhancing crack tip oxidation and leading to planar (Mode-I) crack growth. Alternatively, it is also argued that the temperature, and therefore, strain rate dependence of yield strength, and particularly the anomalous yield strength dependence of gamma prime on temperature, can also explain the transition from planar Mode-I to cyrstallographic crack propagation as temperature and frequency are varied. Interestingly, the two types of crack growth modes could be seen on one specimen [2], implying that the transition from one mode to the other is also dependent on the stress state. Chan et al. [41] investigated the fatigue crack growth in PWA 1484 tested at 593 °C, $R = 0.5$ and 20 Hz, and their results indicated that Mode-I crack growth and crystallographic {1 1 1} crack growth are competing process that exhibit different crack growth rates. The dominance of one crack growth morphology over another is dictated by the crack growth rate response of individual crack morphologies at a given stress intensity factor range and the local stress intensity factor range when the crack alters its path. But a quantitative analysis on the transition, including the effect of temperature, loading frequency and stress state is not available yet.

Our results indicate that, with the 20 kHz frequency employed in these ultrasonic fatigue studies, fatigue crack propagation on {1 1 1} planes is still possible even at temperatures as high as 1000 °C. Either the "environmental" or the "strain-rate" mechanisms described above are consistent with our observations and further work is underway to examine this transition and the associated strain localization that occurs during ultrasonic fatigue.

4. Conclusions

An ultrasonic fatigue testing system operating at elevated temperature was developed to explore the high-cycle fatigue behavior of nickel-base single-crystal superalloys under

conditions relevant to the operation of gas turbine engines. The capability of this system was demonstrated using a single crystal superalloy (PWA1484) at a temperature of 1000 °C and loading frequency of approximately 20 kHz. The S–N data generated from the ultrasonic testing system was consistent with comparable fatigue data obtained on the same material using conventional fatigue test methods. Interior Ta-rich carbides were the major microstructural feature responsible for crack initiation in the alloy, consistent with the low porosity in the alloy and the observations of strain localization at the carbides. Crack growth under ultrasonic loading at 1000 °C for PWA 1484 occurred on {1 1 1} octahedral slip planes, rather than perpendicular to the loading axis, as usually observed for single crystal superalloys at high temperatures (>850 °C) and conventional servo-hydraulic loading frequencies (<100 Hz).

Acknowledgements

The authors gratefully acknowledge the financial support of the AFOSR and DARPA through AFOSR contract #F49620-03-1-0069, and GE Aviation for providing the samples and carrying out the HIP and heat treatment. The authors acknowledge Dr. Ken Wright (GE Aviation) for providing materials and for helpful discussions.

References

[1] J. Telesman, L.J. Ghosn, J. Eng. Gas Turbine Power 118 (1996) 399–405.
[2] P.K. Wright, M. Jain, D. Cameron, in: K.N. Green, H. Harada, T.E. Howson, T.M. Pollock, R.C. Reed, J.J. Schirra, S. Walston (Eds.), Superalloys 2004, TMS, Seven Springs, Pennsylvania, USA, 2004, pp. 657–666.
[3] H. Mayer, M. Papakyriacou, R. Pippan, S. Stanzl-Tschegg, Mater. Sci. Eng. A 314 (2001) 48–54.
[4] X. Zhu, A. Shayam, J.W. Jones, H. Mayer, J.V. Lasecki, J.E. Allison, Int. J. Fatigue 28 (2006) 1566–1571.
[5] I. Marines, G. Dominguez, G. Baudry, J.-F. Vittori, S. Rathery, J.-P. Doucet, C. Bathias, Int. J. Fatigue 25 (2003) 1037–1046.
[6] C.J. Szczepanski, A. Shyam, S.K. Jha, J.M. Larsen, C.J. Torbet, S.J. Johnson, J.W. Jones, in: J.M. Larsen, L. Christodoulou, J.R. Calcattera, M.L. Dent, M.M. Derriso, W.J. Hardman, J.W. Jones, S.M. Russ (Eds.), Materials Damage Prognosis, TMS, Warrendale, Pennsylvania, USA, 2005, pp. 315–321.
[7] R. Morrissey, T. Nicholas, in: T. Sakai, Y. Ochi (Eds.), Very High Cycle Fatigue, Soc. Mater. Sci., Japan, Kusatsu, Japan, 2004, pp. 156–162.
[8] A. Shyam, C.J. Torbet, S.K. Jha, J.M. Larsen, C.J. Szczpanski, T.M. Pollock, J.W. Jones, in: K.N. Green, H. Harada, T.E. Howson, T.M. Pollock, R.C. Reed, J.J. Schirra, S. Walston (Eds.), Superalloys 2004, TMS, Seven Springs, Pennsylvania, USA, 2004, pp. 259–268.
[9] H. Mayer, Int. Mater. Rev. 44 (1999) 1–34.
[10] A.D. Cetel, D.N. Duhl, in: D.N. Duhl, G. Maurer, S. Antolovich, C. Lund, S. Relchman (Eds.), Superalloys 1988, The Metallurgical Society Inc., Seven Springs, Pennsylvania, USA, 1988, pp. 235–244.
[11] D.N. Duhl, A.D. Cetel, U.S. Patent #04719080, United Technologies Corporation, 1988.
[12] S.P. Timoshenko, J.N. Goodier, Theory of Elasticity, McGraw-Hill, New York, 1970.
[13] P. Bajons, W. Kromp, Ultrasonics 16 (1978) 213–217.
[14] E. Eisner, J. Acous. Soc. Am. 35 (1963) 1367–1377.
[15] D.W. MacLachlan, D.M. Knowles, Fatigue Fract. Eng. Mater. Struct. 24 (2001) 503–521.
[16] S. Suresh, Fatigue of Materials, Cambridge University Press, Cambridge, 1998, p. 223.
[17] J.R. Mihalisin, J. Corrigan, M. Launsbach, R. Baker, in: K.N. Green, H. Harada, T.E. Howson, T.M. Pollock, R.C. Reed, J.J. Schirra, S. Walston (Eds.), Superalloys 2004, TMS, Seven Springs, Pennsylvania, USA, 2004, pp. 795–800.
[18] S. Tin, T.M. Pollock, W. Murphy, Metall. Trans. 32 (2001) 1743–1753.
[19] S. Tin, T.M. Pollock, Mater. Sci. Eng. A 348 (2003) 111–121.
[20] E.W. Ross, K.S. O'Hara, in: R.D. Kissinger, D.J. Deye, D.L. Anton, A.D. Cetel, M.V. Nathal, T.M. Pollock, D.A. Woodford (Eds.), Superalloys 1996, TMS, Seven Springs, Pennsylvania, USA, 1992, pp. 19–26.
[21] L.Z. He, Q. Zheng, X.F. Sun, H.R. Guan, Z.Q. Hu, A.K. Tieu, C. Lu, H.T. Zhu, Mater. Sci. Eng. A 397 (2005) 297–304.
[22] L.R. Liu, T. Jin, N.R. Zhao, Z.H. Wang, X.F. Sun, H.R. Guan, Z.Q. Hu, Mater. Sci. Eng. A 385 (2004) 105–112.
[23] Q.Z. Chen, N. Jones, D.M. Knowles, Acta Mater. 50 (2002) 1095–1112.
[24] L.R. Liu, T. Jin, N.R. Zhao, X.F. Sun, H.R. Guan, Z.Q. Hu, Mater. Sci. Eng. A 361 (2003) 191–197.
[25] J. Reuchet, L. Remy, Mater. Sci. Eng. 58 (1983) 19–32.
[26] B. Baufeld, E. Tzimas, H. Mullejans, S. Peteves, J. Bressers, W. Stamm, Mater. Sci. Eng. A 315 (2001) 231–239.
[27] S. McHugh, Math. Comput. Modell. 14 (1990) 933–941.
[28] M.M. Shenoy, R.S. Kumar, D.L. McDowell, Int. J. Fatigue 27 (2005) 113–127.
[29] S. Tin, T.M. Pollock, Metall. Trans. 34A (2003) 1953–1967.
[30] D.J. Duquette, M. Gell, Metall. Trans. 3 (1972) 1899–1905.
[31] T.M. Pollock, A.S. Argon, Acta Metall. Mater. 40 (1992) 1–30.
[32] D.J. Duquette, M. Gell, J.W. Piteo, Metall. Trans. 1 (1970) 3107–3115.
[33] D.J. Duquette, M. Gell, Metall. Trans. 2 (1971) 1325–1331.
[34] G.R. Leverant, M. Gell, Metall. Trans. 6A (1975) 367–371.
[35] D.C. Wu, D.W. Hoeppner, Scripta Mater. 19 (1985) 493–498.
[36] J.S. Crompton, J.W. Martin, Mater. Sci. Eng. 64 (1984) 37–43.
[37] N.K. Arakere, G. Swanson, J. Eng. Gas Turbines Power 124 (2002) 161–176.
[38] N.K. Arakere, J. Eng. Gas Turbine Power 126 (2004) 590–603.
[39] R.A. Naik, D.P. Deluca, D.M. Shah, J. Eng. Gas Turbine Power 126 (2004) 391–400.
[40] P. Lukas, L. Kunz, M. Svoboda, Int. J. Fatigue 27 (2005) 1535.
[41] K.S. Chan, J. Feiger, Y.-D. Lee, R. John, J. Hudak, J. Eng. Gas Turbine Power 127 (2005) 2–7.

4th International Conference on Very High Cycle Fatigue
Edited by: J.E. Allison, J.W. Jones, J.M. Larsen and R. Ritchie
TMS (The Minerals, Metals & Materials Society), 2007

Very high cycle fatigue behavior of nickel-based superalloy René 88DT at 593 °C

Jiashi Miao[1], T. M. Pollock[1], J. W. Jones[1]

[1]Department of Materials Science and Engineering, University of Michigan, Ann Arbor, MI-48109, USA

Keywords: Very high cycle fatigue, nickel-based superalloy, crack initiation, crystallographic facets

Abstract

The very high cycle fatigue behavior of a polycrystalline nickel-based superalloy, René 88 DT, was studied in the lifetime regime of 10^5~10^9 cycles at 593 °C in laboratory air using an ultrasonic fatigue testing apparatus operating at 20 kHz. Fatigue failures were observed at lifetimes beyond 10^8 cycles, and the variability in fatigue life increased with decreasing stress levels. Fractographic analysis indicated that all fatigue cracks initiated internally. Most of crack initiation sites consisted of large crystallographic facets and no inclusions were observed. These large crystallographic facets were formed by fatigue crack initiation and early crack growth in large grains with dimensions much larger than the average grain size. Quantitative fracture surface analysis showed that the crystallographic facets at the crack initiation sites are oriented close to 45 degrees to the loading axis and correspond to maximum shear stress planes. Crystallographic orientations of grains near internal crack initiation sites were revealed using EBSD combined with metallographic serial sectioning. Cyclic strain localization within a favorably oriented large grain and early crack growth in similarly oriented neighboring grains is the likely mechanism controlling the VHCF lifetime in this alloy.

Introduction

Recent studies have revealed that conventional fatigue limits do not exist for many engineering alloys, with fatigue failures occurring in the very high cycle regime (lifetime $>10^7$ cycles) [1, 2]. For materials with a high density of defects such as pores and inclusions, internal defects are the primary crack initiation sites in the very high cycle regime [3, 4]. However, for materials prepared by advanced processing techniques that significantly reduce the content of defects, microstructure heterogeneities are expected to be the main crack initiation sites. In the very high cycle regime, fatigue crack initiation (rather than crack propagation) is thought to be the life-determining process [5]. Conventional fatigue life predictions based on damage-tolerant methodologies, are, therefore, not effective in accurately predicting very high cycle fatigue life. Additionally, the uncertainty in life prediction increases as the fatigue life shifts from the low cycle regime to the very high cycle regime. A thorough understanding in fatigue crack initiation and small crack growth behavior is therefore crucial for building physically-based life prediction models that accurately predict fatigue life in the very high cycle regime.

Nickel-based superalloys have been widely used in turbine engine components in aerospace and power-generation industries. Better understanding of the fatigue behavior of superalloys in the

very high cycle regime can therefore directly benefit safe extension of the residual life of these components and the development of new alloy systems.

In this study, the fatigue behavior of a polycrystalline nickel-based superalloy, René 88 DT, was studied in the very high cycle regime using ultrasonic fatigue. Comparisons between very high cycle fatigue behavior generated by ultrasonic fatigue and fatigue behavior generated at conventional frequency were made, and a detailed study of the role of microstructure heterogeneities, particularly grain size, orientation and spatial distribution, on crack initiation in this alloy is described.

Material and Experimental Procedures

Materials

The René 88 DT used in this study was prepared by powder metallurgy techniques that significantly reduce chemical inhomogeneity and initial defect sizes in the alloy [6]. René 88 DT is strengthened primarily by precipitation of a gamma prime phase (γ') [7]. Figure 1 (a) shows the typical microstructure of the alloy. The grain size was measured using the line intercept method on optical micrographs. The distribution of grain size is illustrated in figure 1 (b). The mean grain size, excluding the presence of annealing twins, is about 26μm. Large grains on the order of two to five times of the average grain size and large grain clusters exist in the microstructure. . Annealing twins are prevalent in the microstructure. The fraction of annealing twin boundaries is approximately 0.58. Texture analysis based on EBSD scans indicates there is no significant macrotexture.

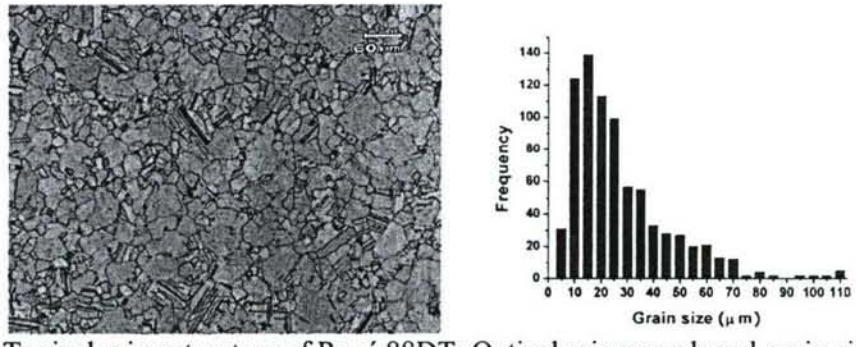

Figure 1. Typical microstructure of René 88DT: Optical micrograph and grain size distribution

Experimental Procedures

Cylindrical ultrasonic fatigue specimens with a gage diameter of 5mm and gage length of 16mm were used in this study. The detailed design methodology and geometry of the specimens can be found elsewhere [8]. In order to eliminate the influence of surface residual stresses resulting from mechanical machining, the gage sections of all fatigue specimens were electropolished to remove approximately 100μm from the diameter. Ultrasonic fatigue testing was conducted under uniaxial tension with a resonance frequency close to 20 kHz, and a stress ratio R =0.05 at 593°C in laboratory air. Fatigue cycles were applied in pulses of 500 ms separated by pauses of 900 ms to allow accurate control of specimen temperature. Fracture surfaces of all failed specimens were examined using scanning electron microscopy. The geometric orientation of crystallographic facets at crack initiation sites was quantitatively studied using a three dimensional reconstruction program developed in the environment of IDL (Interactive Data Language). This method uses SEM stereo pairs to automatically reconstruct the fracture surface. The EBSD studies were performed using TSL OIM software on a FEG XL30 SEM.

Results and Discussion

S-N data

The stress-life data for René 88 DT generated by ultrasonic fatigue at 593°C, along with 10 Hz, R = 0.05 fatigue test results [9] for the same material are presented in Figure 2.. Ultrasonic fatigue testing was conducted by displacement control at low loading stresses and in the long life regime, while conventional fatigue testing was performed in load control at high stresses. As indicated in Figure 2, fatigue failure still can occur in this alloy for lifetimes beyond 10^8 cycles. It is noteworthy that the variability in fatigue life increases in the very high cycle fatigue regime. The variability in fatigue life exceeds two orders of magnitude at σ_{max} = 600MPa, while the variability in fatigue life at σ_{max} = 940MPa is only one order of magnitude.

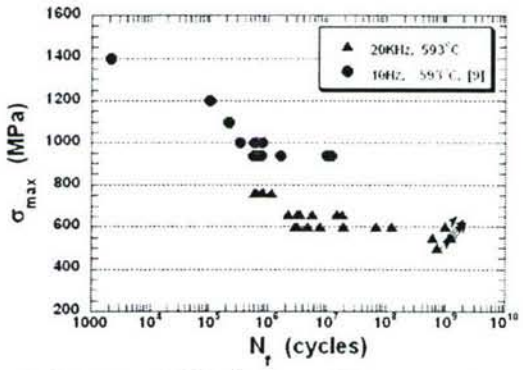

Figure. 2. S-N data of Rene 88 DT at 593°C（Data with arrow sign represent run-out results）

Fractography

Fractographic analysis indicated that all specimens failed by internal or subsurface crack initiation. Most crack initiation sites (95%) consist of large crystallographic facets with no defects such as inclusions or pores observed. A few specimens failed by crack initiation from large inclusions. Caton et al. [9] studied conventional fatigue behavior of the same material in the stress range of 940MPa - 1400MPa at 593°C and found that all fatigue cracks initiated internally except for specimens tested at the highest stress levels. They observed two types of crack initiation sites: crystallographic facets and non-metallic inclusions. The increase of fatigue life variability is thought to be due to superposition of the variability of two types of crack initiation mechanisms [10]. Apparently there is a transition of fatigue crack initiation mode with decreasing stress levels. At low stresses, fatigue cracks prefer to initiate from large grians forming crystallographic facets at the crack initiation sites. The large variability in fatigue life in the very high cycle regime is therefore likely caused by the variation in local microstructure associated with fatigue crack initiation and early small crack growth.

Matching half fractography of crystallographic facets at crack initiation sites is presented in fFigure 3. Large facets were formed by fracture and crack growth within large grains. The size of these grains is in the range of 60μm~120μm, which is much larger than the mean grain size of this alloy.

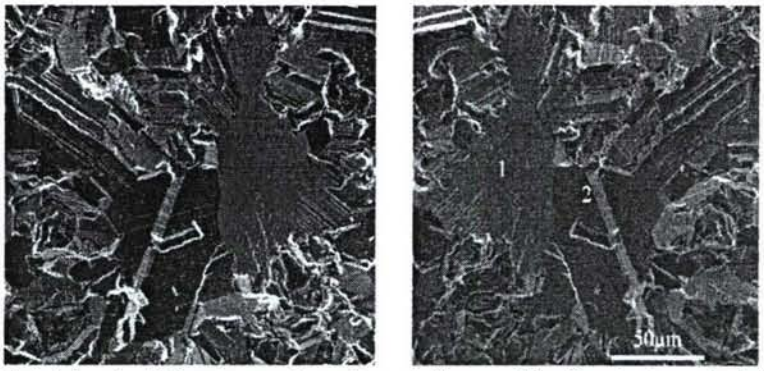

Figure 3. Matching half fractography of crystallographic facet at crack initiation site

The specimen surface oxidized slightly during ultrasonic fatigue testing at 593°C. Strain localization within large grains at the surface resulted in the formation of slip bands or persistent slip bands as shown in Figure 4, which shows that the oxide layers were spalled off, revealing localized cyclic deformation. For room temperature ultrasonic fatigue tests of the same alloy at low stress, crack initiation occurs at the specimen surface where strain localization within or more large grains results in the formation of persistent slip bands and microcracks. However, it is likely that surface oxidation at elevated temperature retards crystallographic crack initiation at the surface. Thus, cyclic strain localization in favorably oriented large grains in the specimen interior becomes dominant.

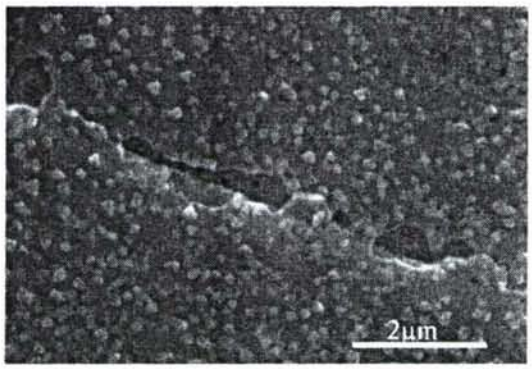

Figure. 4. Surface oxide layer and localized deformation formed during fatigue test at 593°C

There are two main types of facets at the crack initiation sites, identified in this paper as either single plane facets or chevron facets. The crystallographic facets in Figure 3 are typical examples of single plane facets. Figure 5 (a) shows an example of crystallographic facets with the chevron shape at the crack initiation site. The shapes of the facets were examined in detail using three dimensional reconstruction methods. The rectangle region in Figure 5 (a) was subject to 3D reconstruction. Figure 5 (b) shows the 3D view of the reconstruction region. The 3D results indicate that facet planes F1 and F2, in figure 5 (a), are orientated with respect to the loading axis about 45 degrees and 46 degrees, respectively. Thus, both facet planes are close to maximum shear stress planes. The angle between two facets planes is 44 degrees.

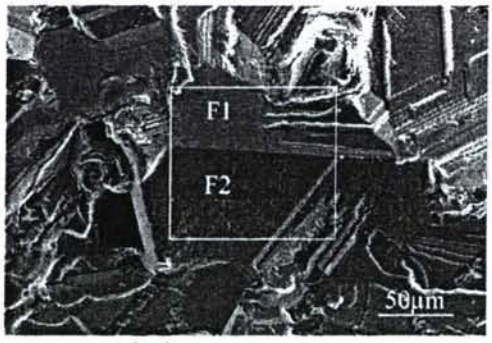

(a) (b)

Figure 5. Three dimensional reconstruction of chevron crystallographic facet at crack initiation site: (a) crack initiation site (d) 3D view of crystallographic facet with chevron shape.

Microstructure within Crack Initiation Sites

In order to study the specific microstructure associated with internal fatigue crack initiation and early small crack growth, metallographic serial sectioning was used to reveal the microstructure within the crack initiation site. Metallographic serial sectioning was completed by mechanical grinding and polishing with sectioning planes normal to the fracture surface. At periodic intervals of sectioning, orientation information of the microstructure beneath fatigue fracture surface was collected using EBSD.

Figure 6 (a) shows the crack initiation site before sectioning. The large crystallographic facet at the crack initiation site has a chevron shape. Figure 6 (b) shows the metallographic sectioning plane directly cuts through the chevron-shaped crystallographic facet at the crack initiation site. An EBSD reconstructed grain boundary map in Figure 6 (c) illustrates the microstructure details of the crack initiation grain. Both facet planes of the chevron facet are within one large grain and parallel to annealing twin boundaries, indicating that they are of {111} orientation. 3D reconstruction results showed the angles between the normals of the two facet planes and loading axis are 41 degrees and 43 degrees, respectively. The angle between two facet planes was 37 degrees. Thus, the fatigue crack initiated along octahedral planes that are oriented close to the orientation for maximum shear stresss. The special geometrical relationship between two facet planes provides an easier path for fatigue crack propagation within the large grain. The Schimd factors for the large grains at which cracks initiated are are greater than 0.43. Serial sectioning results indicate that in the neighborhood of the grain at which fatigue crack initiation occurred, a cluster of grains with similar orientation exists. As shown in Figure 6 (d), the orientations of these grains Figure 6 (a) are close to <001>. During ultrasonic fatigue, the cyclic stresses are much lower than the overall yield stress for the alloy and most grains only experience elastic deformation. In the very high cycle regime cyclic plastic deformation can assume to be localized in favorably oriented large grains or grain clusters where the grains have asimilar relative orientation that contributes to both fatigue crack initiation (in one grain) and early small crack growth in the neighboring grains. This scenario is supported by the results presented in Figure 3. Three-dimensional reconstruction results indicate that the facet planes within two large grains at crack initiation are nearly parallel to each other. A fatigue crack initiated from grain 1 and then propagated to grain 2, leaving a smooth transition between the two resulting facets, as would be expected if the two grains have similar crystallographic orientation. For such an arrangement of large grains, fatigue crack initiation and early propagation would be expected to be easier.

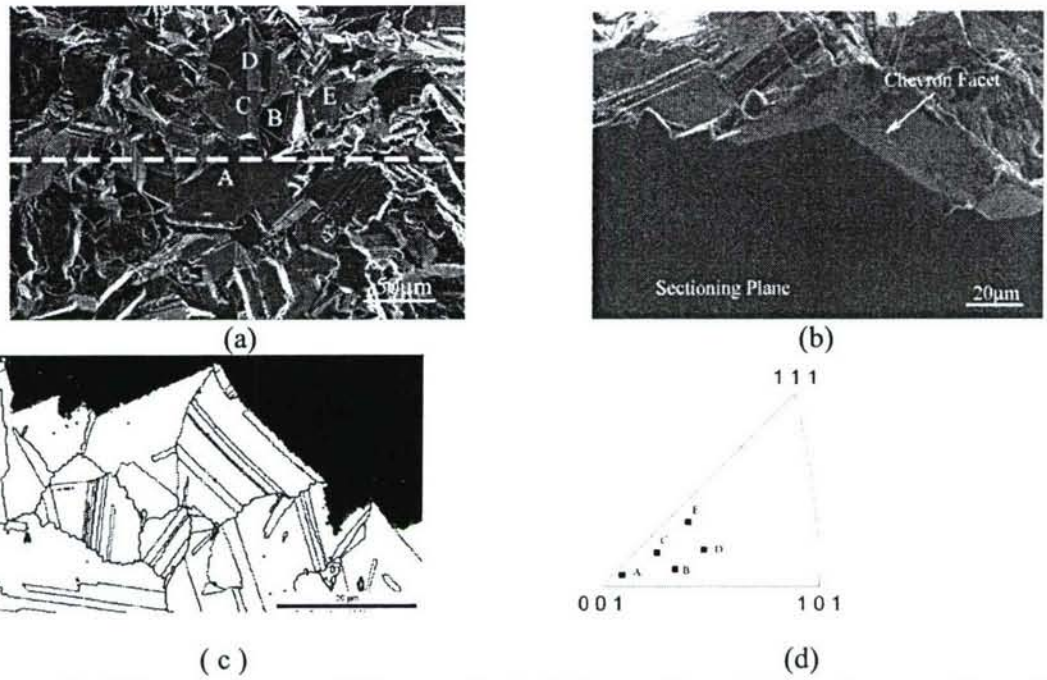

Figure 6. Microstructure within crack initiation site: (a) fracture surface before sectioning,(dashed line indicates the position of sectioning plane in figure (b). (b) metallographic sectioning plane. (c) reconstructed grain boundary (black lines represent random grain boundaries, blue lines represent annealing twin boundaries), (d) grains with similar orientation near crack initiation site.

Conclusions

The very high cycle fatigue behavior of the nickel-based superalloy René 88 DT was investigated in the life time regime of 10^5~10^9 cycles at 593°C using ultrasonic fatigue instrumentation. All fatigue cracks initiated internally at this elevated temperature. Compared with conventional (10Hz) fatigue results at high loading stresses, nearly all fatigue cracks in current study originated from crystallographic initiation sites associated with large grains with diameters >50. Crystallographic facets at crack initiation sites can be divided into two groups according to their geometry: single plane facet and chevron facet. The 3D results showed that crystallographic facets at crack initiation sites are oriented at an angle close to 45 degrees to the loading axis. By using metallographic serial sectioning combined with EBSD, microstructural and crystallographic details related to internal crystallographic crack initiation sites was revealed. Preliminary results showed that clusters of grains with similar orientation are the most favored crack initiation sites because they promote the necessary strain localization and early crack propagation necessary to cause fatigue failure.

Acknowledgements

This work was supported by the Air Force Office of Scientific Research (F49620-03-1-0069, Dr. J.Tiley, Program Manager) and DARPA (Dr. Leo Christoudolou, Program Manager). The authors thank Mr. Chris Torbet for technical support for ultrasonic fatigue testing.

References

[1] Bathias, C. There is no infinite fatigue life in metallic materials", Fatigue Fract Engng Mater Struct 1999; 22: 559-565.

[2] Y (Yukitaka) Murakami, T Nomoto, T Ueda, and Y (Yasuo) Murakami. On the mechanism of fatigue failure in the superlong life regime ($N > 10^7$ cycles). Part I: Influence of hydrogen trapped by inclusions. Fatigue Fract Engng Mater Struct 2000; 23: 893-902.
[3] X. Zhu, A. Shyam, J.W. Jones, H. Mayer, J.V. Lasecki and J.E. Allison. Effects of microstructure and temperature on fatigue behavior of E319-T7 cast aluminum alloy in very long life cycles. Int J Fatigue 2006;28:1566-1571.
[4] J. Huang, J. E. Spowart and J. W. Jones. Fatigue behaviour of SiC_p-reinforced aluminium composites in the very high cycle regime using ultrasonic fatigue. Fatigue Fract. Engng Mater. Sruct 2006; 29:507-517.
[5] Hael Mughrabi. Specific features and mechanisms of fatigue in the ultrahigh-cycle regime. Int J Fatigue 2006; 28: 501-1508.
[6] Krueger, D D, Kissinger, R D and Menzies, R G. Development and introduction of a damage tolerant high temperature Nickel-Base Disk Alloy, Renee 88DT. Superalloys 1992; Champion, Pennsylvania; USA, 277-286.
[7] S. T. Wlodek, M. Kelly and D.A.Alden. The structure of Rene 88 DT. Superalloys 1996, Champion, Pennsyslvania; USA, 129-136.
[8] A. Shyam, C. J. Torbet, S. K. Jha, J. M. Larsen, M. J. Caton, C. J. Szczepanski, T. M. Pollock, J. W. Jones. Development of ultrasonic fatigue for rapid, high temperature fatigue studies in turbine materials. Superalloys 2004; Champion, Pennsylvania; USA, 259-268.
[9]Caton, M.J, Jha, S.K, Rosenberger, A.H and Larsen, J.M. Divergence of mechanisms and the effect on the fatigue life variability of Rene 88DT. Superalloys 2004; Champion, Pennsylvania; USA, 305-312.
[10] Jha, S.K, Caton, M.J, Larsen, J.M, Rosenberger, A.H, Li. K. Z and Poter,W.J. Superimposition mechanisms and their effect on the variability in fatigue lives of nickel-based superalloy. Materials Damage Prognosis; TMS, 2005, 343-350